ADVANCED FUNCTIONAL MATERIALS
www.afm-journal.de

The Chemistry and Promising Applications of Graphene and Porous Graphene Materials

Haibo Huang, Haodong Shi, Pratteek Das, Jieqiong Qin, Yaguang Li, Xiao Wang, Feng Su, Pengchao Wen, Suyuan Li, Pengfei Lu, Fangyan Liu, Yuejiao Li, Ying Zhang, Yi Wang, Zhong-Shuai Wu, and Hui-Ming Cheng**

Graphene and graphene oxide (GO), as wonder materials, have penetrated nearly every field of research. One of their most attractive features is the functionality and assembly of graphene or GO, in which they can be considered to be chemically functionalized building blocks for creating unconventional porous graphene materials (PGMs) that not only combine the merits of both porous materials and graphene, but also have major advantages over other porous carbons for specific applications. The chemistry and approaches for functionalizing graphene and GO are first introduced, and typical procedures for pore creation (e.g., in-plane pores, 2D laminar pores, and 3D interconnected pore assemblies), self-assembly, and tailoring mechanisms for PGMs to highlight the significance of precise control over the pore morphology and pore size are summarized. Because of their unique pore structures, with different morphologies and intriguing properties, PGMs serve as key components in a variety of applications such as energy storage, electrocatalysis, and molecular separation. Finally, the challenges relating to PGMs from the understanding of chemical self-assembly to specific applications are discussed, and promising solutions on how to tackle them are presented. This provides an insightful outlook for the future development of the chemistry and applications of PGMs.

1. Introduction

Porous materials (PMs) have received extensive attention for applications in energy storage and conversion, catalysis, gas adsorption and separation, and environmental protection, due to their extraordinary chemical and physical properties,[1–4] such as tunable porosity, high specific surface area (SSA), large accessible internal space, variable chemical compositions, low mass density, and/or interconnected pore structures with different length scales. In particular, their extremely high ratio of surface area to mass or volume allows intimate interactions with diverse organic or inorganic species to take place both at the surface and in the interior porous space. According to pore size, PMs in principle are divided into microporous, mesoporous, and macroporous. Generally, hierarchically PMs with the multiple levels of pore size have bimodalities, or even trimodalities.[1]

Among the many PMs, porous nanocarbon materials are extremely appealing due to their high electrical conductivity, low mass density, excellent thermal conductivity, high biocompatibility, and good chemical stability under nonoxidizing conditions.[5] In addition, many different atoms are bond with them using different hybrid orbitals (sp, sp^2, sp^3), enabling the production of PMs with the desired morphologies and wonderful properties for various applications.[5,6]

Graphene, a typical 2D sheet of sp^2-hybridized carbon, has superior chemical and physical properties, i.e., high SSA

Dr. H. B. Huang, H. D. Shi, P. Das, J. Q. Qin, Dr. Y. G. Li, X. Wang, F. Su, Dr. P. C. Wen, Dr. S. Y. Li, Dr. P. F. Lu, Dr. F. Y. Liu, Y. J. Li, Y. Zhang, Y. Wang, Prof. Z.-S. Wu
Dalian National Laboratory for Clean Energy
Dalian Institute of Chemical Physics
Chinese Academy of Sciences
457 Zhongshan Road, Dalian 116023, China
E-mail: wuzs@dicp.ac.cn

H. D. Shi, P. Das, J. Q. Qin, X. Wang, F. Su, Y. J. Li, Y. Zhang, Y. Wang
University of Chinese Academy of Sciences
Beijing 100049, P. R. China

The ORCID identification number(s) for the author(s) of this article can be found under https://doi.org/10.1002/adfm.201909035.

Prof. H.-M. Cheng
Shenyang National Laboratory for Materials Science
Institute of Metal Research
Chinese Academy of Sciences
Shenyang 110016, China
E-mail: cheng@imr.ac.cn

Prof. H.-M. Cheng
Tsinghua-Berkeley Shenzhen Institute
Tsinghua University
Shenzhen 518055, China

Prof. H.-M. Cheng
Advanced Technology Institute
University of Surrey
Guildford, Surrey GU2 7XH, UK

DOI: 10.1002/adfm.201909035

(2630 m^2 g^{-1}), high Young's modulus (1.0 TPa), extraordinary intrinsic electron mobility (200 000 cm^2 v^{-1} s^{-1}), and excellent thermal conductivity (5000 W m^{-1} K^{-1}).[7–9] By virtue of these attractive properties, graphene has inspired research interest in energy storage and conversion,[10,11] catalysis,[12] gas adsorption and separation,[13] drug delivery,[14] green chemistry, and the environment.[15] Graphene oxide (GO) and reduced graphene oxide (rGO) are two typical mono-layer graphene derivatives containing oxygenate groups and defects. Furthermore, they can bond with many different atoms by sp, sp^2, and sp^3 hybrid orbitals to produce porous graphene (PG) that efficiently combine the merits of both PMs and graphene.[9] The structure and properties of porous graphene materials (PGMs) derived from both GO and rGO are highly dependent on their surface/interface, assembly and functionalization chemistry, which determine the functions of the PG for targeted specific applications.

According to the pore formation mechanisms, PGMs can be classified into three categories: monolayer PG with in-plane pores, stacked 2D laminar PG with interlayer pores, and 3D interconnected porous frameworks, all of which have many merits over conventional porous nanocarbons.[16,17] First, the high mechanical strength of graphene efficiently reinforces the porous structure. Second, the outstanding thermal and chemical stability of graphene enables its porous derivatives to be durable in tough environments. Third, electrically conductive graphene serves as a desired current collector for fast electrons transportation through the porous framework. Last but not the least, GO, rGO, and graphene with heteroatom-doping can serve as alternative substrates for modifying a variety of inorganic or organic species to produce new PG hybrids with designable functionalities. Because of these advantages, a plethora of applications, including supercapacitors,[18–22] batteries,[23–27] and molecular separation,[28–30] have been widely explored, in which the chemistry of graphene and GO play significant roles in the design and construction of well-defined PMs.

Given the widespread interest in graphene, advances in its synthesis, characterization, and applications have been previously reviewed.[31–36] However, most of the literatures focus only on the synthesis chemistry[32,37] and electrochemistry[38] of graphene, or certain specific applications of graphene-based materials.[39–41] A comprehensive description of graphene and GO chemistry that involves the surface, interface, assembly, and functionalization chemistry is missing. Although, the preparation of PGMs and their promising applications have been extensively investigated in many fields, the key roles of chemistry in "structure-determining-performance" for targeted applications using PG has not been clearly elucidated.

In an attempt to fill this gap, this review will deeply discuss the chemistry of graphene and GO, and provide a comprehensive overview of their surface chemistry, pore-forming mechanisms, pore-tailoring approaches, and functionalization chemistry as influenced by different driving forces such as ionic interactions, hydrogen bonds, π–π interactions, and van der Waals forces, which are critical for understanding the significant roles of PGMs in their applications (**Figure 1**). Given their unique porous structures with different morphologies and properties, the fabrication methods of three typical PGMs with in-plane pores, 2D laminar pores, and 3D interconnected pore assemblies, will be systematically summarized to highlight the importance of controlling the porous structure. Furthermore, a variety of applications, e.g., supercapacitors, lithium sulfur batteries, lithium ion batteries, non-lithium batteries (Na/K/Mg/Al batteries),

Haibo Huang received her Ph.D. degree from Jilin University in 2016 and joined the 2D Materials & Energy Devices group at Dalian Institute of Chemical Physics (DICP), Chinese Academy of Sciences (CAS) in 2017 as a postdoctoral fellow, advised by Prof. Zhong-Shuai Wu. Her research interests focus on bioinspired construction and application of 2D materials for energy-storage devices such as aluminum ion and Li-S batteries.

Zhong-Shuai Wu received his Ph.D. from the Institute for Metal Research, CAS in 2011, and worked as a postdoctoral fellow at the Max Planck Institute for Polymer Research in Mainz, Germany from 2011 to 2015. He then became a full Professor and Group Leader of 2D Materials & Energy Devices at DICP, CAS. In 2018, he was promoted to be a DICP Chair Professor. His research interest includes graphene and 2D materials, microscale electrochemical energy storage devices, supercapacitors, batteries, and catalysis.

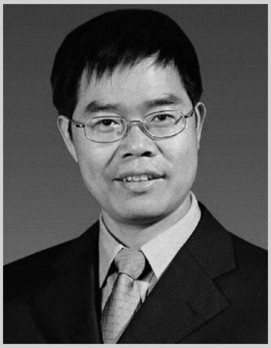

Hui-Ming Cheng received his Ph.D. in materials science from the Institute of Metal Research, CAS. He worked at AIST and Nagasaki University in Japan, and MIT in USA, in the 1990s. Currently he is a Professor and Director of the Advanced Carbon Research Division of Shenyang National Laboratory for Materials Science, IMR, CAS, and the Low Dimensional Material and Device Laboratory of the Tsinghua Berkeley Shenzhen Institute, Tsinghua University. His research focuses on carbon nanotubes, graphene, 2D materials, energy-storage materials, photocatalytic semiconducting materials, and bulk carbon materials.

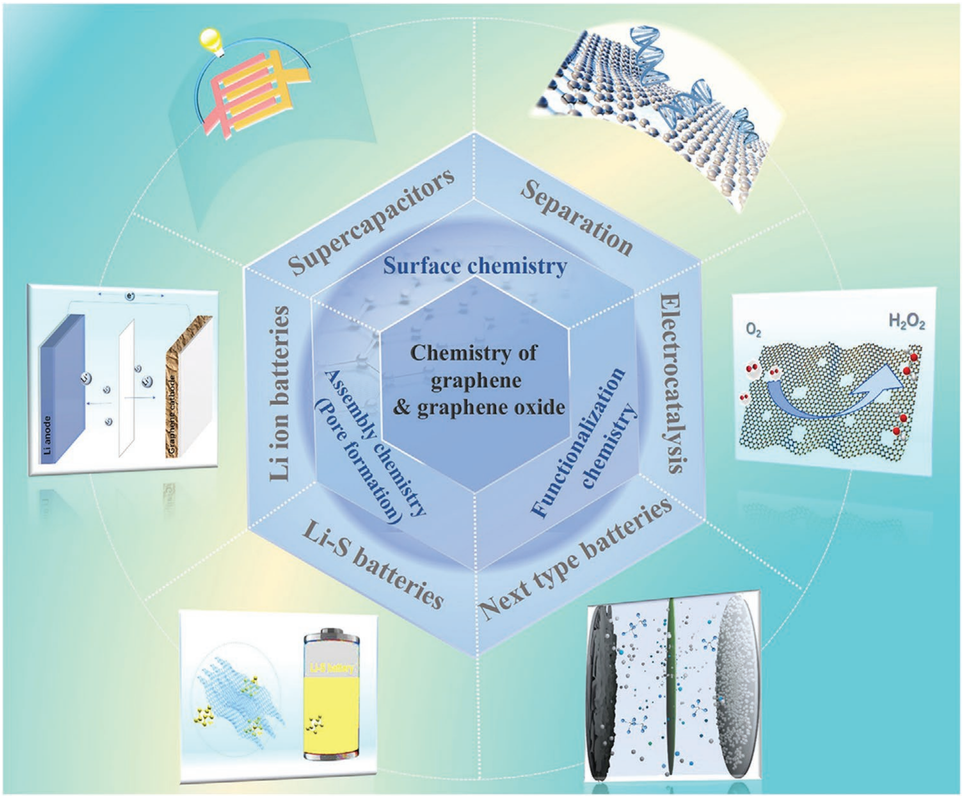

Figure 1. Schematic representing the chemistry of graphene and GO for specific applications.

electrocatalysis, and molecular separation with PGMs serving as key components will be analyzed and summarized. Finally, the unresolved challenges and future perspectives in this field will be considered to accelerate the development of PGMs for diverse functional applications and shed new light on their future directions.

2. Surface Chemistry of Graphene and GO

Since graphene's discovery,[42] chemically modified graphene (CMG) has been synthesized for various applications,[43,44] thus, illuminating different functional groups, especially, oxygen-containing functional groups (OCFGs) on the surface of GO. In addition, they also induce defect formation in the form of edges, doped- heteroatoms, other functional groups, and moieties.

2.1. Functional Groups

Graphene is a subset of graphite containing sp^2-hybridized carbon atoms positioned in a honeycomb lattice in two dimensions.[42,45,46] Each carbon atom contributes to the delocalized electron network by virtue of its π orbital. Ideally, graphene is pristine without any functional groups. As one of the graphene derivatives, GO can be described as functionalized graphene with many OCFGs like carbonyl, carboxyl, hydroxyl, epoxy groups attached to the edges and basal plane (**Figure 2**).[8,47,48]

Due to the presence of these OCFGs, GO exhibits lots of unique properties.[8,47,49,50] For example, unlike graphene, the highly negative charge on the surface of GO enables excellent colloidal dispersion in aqueous medium.[13,31] This allows the use of solution-based film fabrication protocols, such as self/co-assembly, vacuum filtration, drop casting, and spin-coating. Additionally, nanoscale wrinkles and defects manifest in the basal plane due to the amorphous region of graphene caused by various functional groups.[8,51] In addition, these OCFGs offer many reactive sites for all kinds of surface modification reactions, which is helpful for the development of a suite of functionalized GO-based membranes with remarkably improved performance.[52]

2.2. Defects

The main reason behind defect production is the reconstructions in the atomic network permitting a coherent defective lattice in the absence of other coordinated atoms. In addition, thanks to the adsorbed atoms, these reconstructed defects partially enhance the structural properties. Typically, defect on graphene manifest as point defects that are 0D vacancies and interstitial atoms, such as single defects,[53] Stone–Thrower–Wales defects,[54] and multiple defects.[55] Graphene edge may also be considered as a defect,[54,56,57]

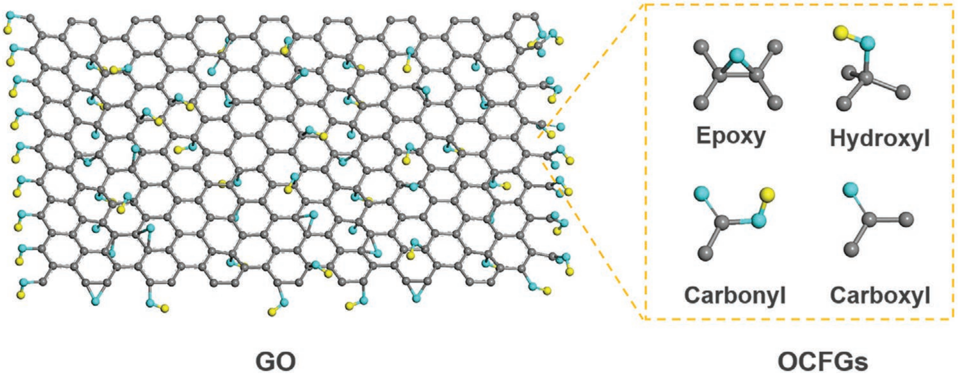

Figure 2. Schematics of the molecular structure of GO with four types of OCFGs.

and is discussed in details in the next subsection. There are three mechanisms causing defects in graphene: i) crystal growth,[58] ii) irradiation with energetic particles,[59–62] and iii) chemical treatment.[61]

The functionalized or defective graphene (DG) obtained by the above methods can significantly affect its electronic, magnetic, mechanical, and chemical properties. It is suggested from theoretical simulations that OCFGs and other functional groups could easily be connected with dangling bonds at a vacancy on graphene. Such reconstruction of defects can enhance local activity. From a theoretical point of view, the overlap of p-orbitals of graphene determines the electronic properties.[59] Therefore, the defects affect the electronic properties of graphene seriously.

2.3. Edge

Graphene edges have been explored extensively over the last few years, as a result of their unique electronic, chemical, and magnetic properties.[60–64] Graphene nanoribbons (GNRs) with narrow widths can generate crystallographic orientation of the edges. Defined by the orientation of the hexagons relative to the ribbon length, the achiral edges in GNRs can be divided into zigzag and armchair edges (**Figure 3**a–c).[60]

The structural features of GNRs are directly dependent on the various fabrication methods.[64] Significant efforts have been devoted to the large-scale production of GNRs with bottom-up and top-down approaches, such as chemical vapor deposition (CVD),[65] nanofabrication,[66–67] sonochemical method,[68] nanowire lithography,[69,70] cutting with a diamond knife,[71] nanoscale cutting of graphene using nickel nanoparticles,[72,73] and unzipping of carbon nanotubes (CNTs) (Figure 3d–f).[61,74–76] Among them, CVD offers a simple method for the fabrication of high-quality GNRs in a relatively short time.[65] CVD growth of ribbon-like filaments of graphite by the decomposition of a reactant gas containing $CO/H_2/Fe(CO)_5$ at 400–700 °C was first reported by Maeda's group.[77] Further, the modification in reactant gas/solution can yield different products.[78] For example, with ferrocene/tetrahydrofuran, iron-filled multiwall CNTs (MWCNTs) was produced while with ferrocene/ethanol/thiophene under the same heating condition of 950 °C, pure graphitic nanoribbons were yielded.[65] Overall, the CVD strategy provides an efficient method to synthesize high-quality GNRs with open edges.[79]

The alternative synthesis method for GNRs is the unzipping of CNTs along their longitudinal direction. Pioneered by Kosynkin et al.,[74] this method involves the unzipping of MWCNTs using chemical treatment with H_2SO_4 and $KMnO_4$. The resulting nanoribbons have the length of 4 µm, width of 100–500 nm, and 1–30 graphene layers. However, the use of strong oxidizing agents led to a significant decrease in electrical conductivity. Since then, many ingenious routes for obtaining purer and longer GNRs with fewer defects have been explored. It has been noted that the presence of a second acid ($C_2HF_3O_2$ or H_3PO_4) in addition to the previously discussed $H_2SO_4/KMnO_4$ mixture prevents the generation of vacancies in the GNRs due to diol group protection. Incredibly, this study resulted in long and narrow GNRs (>5 mm length, <100 nm width) with atomically sharp edges.[80] Intercalating CNTs with alkali-metal (Li) and ammonia as co-intercalants and their subsequent removal is yet another unzipping method.[76] In addition, transition metals can also be used to cut through graphene sheets, e.g., cutting MWCNTs into GNRs under a hydrogen flow by selectively etching with Ni nanoparticles.[72]

Apart from these chemical routes, some mechanical strategies also show promise for obtaining high purity GNRs. For example, it is known that oxygenation can create defects on the graphene basal plane. By extending this concept to MWCNTs, a mild gas-phase oxidation can allow oxygen to create "etch-pits" on their sidewalls, which when followed by a solution-phase sonication step facilitates the unzipping of MWCNTs to obtain GNRs with remarkably low I_D/I_G ratio, indicative of high-quality GNRs with excellent electrical conductivity and mobility.[79]

The fabrication of GNRs has made significant advances in the large-scale production of narrow ribbons and smooth edges in the last few years. Momentous progress has been reported in transmission electron microscopy (TEM) characterization of the atomic structure at graphene edges.[62,81,82] After exposure to electron beam irradiation for a long time, each graphene layer edge shows irregular structures (Figure 3g). The material receives significant resistive Joule heating when the voltage is across the surface of ribbon, which results in atomically discernible armchair edges, smooth zigzag, and edge junctions (Figure 3h,i).

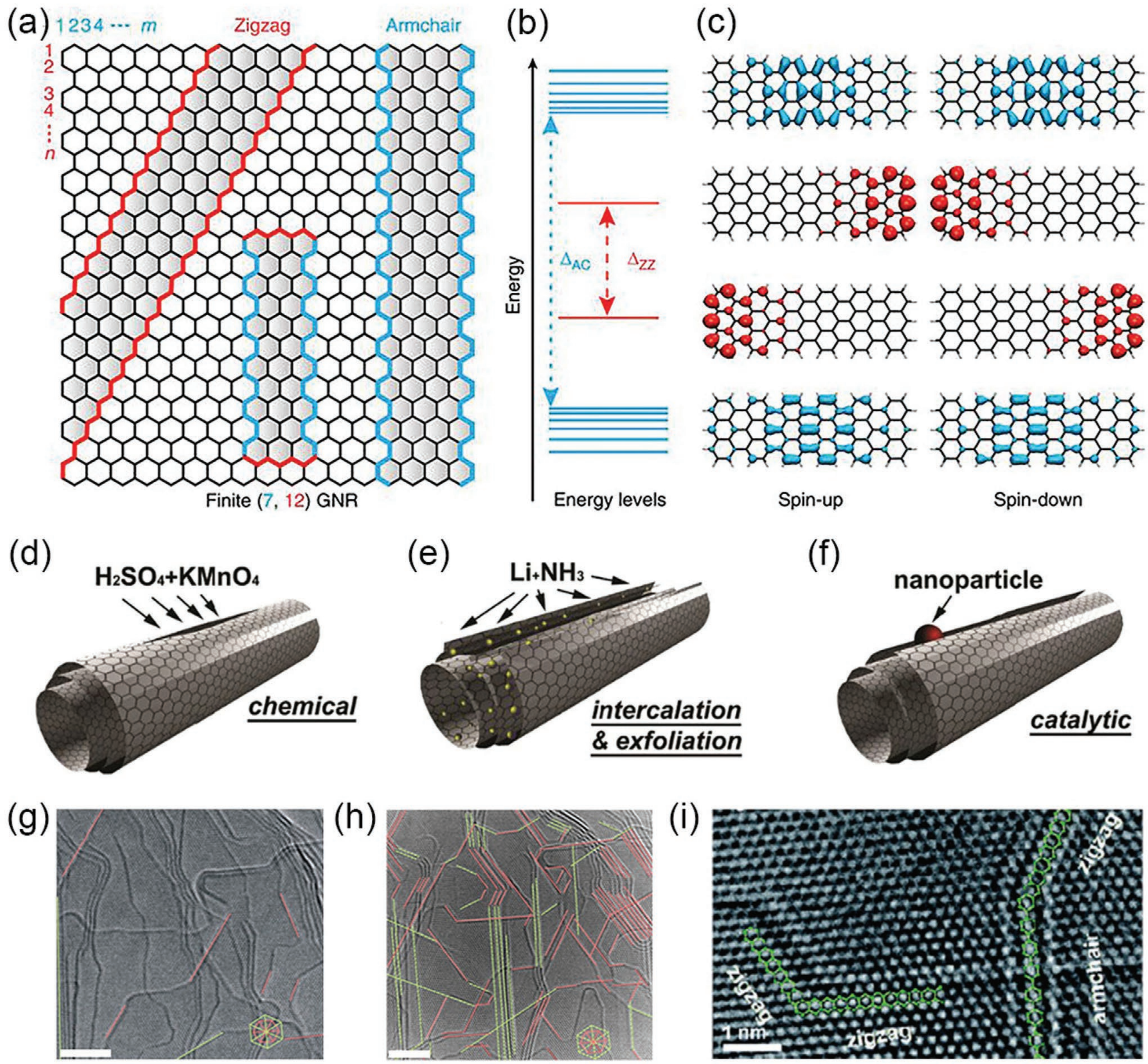

Figure 3. a) Zigzag and armchair edges in monolayer GNRs. b) Energy levels. c) Kohn–Sham spin-orbitals of edge-localized states and the energetically closest bulk states. a–c) Reproduced with permission.[60] Copyright 2016, Nature Publishing Group. d–f) Schematic showing the method used for unzipping doped nanotubes to form GNRs: d) chemical route, e) intercalation–exfoliation of MWCNTs, f) catalytic approach. d–f) Reproduced with permission.[61] Copyright 2010, American Chemical Society. g) TEM image showing irregular edges and h) zigzag and armchair edges. i) High-resolution TEM (HRTEM) image showing well-defined zigzag and armchair edges. g–i) Reproduced with permission.[62] Copyright 2009, the American Association for the Advancement of Science.

3. Different Pore Structures and Tailoring Approaches

3.1. In-Plane PG

The term "in-plane PG" refers to graphene sheets with in-plane nanopores. Two main techniques are used to generate monolayer PG nanosheets. One is bottom-up synthesis with organic molecular precursors and/or pore templates,[83–85] and the other is a top-down approach by defect generation in the graphene.[86–91] In general, such porous nanosheets are ultrathin and have large SSA, controlled pore size, and high electrical conductivity, exhibiting enormous potential for applications in molecular separation, sensing, catalysis, energy storage, and conversion.[92,93]

Bottom-up synthesis is essential for the formation of PG with strong crystallinity and well-defined pore structure.[84] The regular 2D polyphenylene network (i.e., graphene with single-atom wide pores) was first fabricated by Bieri and co-workers (**Figure 4**a).[83] The formation mechanism of this

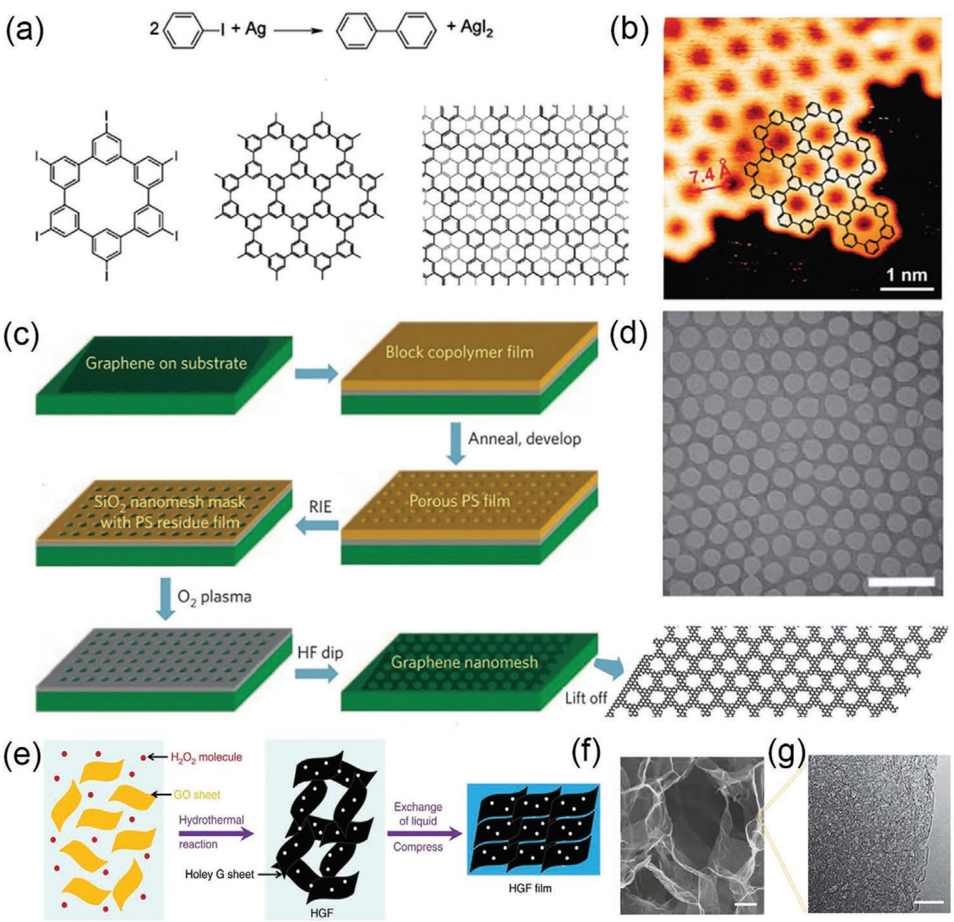

Figure 4. a) Bottom-up organic synthesis of PG by a surface-promoted aryl–aryl coupling reaction (top) and the three PG structures obtained (bottom): a cyclohexa-m-phenylene (CHP) structure, a polyphenylene super-honeycomb network, and a polyphenylene superhoneycomb network, from left to right. b) STM image of an edge of the polyphenylene superhoneycomb network. a,b) Reproduced with permission.[83] Copyright 2009, Royal Society of Chemistry. c) Schematic of the preparation of graphene nanomesh. d) TEM image of graphene nanomesh. c,d) Reproduced with permission.[94] Copyright 2010, Nature Publishing Group. e) Schematic of the preparation process of HGFs and HGF films. f) SEM image of HGF. g) TEM image of holey graphene in HGFs (scale bars: f) 1 µm, g) 10 nm). e–g) Reproduced with permission.[95] Copyright 2014, Nature Publishing Group.

2D polymer network was originated from Ag (111)-induced surface aryl–aryl coupling, which then conjugated to the hexaiodo-substituted macrocycle cyclohexa-m-phenylene completely. The high-resolution scanning tunneling microscope (STM) image showed an edge of the polyphenylene superhoneycomb network with uniform pore spacing of 7.4 Å, demonstrating that nanoporous graphene materials could be precisely prepared by proper molecular design (Figure 4b). Various other methods for creating in-plane pores in monolayer graphene, such as oxidative etching,[89] electron or ion beam irradiation,[90,96] oxygen plasma etching,[88] and chemical agents[86,94,97–101] have been explored to obtain monolayer PG.[84,92,102] For instance, the in-plane pores (≈3.5 nm) can be generated in suspended graphene sheets by the controlled exposure to focused electron beam irradiation.[86] Nevertheless, this method is not suitable for large-scale manufacture of PG with large pore size distribution. Meanwhile, chemical methods have also been explored.[87] Duan's group reported a PG nanomesh produced using block copolymer lithography (Figure 4c).[94] Specifically, as the protecting layer, a silicon oxide film was first covered onto graphene, and a poly(styreneblock-methyl methacrylate) (PS-*b*-MMA) block copolymer thin film was then fabricated as the etching template. Afterwards, CHF_3 oxygen plasma etching and plasma-based reactive ion etching were used to generate holes in the monolayer graphene. TEM studies clearly showed the well-arranged nanohole structure with an average neck width of 7.1 nm (Figure 4d). Such graphene nanomesh-based room-temperature transistors could drive nearly 100 times larger currents with a comparable on–off ratio tuned by varying the width of individual GNRs. However, the use of a toxic gas (CHF_3), high cost, and inefficient production are detrimental to the acceptance of this strategy.

Chemical activation is another top-down approach for introducing in-plane pores in graphene. In 2011, a simple KOH activation method to prepare PG with a large number of in-plane micropores and mesopores was reported by Ruoff's group.[99] The activated microwave-exfoliated GO (a-MEGO) showed abundant micropores and mesopores with a size distribution between 1 and 10 nm, and had ultra-high SSA of up to

3100 m^2 g^{-1}, and high electrical conductivity. 3D holey graphene framework (HGF) with hierarchically porous structure was prepared by the low temperature etching of graphene to create nanopores and subsequently self-assembling into the 3D network (Figure 4e).[95] During the hydrothermal process, H_2O_2 molecules can partially oxidize to etch the carbon atoms around the more active defective sites of GO, leaving behind carbon vacancies to create the nanopores. The pore sizes of 3D HGFs include sub- and several micrometers with one- or few-layers graphene as pore walls (Figure 4f,g). The hierarchical porous structure ensures efficient ion diffusion to allow the production of HGF-based supercapacitors with both high volumetric and gravimetric energy densities. In addition, Zhou et al. demonstrated a general and scalable synthesis approach for PG by the carbothermal reaction between graphene and metal oxide nanoparticles.[103] On the surface of GO nanosheets, oxometalates (OM) or polyoxometalates (POM) were thermally decomposed into metal oxide nanoparticles in which the neighboring carbon atoms in graphene layer were oxidized to carbon dioxide or carbon monoxide. Consequently, abundant pores or defects were generated on graphene to obtain PG by a thermal reaction. Using K_2TiO_3, uniform nanopores of 1–10 nm size were observed. It is suggested that the top-down approaches for obtaining mesoporous graphene can be fast, low cost, and have a high yield.

In monolayer PG, a bottom-up synthesis strategy can precisely control the pore structure and morphology, but is time-consuming and suffers from complicated protocols. For the top-down techniques, photo-, electron-, and plasma-etching have been used for the preparation of PG films.[89,93–96,102] Chemical etching is a relatively cost-effective and simple process for the large-scale fabrication of PG, but the defects introduced eventually affect the conductivity and mechanical properties.[104]

3.2. 2D Laminar PG

Besides monolayer PG,[105] producing 2D laminar sandwich-like PG hybrids by the direct loading of porous functionalized moieties onto graphene has been demonstrated as an efficient strategy to prevent the restacking.[106–108] So far, 2D porous polymers, metal oxides, silica, and carbon-based nanohybrids have been reported widely.[109–112] These hybrids were prepared based on the interaction forces between graphene and other precursors, without the assistance of a template. Zhuang et al. fabricated a simple catalyst-free and graphene-inspired strategy for the large-scale synthesis of Schiff-base-type porous polymer[109] nanosheets displaying high nitrogen content of 43.9 wt%, and single-sheet porous structure. Furthermore, they could serve as robust precursors for the formation of heteroatom-doped porous carbon nanosheets by template-free pyrolysis. As another example, Tong et al. prepared uniform sandwich-like mesoporous Nb_2O_5/graphene/mesoporous Nb_2O_5 nanosheets using a two-step hydrolysis approach to produce high-rate and high-capacity sodium ion batteries.[113] Specifically, the mesopores were constructed by several nanometer-sized Nb_2O_5 particles on graphene. Because of its uniform 2D feature, large SSA, and highly mesoporous structure, electrodes fabricated from these nanosheets displayed excellent electrochemical performance.

The creation of PG hybrids with well-defined porous structures is very important in specific applications.[92] In general, 2D-ordered PG hybrid nanosheets are obtained by the decoration of functional components on graphene with soft- and hard-templates.[92] For example, 2D sandwich-like graphene-based mesoporous silica (GM-silica) sheets have been fabricated with cetyltrimethylammonium bromide as soft template (**Figure 5**a).[107] After annealing, 2D sandwich-like GO-based mesoporous silica (GOM-silica) nanosheets were reduced to GM-silica, showing a free-standing nanosheet morphology.

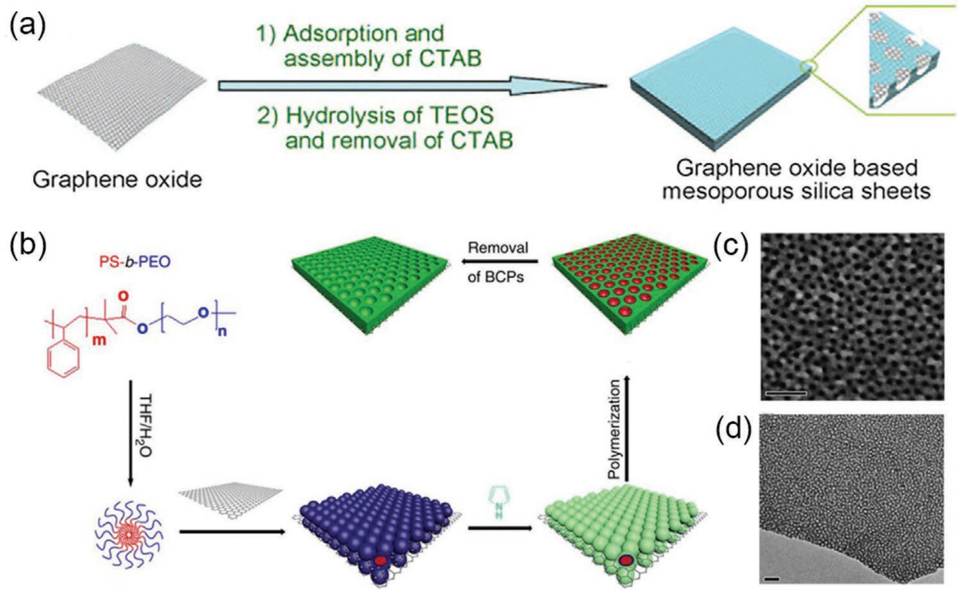

Figure 5. a) Schematic of the fabrication of GOM–silica nanosheets. Reproduced with permission.[107] Copyright 2010, WILEY-VCH. b) Schematic of the fabrication, c) SEM, and d) TEM images of mPPy@GO nanosheets. b–d) Reproduced with permission.[114] Copyright 2015, Nature Publishing Group.

It is worth noting that the GM-silica nanosheets could serve as a hard template for generating graphene-based mesoporous carbon (GM-C), with well-organized mesopores with the size of ≈2 nm. Beside this, patterning 2D free-standing surfaces (e.g., graphene) with mesoporous conducting polymers, such as polypyrrole and polyaniline is a versatile route to develop 2D PG hybrid nanosheets.[114–116] In a typical fabrication, spherical micelles of the block copolymer polystyrene-*b*-poly(ethylene oxide) were used as a soft template for polymerizing the polypyrrole on the GO surface to produce mesoporous GO-based polypyrrole (mPPy@GO) and GO-based polyaniline (mPANi@GO) nanosheets (Figure 5b). Notably, mPPy@GO nanosheets had a 2D free-standing morphology, tunable pore sizes ranging from 5 to 20 nm (Figure 5c,d), an adjustable thickness of 35–45 nm, and large SSA of 85 $m^2 g^{-1}$. Such a novel structure of 2D mPPy@GO nanosheets delivered excellent capacitance and rate performance as electrodes of supercapacitors and micro-supercapacitors (MSCs).

To summarize, 2D laminar PG hybrids with disordered or ordered pores couple the merits of graphene and porous functional materials while eliminating their individual drawbacks. They not only have the morphological characteristic of 2D graphene and a micro-/mesoporous structure, but also show excellent properties such as large SSA, ultrathin thickness, and impressive electrical conductivity, making them useful in medicine, biology, catalysis, environmental protection, energy storage, and energy conversion.

3.3. 3D Interconnected PG

3.3.1. Hydrothermal/Solvothermal Assembly

3D PG can not oly provide continuously interconnected 3D structures with a large surface area, low weight density, and high conductivity,[117–120] but also is a good support for loading metals and metal oxides. Wu et al. reported a 3D N-doped graphene aerogel (N-GA)-supported Fe_3O_4 nanoparticle (Fe_3O_4/N-GA) material as an efficient catalyst for the oxygen reduction reaction (ORR, **Figure 6**a).[117] Scanning electron microscopy (SEM) revealed an efficient assembly between graphene nanosheets and Fe_3O_4 NPs, in which a 3D interconnected PG framework with continuous macropores was observed. Soon after, Xu et al. reported the preparation of graphene/$Ni(OH)_2$ hydrogels by using a one-step hydrothermal approach[121] suggesting that a hydrothermal process which induced the 3D self-assembly of graphene with a porous structure by noncovalent driving forces may promote uniform chemical doping and in situ growth of metal oxide/hydroxide moieties on 3D graphene framework. Using hydrothermal and solvothermal reduction,[122] a series of heteroatom-doped graphene graphene/CNTs,[123,124] graphene/polymers,[125,126] hydrogels/aerogels,[127,128] graphene/metal oxide and sulfide[129,130] composite, and hydrogels/aerogels graphene/metal nanoparticles[131,133] have been explored, which greatly expand the diversity and functions of 3D PG. Particularly interesting is the fact that, simple solvothermal treatment of an amphiphilic GO and activated carbon particles dispersion can be employed to prepare graphene/activated carbon organogels.[134] Therefore, the solvothermal and hydrothermal reduction strategies are simple and effective routes to directly assemble 3D graphene networks by involving neither extra chemicals nor post treatment.

3.3.2. Chemical Reduction

The chemical reduction of GO is another efficient method for the assembly of 3D graphene networks by the major driving forces of hydrogen bonds and π–π stacking interactions, using reducing agents, e.g., L-ascorbic acid, hydrogen iodide, hydroquinone, sodium hydrogen sulfite, and sodium sulfide.[135–138] Chemical reduction can be accomplished under lower temperature and shorter hours compared to hydrothermal reduction.[139] Owing to the restoration of the π-conjugation and a more complete reduction, PG obtained by chemical reduction has higher electrical conductivity than those produced by hydrothermal reduction. In addition, the macroporous graphene hybrids constructed by this method can maintain high flexibility very well after the self-assembly.[140]

In addition to the chemical routes, 3D self-assembled graphene framework can be obtained by an electrochemical deposition–reduction strategy (Figure 6b).[118,141] The as-prepared PG hydrogels, consisting of perpendicularly aligned graphene strongly bonded to the electrode, are not only electrically conductive but also accessible to electrolyte ions serving as a new electrode for the further electrodeposition of secondary functional components.

3.3.3. Hard Template Method

In addition to the two above methods, template-induced CVD has emerged as a promising strategy to produce a 3D interconnected flexible porous network of high-quality graphene, using porous nickel foam as a sacrificial template, with methane or ethanol as the carbon source. Chen et al. fabricated a typical 3D graphene foam (GF) by using porous nickel (Ni) foam as a template for the CVD growth of graphene from CH_4 at 1000 °C under ambient pressure (Figure 6c).[119] The GF inherited the interconnected 3D scaffold of the Ni foam template with a high porosity and only few-layer graphene on the walls of the foam. Such unique GFs have enormous potential for use as foldable, flexible, and stretchable conductors and energy storage devices.

Colloidal synthesis is another template method for the preparation of 3D interconnected PGMs.[18,142] 3D self-supported interconnected graphene framework was prepared by vacuum filtration and post-treatment method with CMG and a self-assembled polystyrene sphere (PS) (Figure 6d).[18] Compared to the CVD template method, this PS-template synthesis can easily control the pore diameter of the obtained graphene framework by adjusting the size of PS. Moreover, the obtained 3D macroporous CMG films provide rapid paths for electronic and ionic transport, thus providing ample potential for energy storage and conversion applications.

3.3.4. Laser-Induced Reduction

Since 1994, laser has been widely applied for producing micron-sized features and 3D microdevices by exploiting localized

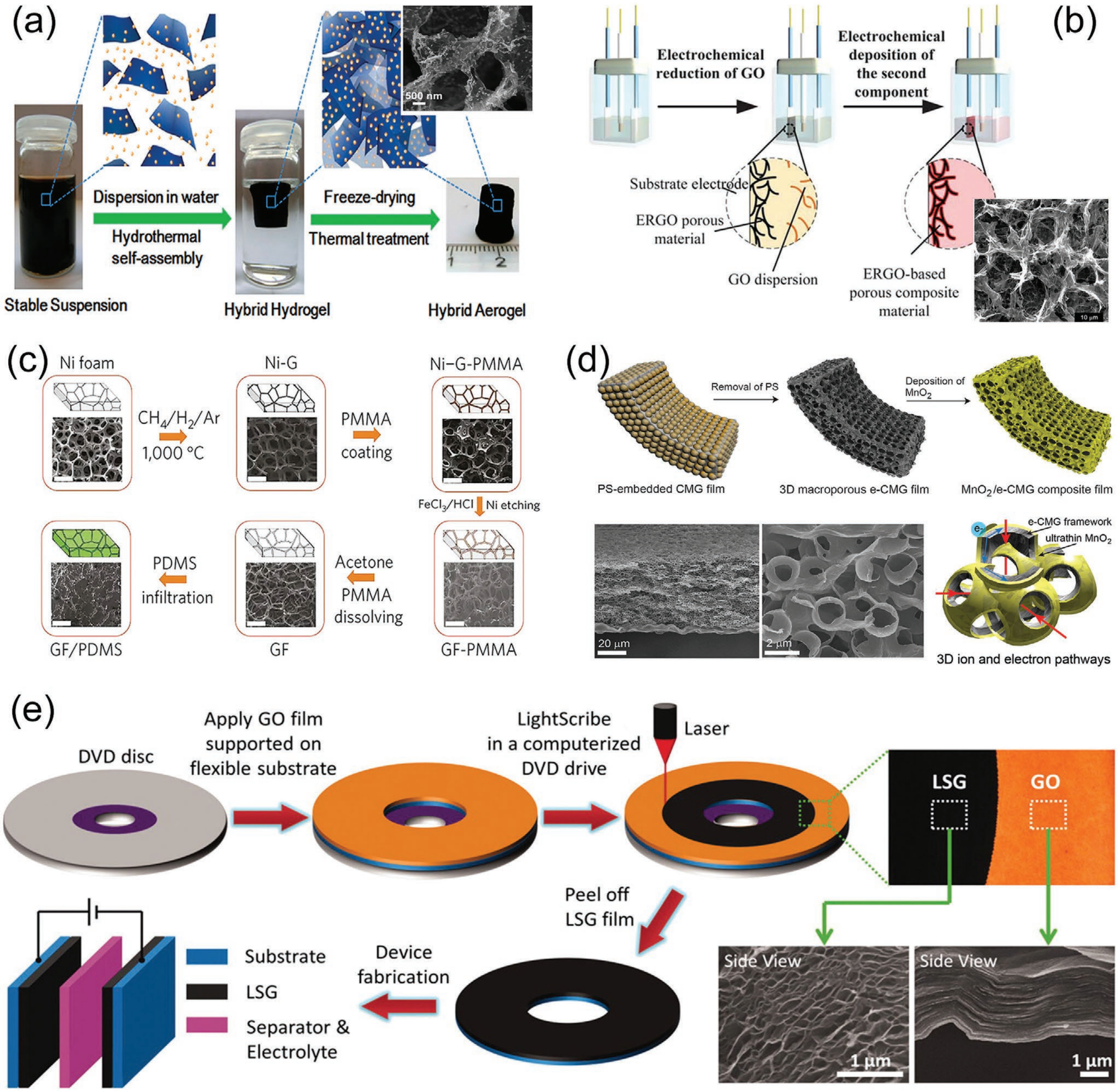

Figure 6. a) Fabrication process for 3D Fe_3O_4/N-GAs catalyst. Inset: SEM image of 3D macroporous-structured Fe_3O_4/N-GA. Reproduced with permission.[117] Copyright 2012, American Chemical Society. b) Diagrammatic of the preparation method for ERGO-based composite materials. Inset: SEM image of ERGO on copper foil. Reproduced with permission.[118] Copyright 2012, Royal Society of Chemistry. c) Synthesis of 3D GF and integration with PDMS. Reproduced with permission.[119] Copyright 2011, Nature Publishing Group. d) Schematic of the procedure to fabricate 3D macroporous MnO_2/e-CMG film. Inset: SEM images of the e-CMG film, and 3D ionic and electronic transport paths in the MnO_2/e-CMG electrode. Reproduced with permission.[18] Copyright 2012, American Chemical Society. e) Schematic showing the fabrication process of LSG-based supercapacitors. Reproduced with permission.[120] Copyright 2012, American Association for the Advancement of Science.

heating.[143] Later, laser-reduction became a straightforward, scalable patterning approach for producing graphene-based nanomaterials.[144] The structure of a laser-induced PG can be designed and altered by adjusting the laser energy and substrate material. LightScribe DVD optical drive has been used to produce the direct laser reduction of GO to graphene patterns by El Kady and co-workers (Figure 6e).[120] GO film was converted into a laser-scribed graphene (LSG) film by laser beam reduction, in which the gas produced by laser reduction generated 3D porous nanostructures with large accessible SSA (1520 $m^2\ g^{-1}$). Further, a one-step scalable approach using CO_2 laser irradiation of commercial insulating polyimide under ambient conditions was developed for the preparation of a PG film,[145] which is promising for use in microscale energy storage devices. Very recently, Wu's group demonstrated the fast and simplified production of integrated MSCs based on laser-induced graphene films with 3D interconnected porous network, large SSA (203 m^2 g^{-1}), and high electrical conductivity (8.5 S cm^{-1}).[146] Importantly, the obtained all-solid-state planar-integrated MSCs showed high capacitance and outstanding rate capability, indicative of great potential as on-chip power sources for miniaturized electronics.

3.4. Hierarchically PG (HPG)

Owing to their diversity and enhanced performance, HPG with two or three type pores have attracted considerable attentions. So far, several key approaches for fabricating of HPGs with bimodal porous structures have been developed, including assembly and post-treatment,[147] colloidal crystal templating,[24] freeze drying,[148] supercritical fluid,[149] and hydrothermal method.[150] Besides, HPGs can be synthesized by altering the chemical and physical parameters of phase separation, templating replication, and post-treatment.[151] Importantly, HPG can efficiently combine the structural advantages of each individual porous structure, showing large accessible space, low mass density, high SSA, variable chemical compositions, and interconnected hierarchical porosity. Therefore, the HPG materials are benefit benefical for large ion storage, fast ion diffusion, and rapid electron transportation, endowing them with technological importance in energy storage and conversion, catalysis, and separation. For instance, Xiao et al., reported hierarchically porous air electrodes with functionalized graphene sheets that contain lattice defects and hydroxyl, epoxy, and carboxyl groups by a colloidal microemulsion approach.[24] The resultant 3D air electrodes were consisted of interconnected hierarchical porous structure of both micropore and mesopores, which were more suitable for Li-O_2 battery in comparison with 2D layered structure. In order to meet the practical demand of flexible supercapacitors for high mechanical strength and porous structure, Wang's group developed the flexible graphene films with interconnected mesopore and macropore structures through post-reduction of a blade-cast GO hydrogel.[147] The as-prepared PG film prossessed high strength, superior toughness, large SSA, and high electrical conductivity, making them one very promising electrode candidate for high-performance flexible supercapacitors. Further, Chen and Qiao demonstrated a 3D oxygen evolution reaction (OER) catalyst with hierarchical pores for water splitting.[152] Benefiting from the unique in- and out-plane pores structure, 3D conductive network, and N-doped graphene, the OER catalytic activity was remarkably promoted, which was well comparable to those of some noble metal catalysts, e.g., IrO_2.

4. Functionalization Chemistry of PG

Even though graphene's astounding properties are suitable for different purposes, there may be some challenges like dispersion in a particular medium, a low intrinsic limit on certain properties or difficulties in processing that restrict their universal application. Such shortcomings can be overcome by the chemical functionalization of graphene or GO. There are two ways of functionalizing graphene, including noncovalent interactions and covalent bonds.

4.1. Covalent Functionalization

The purpose of covalent modification of graphene is converting sp^2 carbons to sp^3, which has a preferential tetrahedral geometry with longer bonds.[153] This transformation affects the sp^3 carbons directly while creating a geometric distortion that extends over several lattice positions. Compared to graphene, the covalent functionalization of GO imposes fewer restrictions on the delocalized π network,[8] because it contains OCFGs, including epoxy, hydroxyl, carbonyl, and carboxyl functional groups.[47] Thanks to the presence of the oxygen groups on the surface, GO can often be the raw material for the formation of PG and PG derivatives through the covalent attachment of organic groups to its surface. As a typical study, in situ lithiation synthesis of a nanosize lithium sulfide/graphene aerogel with C—O—S bond interaction efficiently suppresses the shuttling of polysulfides in Li-S batteries.[154]

4.2. Noncovalent Functionalization

Noncovalent functionalization exists in all types of materials, and is critically important for determining the materials' structure, stability, and function. Compared to covalent functionalization, some notable characteristics of noncovalent functionalization are as follows: i) noncovalent functionalization is largely preferred to functionalize graphene and GO because although it introduces new chemical groups, the electronic properties and structure of graphene can still be preserved while dispersibility, reactivity, binding capacity, or other properties can be tuned; ii) the treatment methods offer high flexibility, due to the mild and nonpermanent character of noncovalent interactions; iii) the total energies of noncovalent interaction can rival some covalent bonds.[153,155]

On the basis of driving force, the common styles of noncovalent functionalization can be divided into ion interactions, van der Waals forces, π–π effect, and hydrogen bonding.[155] Among these, it can achieve the noncovalent-functionalized graphene and GO by relying on π–π interactions and van der Waals forces with some polymers and organic molecules. Hydrogen bonds and ionic interactions often occur at the edges and the surface of GO with abundant OCFGs, which does not occur in pristine graphene.

4.2.1. π–π Stacking Interactions

The π–π stacking interaction as a noncovalent interaction plays an important role in graphene's surface chemistry.[156–158] It refers to the weak interactions that often occur between electron-poor and electron-rich regions. It is commonly seen that π–π interactions are mainly divided into two types: a) face-to-face stacking, and b) CH$\cdots\pi$ edge-to-face stacking. The interactions occurring between small molecules are used to functionalize GO and graphene for further processing and property modification on both sides of graphene. Because of the defects and OCFG on the surface of GO or rGO, there are also both acceptor moieties and hydrogen-bond donors from OCFGs that contribute an additional interaction mode. With an increase in degree of reduction of GO, most OCFGs on the basal plane can be removed, leading to a material with an edge-dominant oxygen moiety. The π–π interactions have two major necessary conditions, one is the existence of π systems, and the other is the geometry of the interacting species. Conjugated molecules with abundant double carbon bonds have been applied to construct high-performance graphene-based composites by cross-linking adjacent graphene nanosheets with π–π interactions.[155] Xiao et al. reported that the plane-to-plane conductivity of layer-by-layer stacked CVD graphene films could be increased by insertion of 1-pyrenebutyric acid *N*-hydroxysuccinimide ester into the graphene interlayer.[159] However, other small pyrene derivatives with pendant groups are able to undergo intermolecular bonding and are prone to aggregation through π–π interaction during the formation of graphene-based composites, resulting in low electrical conductivity.[155]

4.2.2. Van der Waals Interactions, Ionic Interactions, and Hydrogen Bonding

Hydrophobic property of graphene promotes its interactions with hydrophobic or partially hydrophobic organic molecules, which are helpful for the dispersion of graphene nanosheets in both aqueous and organic media, as well as the incorporation in polymers. Due to the partial reduction of OCFGs in rGO, hydrophobic interactions also appear in rGO, which is more hydrophobic than oxygen-enriched GO and much closer to graphene's aromatic character. These surface functional groups and the hydrophilicity of GO, and hydrophobic properties of graphene and rGO play an important role in ionic interactions or hydrogen bonds with the analogous ionic parts of molecules or macromolecules.[8] For instance, in a typical hydrothermal method for producing 3D PG structures, strong cross-links of 3D graphene network were formed through π–π stacking, hydrogen bonds, and van der Waals interaction between the partially reduced and functionalized graphene.[136]

4.3. Chemical Doping

Chemical doping is a proven method for adjusting the electrical properties of pristine graphene by controlled doping with electrons and holes, when pristine graphene is unstable in the surrounding environment. The mechanisms of chemical doping in graphene can take two routes: electrical doping (induced by gate voltage)[42,160] and chemical doping (induced by chemical species).[161]

4.3.1. Surface Transfer Doping

Surface transfer doping is achieved by electron exchange between a semiconductor and adsorbed dopants on its surface.[162] It does not disrupt the graphene structure, and most cases of chemical doping are reversible. As a result of chemical doping, graphene can be divided into n-type or p-type.[163,164] Generally, molecules with electron withdrawing nature induce p-type doping on graphene upon adsorption, while donating groups confer n-type doping. The differences between graphene with n- and p-type doping are summarized below. First, p- and n-type doping drives the Dirac point of graphene above and below the Fermi level, respectively. Second, p-type doping is accomplished by adding less than four valence electron atoms, while n-type doping is achieved by adding more than four valence electrons atoms. Third, n-type doping of graphene results in a stiffening of G band (demarcated by a downshift) while p-type doping leads to softening (demarcated by upshift). Correspondingly, the resistivity of p-type (n-type)-doped graphene shifts toward positive (negative) gate voltage compared to Dirac point of pristine graphene.[165]

4.3.2. Substitutional Doping

Different from surface doping, substitutional doping is the substitution of carbon atoms in the graphene honeycomb lattice by different number of valence-electrons atom, which results in the disruption of sp^2 bonding-atoms and involuntary doping.[15] Substitution doping can also be divided into p- and n-type doping. Compared to a carbon atom, a nitrogen atom has an additional electron, and serves as an electron donor for the n-type doping of graphene, while boron has one less electron and acts as an electron acceptor producing p-type doping.[166]

4.3.3. Synthesis of Doped Graphene

Heteroatom-doped graphene is obtained by two different strategies: direct synthesis and post treatment, with the former producing more homogenous doping than the latter. In most cases, the latter leads to surface doping only. Generally, direct synthesis is achieved by CVD, solvothermal, segregation growth, and arc-discharge approaches,[167] while post treatment follows N_2H_4 treatment, and plasma treatment, thermal treatment. A summary of the various approaches used to synthesize heteroatom-doped graphene is given in **Table 1**.

A typical example of n-type doping is the synthesis of N-doped graphene sheet using CVD with NH_3 as the nitrogen source.[168] As shown in **Figure 7**, X-ray photoelectron spectroscopy (XPS) showed that N bonding was incorporated in the forms of "pyrolic", "pyridinic", and "graphitic". Similar to n-type-doped semiconductors, N-doped graphene has a low conductivity, low mobility (200–450 $cm^2\ V^{-1}s^{-1}$), and large on/off current ratio.

High temperature annealing with nitrogenous organic compounds or ammonia as the nitrogen source is a general and efficient method of obtaining N-doped graphene.[174,175,187,190] Taking advantage of their hydrogel behavior together with the mechanical stability of GO sheets, an interconnected macroporous nitrogen-doped freestanding film was constructed (**Figure 8**a).[190] The doping process and reduction of graphene can be accomplished simultaneously, Wu et al.

Table 1. Summary of heteroatom doping on graphene.

Heteroatom species	Synthesis methods	Precursors	Applications	Refs.
Nitrogen	CVD	CH_4/NH_3	FET	[168]
Nitrogen	CVD	NH_3/He	ORR	[169]
Nitrogen	CVD	$NH_3/CH_4/H_2$/Ar	ORR	[170]
Nitrogen	CVD	Acetonitrile	Li ion battery	[171]
Nitrogen	CVD	Pyridine	FET	[172]
Nitrogen	Arc discharge	NH_3 (50%, v/v)	–	[173]
Nitrogen	Thermal treatment	Melamine, formaldehyde		[174]
Nitrogen	Thermal treatment	H_2/Ar	ORR	[175]
Nitrogen	Thermal treatment	Melamine, g-C_3N_4	ORR	[176]
Nitrogen	Plasma	GO, N_2 plasma	Ultracapacitors	[177]
Nitrogen	Plasma	Exfoliated graphite oxide, N_2 plasma	fuel cells	[178]
Nitrogen	Plasma	Graphite oxide, N_2 plasma	Three electrode cell	[179]
Nitrogen	Plasma	Graphite oxide, N_2 plasma	Biosensor	[180]
Nitrogen	N_2H_4 treatment	GO, N_2H_4, NH_3	–	[181]
Nitrogen	N_2H_4 treatment	Exfoliated graphite oxide, N_2H_4	Electrochemical biosensor	[182]
Boron	Thermal treatment	B_2O_3	ORR	[183]
Boron	Thermal treatment	BBr_3	Solar cells	[184]
Boron	Laser	H_3BO_3	Micro supercapacitor	[185]
Boron	CVD	H_2/phenylboronic acid	–	[186]
Nitrogen and boron	Thermal treatment	NH_3/Ar, BCl_3/Ar	Li ion battery	[187]
Nitrogen and boron	Thermal treatment	$C_2H_2N_4$, H_3BO_3	Supercapacitor	[188]
Nitrogen and boron	Arc discharge	B_2H_6	–	[189]

prepared heteroatom (N, B)-doped chemically derived graphene in one step (Figure 8b,c).[187] The oxygen atomic percentage was significantly reduced from 8.55% for the pristine graphene to 3.13% for the N-doped graphene and 6.06% for the B-doped graphene, due to the formation of C—N and C—B bonds by the reaction of OCFG with NH_3 and BCl_3. Importantly, these heteroatom-doped graphene have extremely high rate and large capacity for lithium ion batteries for the following reasons. First, the electrochemical activity and electrical conductivity of graphene in electrochemical process can be simultaneously increased by N or B doping. Second, doped graphene has higher thermal stability than pristine graphene due to the simultaneous reduction and doping process. Third, the increased disorder of surface morphology caused by doping also plays a significant role in improving the electrochemical properties.[170,171] Other heteroatom co-doped PG-based materials have also shown improved electrochemical performance compared to nondoped graphene. For example, a 3D N, S co-doped rGO/carbonized cellulose paper with many nanosize holes used as the interlayer in Li-S batteries, achieved wonderful permselectivity for effective intercepted polysulfides and Li ions, delivering high areal capacity and significant cycling stability (Figure 8d).[191] A nitrogen and iodine co-doped PG with a well-defined microstructure was fabricated by a hydrothermal self-assembly strategy followed by heat treatment at 900 °C (Figure 8e).[192] Compared to un-doped, nitrogen-, or iodine-monodoped PG, the co-doped material showed higher activity for the OER and ORR.

5. Promising Applications of PG

By virtue of the different advantages discussed above in terms of mechanical, electrical, and chemical properties, PGMs have enabled unprecedented advances in terms of device performance in various sectors.[193] As mentioned in previous sections, these improvements are mainly attributed to the combined effects of surface chemistry, dynamic chemistry, and electron-transfer chemistry of functionalized PG. Such effects allow us to chemically tune and precisely functionalize the features that are useful for certain structure-determined performance applications. In the following section, we shall give a concise account of the most attractive progress on chemically functionalized PG-based materials for the key applications such as supercapacitors, Li ion batteries, Li metal/sulfur batteries, next-generation batteries, electrocatalysis, and molecular separation, and attempt to fully analyze and comprehensively understand the inherent relationships between functional chemistry-related materials parameters (e.g., pore structures, morphology, components) of PG and the performance of these devices.

5.1. Supercapacitors

As an important and promising electrochemical energy storage device, supercapacitors have the distinct attributes of a short charge/discharge time, long cycle life, high power density, and environmental friendliness.[194] According to the energy

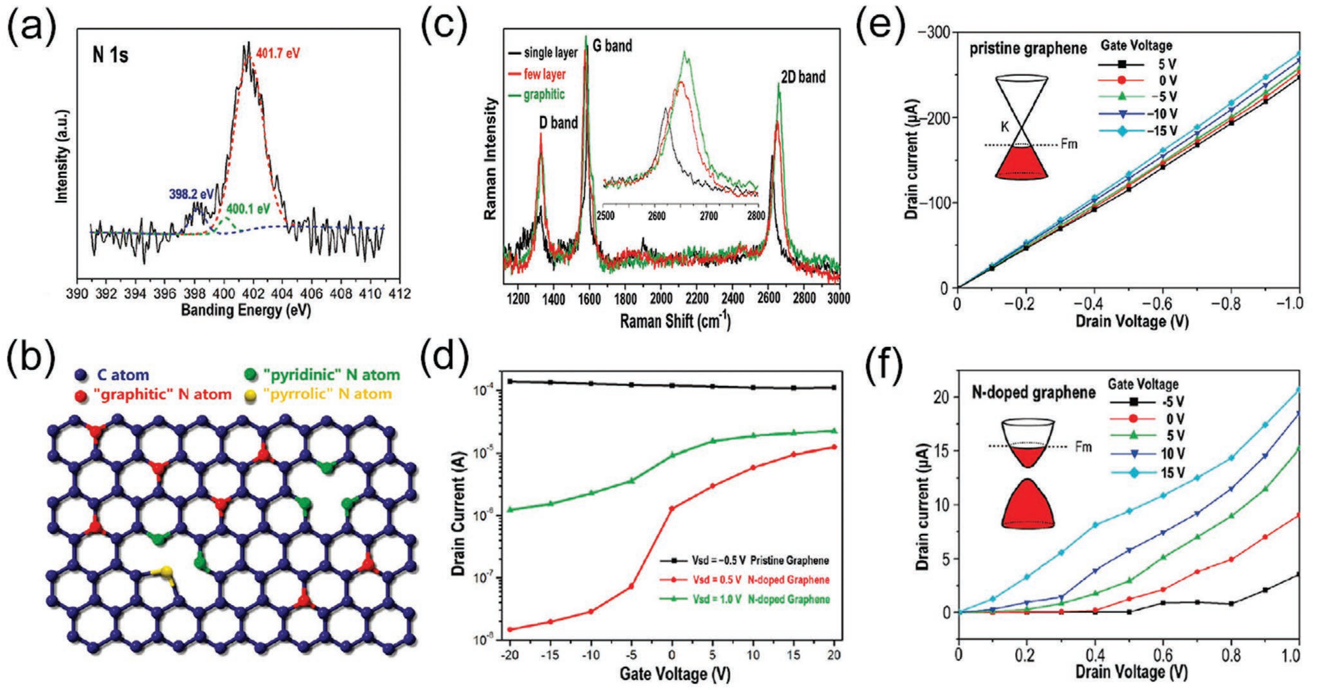

Figure 7. a) N 1s XPS spectrum of N-doped graphene. b) Schematic and c) Raman spectra of N-doped graphene. d) Pristine graphene and N-doped graphene transfer characteristics. e,f) I_{ds}/V_{ds} characteristics at various V_g values for pristine graphene and N-doped graphene field effect transistor (FET) devices. Insets: presumed band structures. a–f) Reproduced with permission.[168] Copyright 2009, American Chemical Society.

storage mechanism, supercapacitors can be simply divided into two types including electrochemical double-layer capacitors (EDLCs) that store charge by the physical absorption of electrolyte ions on the electrolyte/electrode interface, and pseudocapacitors that use fast and reversible faradaic reactions that occur between electrode and electrolyte.[194,195]

5.1.1. EDLCs

Aiming at achieving high capacitance, carbon materials (e.g., activated carbon, porous carbon, CNTs, graphene) require large SSA, an appropriate pore size distribution, abundant heteroatoms, high electrical conductivity, and stable physicochemical properties.[196–200] In this respect, graphene, including PG, would be a perfect candidate for achieving high energy density because of its large theoretical SSA and gravimetric capacitance.[201] However, strong π–π interactions between graphene sheets will actually cause the irreversible aggregation and spontaneous layer restacking during electrode manufacture,[202] which seriously compromises the available SSA and increases the contact resistance.[203] Ions in the restacked film need to travel a much longer distance to find the broken edges or defects of the graphene nanosheet in order to cross each graphene layer, which greatly reduces the ion diffusion rate (**Figure 9**a).[95] In this regard, PGMs by allowing the electrolytes' fast access to the surface of the porous framework promise better performance than other porous carbons.[194,195]

To achieve high SSA without sacrificing other excellent properties, various approaches have been developed to obtain high-performance PG-based materials for supercapacitors. For instance, Zhu et al. demonstrated the chemical activation of exfoliated graphite oxide to synthesize a PG-based carbon with a SSA up to 3100 m^2 g^{-1} and abundant micropores (Figure 9b).[99] The 3D continuous network of highly curved, atom-thin graphene walls ranging from 0.6 to 5 nm pores gives the sp^2-bonded carbon high capacitances of 165, 166, and 166 F g^{-1} at current densities of 1.4, 2.8, and 5.7 A g^{-1}, respectively, in 1-butyl-3-methyl-imidazolium tetrafluoroborate (BMIMBF$_4$/AN) electrolyte in a two-electrode system (Figure 9c,d). In addition, they developed another PG-derived carbon with high SSA of 3290 m^2 g^{-1} by the microwave expansion and KOH activation of graphite oxide.[201] The gravimetric and volumetric specific capacitances of these two graphene-derived porous carbons were measured to be 174 F g^{-1} and 100 F cm^{-3}, respectively, in an EMIMTFSI/AN electrolyte. Usually, a porous structure with low packing density and high SSA tends to provide high gravimetric capacitance, but low volumetric capacitance. To simultaneously obtain both for EDLCs, Xu et al. used HGFs (Figure 4f,g) with nanopores as high-performance binder-free electrodes in supercapacitors.[95] The nanopores in the holey graphene effectively shorten the ion transport distance between neighboring graphene layers, which significantly accelerates ion transfer across the whole HGF assembly. As a result, HGFs not only had a high gravimetric capacitance of 298 F g^{-1}, but also high volumetric capacitance of 212 F cm^{-3} in an organic electrolyte. In addition, the fully packaged device fabricated with HGFs provided volumetric and gravimetric energy densities of 49 Wh L^{-1} and 35 Wh kg^{-1}, respectively, comparable to a traditional lead acid battery. Another study worth mentioning, dealing with porous yet densely packed carbon electrodes with a low ion transport resistance, high SSA, and high packing density

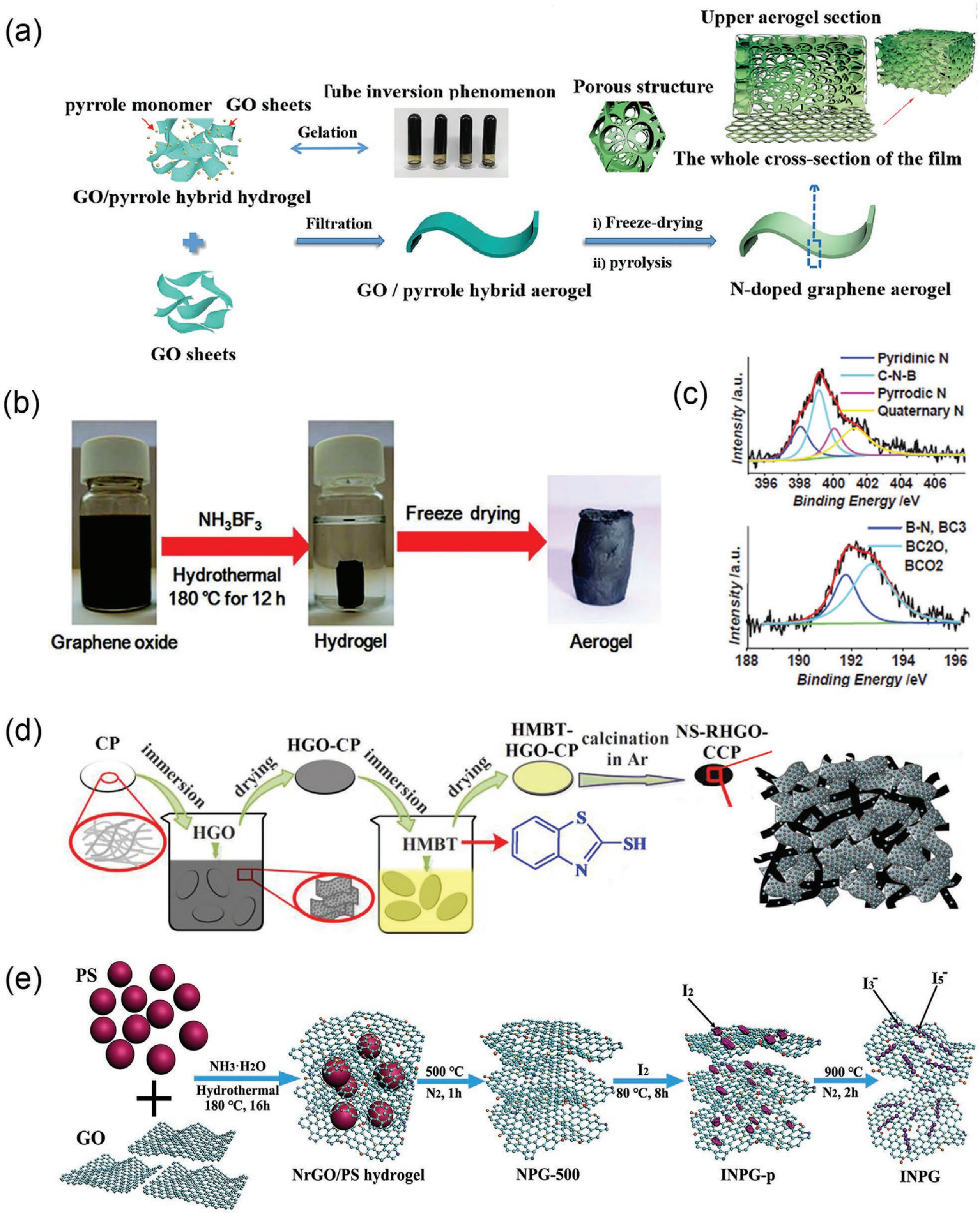

Figure 8. a) Schematic showing the fabrication process of N-doped graphene aerogel films. Reproduced with permission.[190] Copyright 2019, Elsevier. b) Illustration of the fabrication of all-solid-state supercapacitors based on BN-GA. c). N 1s (upper) and B 1s (bottom) XPS spectra of boron and nitrogen co-doped graphene aerogels (BN-GAs). b,c) Reproduced with permission.[187] Copyright 2011, American Chemical Society. d) Illustration of the fabrication process of nitrogen–sulfur co-doped reduced holey graphene oxide/carbonized cellulose paper (NS-RHGO-CCP) interlayer. Reproduced with permission.[191] Copyright 2019, Elsevier. e) Schematic of the synthesis of iodine-doped porous graphene (INPG). Reproduced with permission.[192] Copyright 2019, Elsevier.

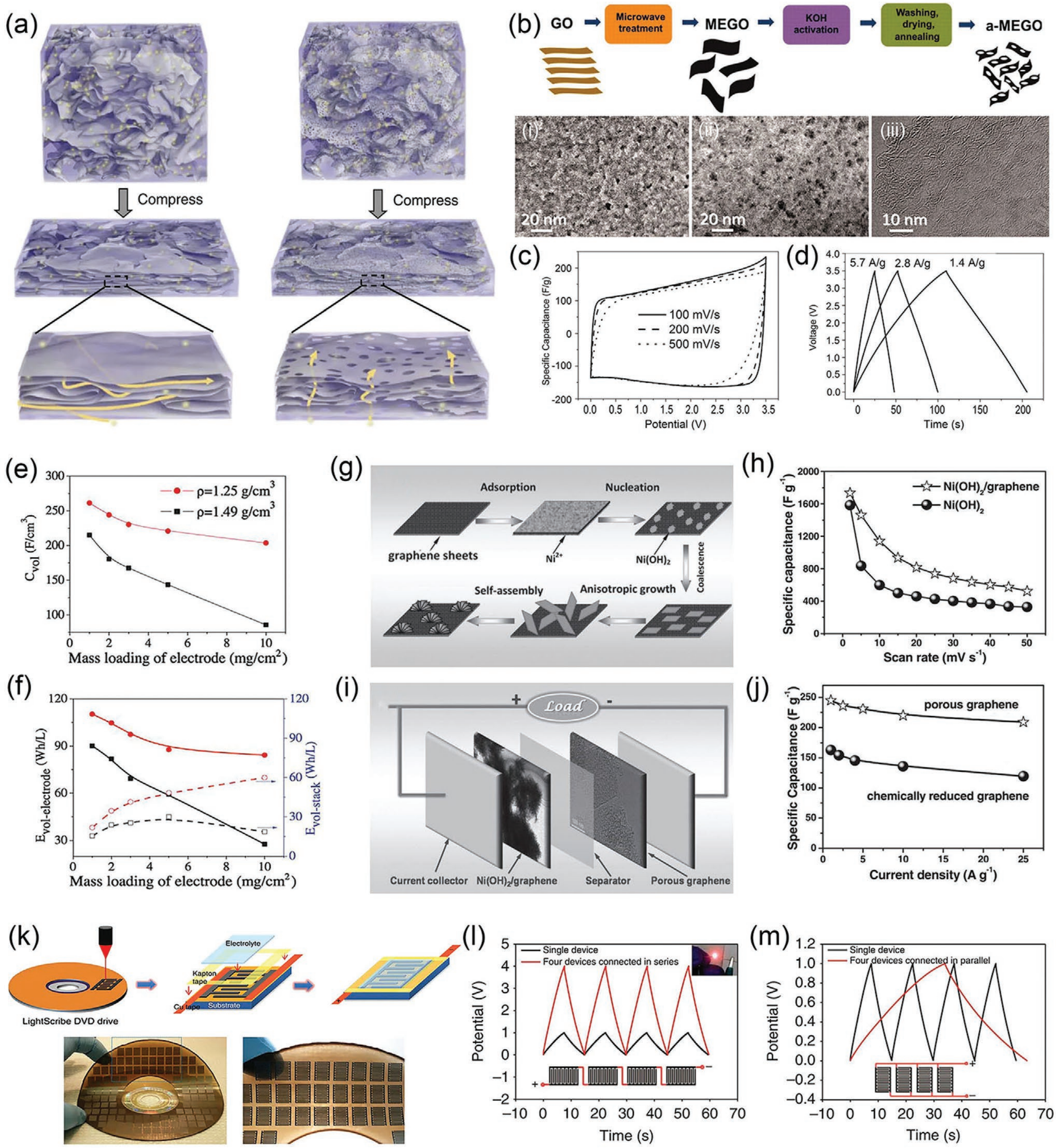

Figure 9. a) Schematic of the HGFs for electrochemical capacitors. Reproduced with permission.[95] Copyright 2014, Nature Publishing Group. b) Schematic showing the generation of pores by chemical activation of MEGO with KOH. Inset: i–iii) Morphologies of 3D a-MEGO. c) CV curves of a-MEGO at different scan rates in BMIMBF$_4$/AN electrolyte. d) Galvanostatic charge/discharge curves of a-MEGO-based supercapacitors under different constant currents. b–d) Reproduced with permission.[99] Copyright 2011, American Association for the Advancement of Science. e) Volumetric capacitance and f) energy density of the EM-CCG film and dried CCG film. e,f) Reproduced with permission.[196] Copyright 2013, the American Association for the Advancement of Science. g) Schematic of the formation of Ni(OH)$_2$/graphene sheets. h) Specific capacitance of Ni(OH)$_2$ and Ni(OH)$_2$/graphene obtained at various scan rates. i) Schematic of asymmetric supercapacitors based on PG as negative electrode and a Ni(OH)$_2$/graphene as positive electrode. j) Specific capacitance of PG and chemically reduced graphene at different current densities. g–j) Reproduced with permission.[197] Copyright 2012, WILEY-VCH. k) Schematic showing the fabrication process for an interdigital LSG-MSC, and photographs of more than 100 LSG-MSCs on a single disk. l,m) Galvanostatic charge/discharge curves of four LSG-MSCs connected in l) series and m) in parallel. k–m) Reproduced with permission.[198] Copyright 2013, Nature Publishing Group.

(1.49 g cm^{-3}) was reported by Yang et al.[196] Electrolyte-mediated chemical-converted graphene (EM-CCG)-based supercapacitors delivered high specific capacitances of 255.5 and 261.3 F cm^{-3} in an aqueous and organic electrolyte, respectively, at 0.1 A g^{-1} (Figure 9e,f). It should be pointed out that the low packing density caused by the abundant porosity is a big obstacle for achieving high volumetric energy density for practical use.

Besides, designing vertically aligned graphene (VG) arrays is of great importance for enhancing ion diffusion to improve the capacitance in particular at high scan rates.[204] For example, Zheng et al, reported high-power micro-supercapacitors (VG-MSCs) based on high-density unidirectional arrays of vertically aligned graphene nanosheets, obtained from a thermally decomposed SiC substrate.[205] Owing to their vertically oriented edges, high electrical conductivity, high-density structurally ordered alignment of graphene, and open intersheet channels, VG-MSCs displayed a high areal capacitance of ≈7.3 mF cm^{-2} and a fast frequency response with a short time constant of 9 ms. This strategy of producing high-density unidirectional VG nanosheets demonstrated the feasibility of manufacturing high-power compact supercapacitors. As another example, Lee et al. realized the fabrication of vertically aligned 3D porous $VOPO_4$-graphene by a general ice-templated self-assembly technique.[206] The resulting 3D $VOPO_4$-graphene showed high SSA, vertically aligned and directionally porous structure, and excellent electrical conductivity, greatly facilitating the diffusion of electrolyte ions and transportation of electrons within the porous framework. As a result, the obtained electrodes exhibited higher capacitance of 527.9 F g^{-1} at 0.5 A g^{-1} compared with ≈247 F g^{-1} of 3D $VOPO_4$ without graphene.

5.1.2. Pseudocapacitors

Pseudocapacitive materials including transition metal oxides (TMO), transition metal hydroxides, conducting polymers, or heteroatom-doped active materials are able to achieve higher energy densities but have an inferior rate performance and cycling life to EDLC materials. To overcome this issue, a promising and reliable strategy is to exploit PG-based hybrids to take full advantage of the combined effect of PG and electroactive components (e.g., TMO, polymers) for pseudocapacitors.[207,208] So far, many hybrids of graphene-TMO and graphene-conducting polymers have been developed, in which the graphene serves as a flexible and conductive substrate for the electroactive materials, thus improving the electrical conductivity and mitigating their agglomeration, and eventually increasing the electrochemical performance. For example, Dong et al. prepared 3D GF/Co_3O_4 composites by using GF as a 3D support to anchor metal oxide particles by a hydrothermal procedure.[209] High specific capacitances of 768, 618, 552, and 456 F g^{-1} were achieved when the composite was measured at 10, 15, 20, and 30 A g^{-1}, respectively. Yan et al. reported a flower-like $Ni(OH)_2$/graphene for use in supercapacitors,[197] which showed higher specific capacitance of 1735 F g^{-1} than that of pure $Ni(OH)_2$ (1600 F g^{-1}) at 1 mV s^{-1}, demonstrating the strong coupling effect. With the scan rate increasing to 50 mV s^{-1}, the $Ni(OH)_2$/graphene still had a specific capacitance of 523 F g^{-1}, indicative of outstanding rate capability (Figure 9g–j).

In addition to the combination of graphene with pseudocapacitive materials, chemical doping of graphene itself is also a very useful strategy to improve the supercapacitive performance by effectively tuning its electron mobility and offering additional pseudocapacitance.[210–212] Graphene doping with nitrogen, boron, sulfur, and other elements for supercapacitors has been extensively investigated,[213–216] and recent advances are summarized in **Table 2**. Typically, nitrogen-doped graphene can be prepared by CVD, arc-discharge, ball milling, microwave plasma-CVD, thermal treatment, and hydrothermal treatment.[217–220] The significance of choosing N-doping is that the electrochemically active nitrogen atoms (pyridinic-N and pyrrolic-N) provide extra pseudocapacitance by the faradic redox reaction while the quaternary-N plays an important role in the improvement of electrical conductivity.[213] For example, pyrrolic-enriched N-doped graphene showed a capacitance of 194 F g^{-1} in 1 M KCl, because the pyrrolic configuration has a better binding energy for electrolyte ions to boost the capacitance.[221] Similarly, B-doped graphene also exhibited better electrochemical performance, which is explained by the fact that the deficiency of electrons in boron atoms is beneficial for attracting electrolyte anions and introducing pseudocapacitance.[213] In addition to monoatomic doping, graphenes with dual or multielement co-doping (e.g., N/P, N/S, and S/P) have been developed, as shown in Table 2.

The trend of electronic devices toward miniaturization and integration into clothes has stimulated extensive research on micro-scale power sources. MSCs with the advantages of high charge/discharge rates and superior cycling stability are promising candidates for miniaturized energy storage which can be integrated with microelectronic systems to provide the required micropower.[222,223] Notably, graphene-based MSCs have drawn increasing attention because the unique structure and properties of graphene and its derivatives are ideal for meeting the demands of MSCs.[224–226] In 2011, Gao et al.[227] reported the large-scale fabrication of monolithic MSCs by laser reduction and patterning of free-standing graphite oxide films. Both in-plane and conventional sandwich configurations were patterned with micrometer resolution. Similarly, EI Kady and Kaner[198] demonstrated a simple and cost-effective method for fabricating graphene-based MSCs (Figure 9k). By using a standard LightScribe DVD burner for direct laser writing of GO films, more than 100 MSCs were readily produced on a single disk, and easily integrated both in series and in parallel to obtain higher operating voltage and capacitance for practical applications (Figure 9l,m), respectively. The as-fabricated LSG-MSCs delivered high power density of 200 W cm^{-3} with exceptional mechanical flexibility and cycling stability, demonstrating promising prospects for practical micro-power sources. Aiming at improving the energy density and specific capacitance, graphene-based composites with a faradic charge storage mechanism have been used as electrode materials for MSCs.[228–230] For example, Wu et al.[231] prepared uniform stacked-layer heterostructure films with a thickness of 105 nm by the alternate deposition of electrochemically exfoliated graphene and redox-active conducting thiophene nanosheets. After a patterning process using oxygen-plasma etching, the resulting MSCs showed a remarkable areal capacitance of 1.3 mF cm^{-2} and a volumetric capacitance of 123 F cm^{-3} at an ultrahigh rate of 100 V s^{-1}.

Table 2. Electrochemical performance of graphene with heteroatom doping.

Host	Elements (content)	Synthesis methods	Specific capacitance	Electrolyte	Measurement system	Cyclability and capacitance retention	Refs.
Graphene	N (10.13 at%)	Hydrothermal	326 F g^{-1}@0.2 A g^{-1}	6 M KOH	Three-electrode	99.69% after 6000 cycles	[213]
Graphene	N (2%)	Thermal reduction	144.9 F g^{-1}@0.5 A g^{-1}	1 M Et_4N BF_4/propylene carbonate	Two-electrode	94.3% after 2000 cycles	[232]
Graphene hydrogels	N (5.86 at%)	Hydrothermal	308 F g^{-1}@3 A g^{-1}	6 M KOH	Three-electrode	92% retention after 1200 cycles	[220]
rGO	N (5.24 at%)	Heat treatment with melamine resin	210 F g^{-1}@0.5 A g^{-1}	$LiPF_6$	Two-electrode	96% retention after 20 000 cycles	[233]
PG	N (not provided)	Hydrothermal	130 F g^{-1}@1 A g^{-1}	$BMIMBF_4$	Two-electrode	96.6% retention after 20 000 cycles	[234]
PG	B (3%)	Fried-Ice	281 F g^{-1}@1 A g^{-1}	2 M H_2SO_4	Three-electrode	100% retention after 4000 cycles	[214]
Graphene	B (4.7%)	Pyrolytic synthesis	172.5 F g^{-1}@0.5 A g^{-1}	6 M KOH	Three-electrode	96.5% retention after 5000 cycles	[235]
Graphene nanoplatelets	B (1.1 at%)	Reduction by a borane-tetrahydrofuran	200 F g^{-1}@0.1 A g^{-1}	6 M KOH	Two-electrode	95% retention after 4500 cycles	[212]
rGO aerogel	S (1.9 at%)	Thermal	445.6 F g^{-1}@0.5 mV s^{-1}	1 M H_2SO_4	Three-electrode	73.4% retention after 1500 cycles	[236]
Graphene films	S (7.1 at%)	Bottom-up synthesis	582 F cm^{-3}@10 mV s^{-1}	H_2SO_4/PVA gel electrolyte	Two-electrode	95% retention after 10 000 cycles	[215]
EG	F (3 at%)	Electrochemical exfoliation	134 F cm^{-3}@1 mV s^{-1}	$EMIMBF_4$/PVDF-HFP gel electrolyte	Two-electrode	93% retention after 5000 cycles	[216]
rGO	S (0.38% at%)/N(0.32 at%)	Solvothermal	254 F g^{-1}@1 A g^{-1}	0.1 M KOH and 0.5 M KCl	Three-electrode	83.54% retention after 5000 cycles	[237]
Porous GAs	S (5.8% at%)/N(4.6 at%)	Thermal	438 F g^{-1}@10 mV s^{-1}	1 M H_2SO_4	Three-electrode	93.4% retention after 10 000 cycles	[148]
GO nanosheets	N (3.0 at%)/B(0.6 at%)	Hydrothermal reaction and freeze-drying processes	239 F g^{-1}@1 mV s^{-1}	H_2SO_4/PVA gel electrolyte	Two-electrode	100% retention after 1000 cycles	[238]
Graphene hydrogel	N/S	Hydrothermal	45 F g^{-1}@1 A g^{-1}	PVA/KOH	Two-electrode	69% retention after 4000 cycles	[239]
GAs	N(5.2%)/S(0.8%)	Hydrothermal	203.2 F g^{-1}@2 A g^{-1}	$EMIMBF_4$	Two-electrode	90% retention after 3000 cycles	[240]
Graphene	N(3.0%)/P(1.2%)	Thermal	219 F g^{-1}@0.25 A g^{-1}	6 M KOH	Two-electrode	86% retention after 20 000 cycles	[241]

5.2. Lithium Batteries

5.2.1. Lithium Ion Batteries (LIBs)

LIBs are popular high-energy-density electrochemical energy storage devices in our daily life. However, a larger amount of energy stored in the active material is usually incompatible with a higher charge–discharge speed (i.e., power density). To this end, it is important to design and fabricate new electrode materials for high rate, high capacity, and long cycle life LIBs. Taking advantages of the inherent properties of graphene, PMs and their exceptional porous structure, PG frameworks provide a flexible space to suffer the large volume changes of LIB electrode materials during the charge–discharge process. In addition, the interconnected structure of PG-based electrochemically active materials can offer 3D electrically conducting paths to facilitate fast ionic transport, and eventually improve the electrochemical performance of the electrodes.[242,243]

The volumetric energy and power density of LIBs have been becoming a surging important parameter for practical applications.[95,244] For instance, Wang et al. reported N-doped holey-graphene monolith with a dense microstructure and high density (1.1 g cm^{-3}). The unique structure not only benefited for electrons transport and ion diffusion channels for Li-ions, but also provided more edges on the sheet to increase Li-ion storage,[245] delivering three times the volumetric capacity (1052 mAh cm^{-3}) of graphite anodes (370 mAh cm^{-3}). Sun et al. reported a 3D Nb_2O_5/HGF composite with tailored porosity (**Figure 10**), and high mass loading without obvious electrochemical performance decrease.[242] Figure 10a shows the synthesis process of the Nb_2O_5/HGF material and its structural advantages compared to Nb_2O_5/G composite. As shown in

Figure 10b,c, the as-prepared sample had a 3D porous structure and an obvious holey structure of the graphene nanosheets. The 3D porous HGF acted as a conductive network and support for Nb_2O_5 nanoparticles. The interconnected graphene network accelerated electron transport, and the porous structure facilitated ion transport in the HGF. Hence, high mass loading and improved power capacity were simultaneously achieved by adjusting the pores of holey graphene in the composite (Figure 10d). Apparently, compared with Nb_2O_5/GF electrode, the Nb_2O_5/HGF electrode showed lower capacity decay at ultrahigh current density. The excellent capacity retention was 90% after 10 000 cycles at 10 C, and Coulombic efficiency was more than 99.9% (Figure 10e). Specifically, the excellent electrochemical performance was attributed to the electron transport and rapid ion transport provided by 3D interconnected graphene network. Another example of creating ion paths throughout the electrode and improving the electrical conductivity of $LiFePO_4$ (LFP) was reported by Wang et al. The combination of N-doped graphene aerogels with LFP provided new and rapid paths for shortened the lithium ion diffusion length and lithium ion transport. A cathode composed of LFP modified by 3D graphene showed excellent cycling stability with a 89% capacity retention over 1000 cycles at 10 C, and high rate capability, e.g., 78 mAh g^{-1} at 100 C.[246]

5.2.2. Lithium Oxygen Batteries (LOBs)

LOBs are considered another promising candidate for energy storage due to their high specific theoretical energy density (3500 W h kg^{-1}). PGMs can satisfy the requirements of the O_2 electrode of LOBs, such as high SSA, excellent electrical conductivity, and electrochemical catalytic activity for the ORR and OER.[24,247–249] For instance, Sun et al. fabricated ruthenium (Ru) nanocrystal-functionalized graphene with different pore sizes as cathode catalysts for LOBs (**Figure 11**a).[247] The highly PG not only facilitated oxygen diffusion through the electrode but also provided sufficient voids for the accommodation of Li_2O_2 (Figure 11b,c). In addition, the adsorbed Ru nanoparticles on the surface of GO can reduce the charge overpotential efficiently and improve the cycling stability at different current densities at 1000 mAh g^{-1} after 200 cycles without obvious capacity decay (Figure 11d–g). Recently, Han et al. demonstrated a novel bicontinuous nanoporous graphene cathode for LOBs, which delivered high energy density, large capacity, and long cycling lifetime.[248] The outstanding performance can be attributed to the combination of tetrathiafulvalene (TTF) redox additive and nanoporous graphene in a dimethyl sulfoxide-based electrolyte. In this case, nanoporous graphene offered conductive surfaces for both oxygen reduction and TTF oxidation, as

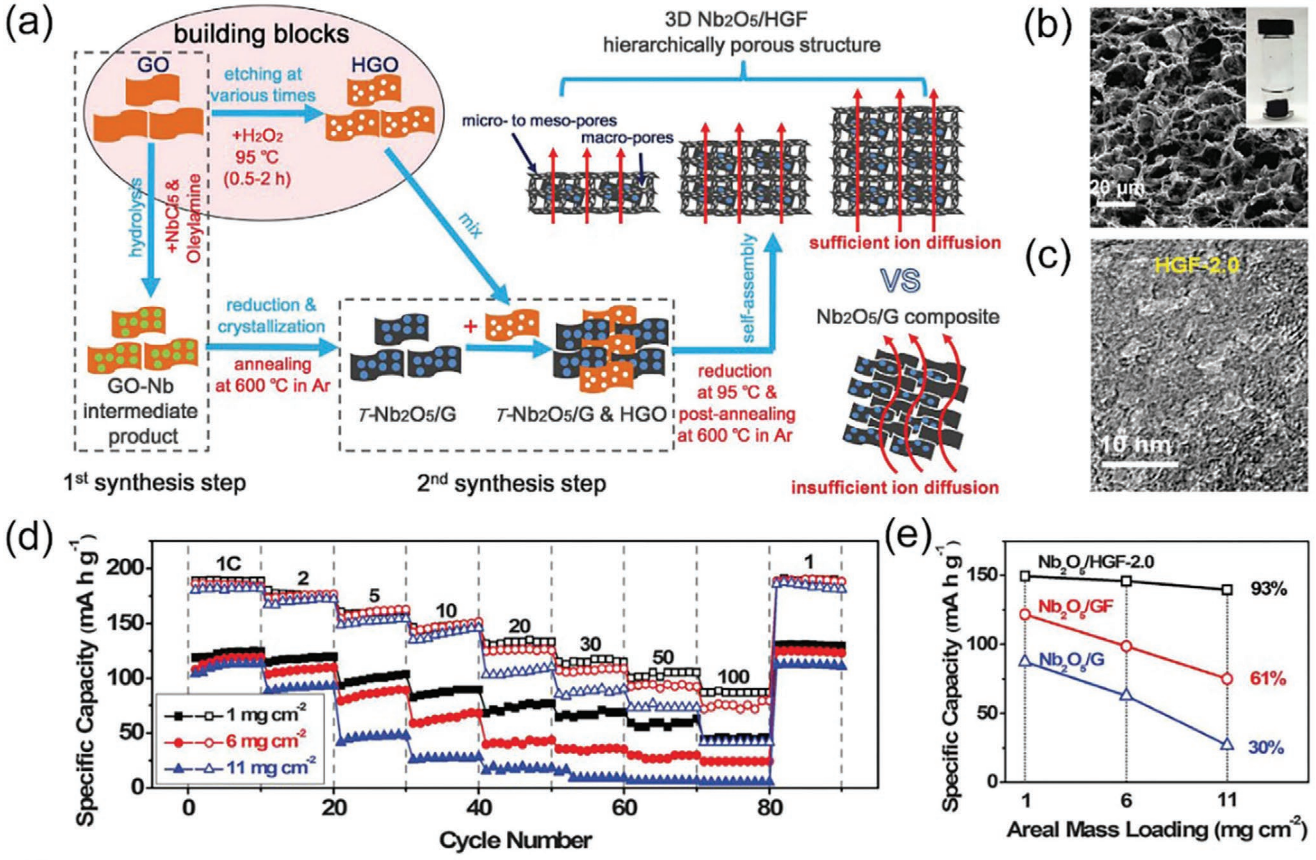

Figure 10. a) Schematic showing the preparation of porous 3D Nb_2O_5/HGF composites. b) Cross-sectional SEM image of 3D porous structure of Nb_2O_5/HGF composite. c) TEM image of graphene sheets with tailored pores. d) Rate performance of Nb_2O_5/HGF-2.0 and Nb_2O_5/G electrodes with different mass loadings. e) Retention of specific capacity at 10 C for three electrodes. a–e) Reproduced with permission.[242] Copyright 2017, American Association for the Advancement of Science.

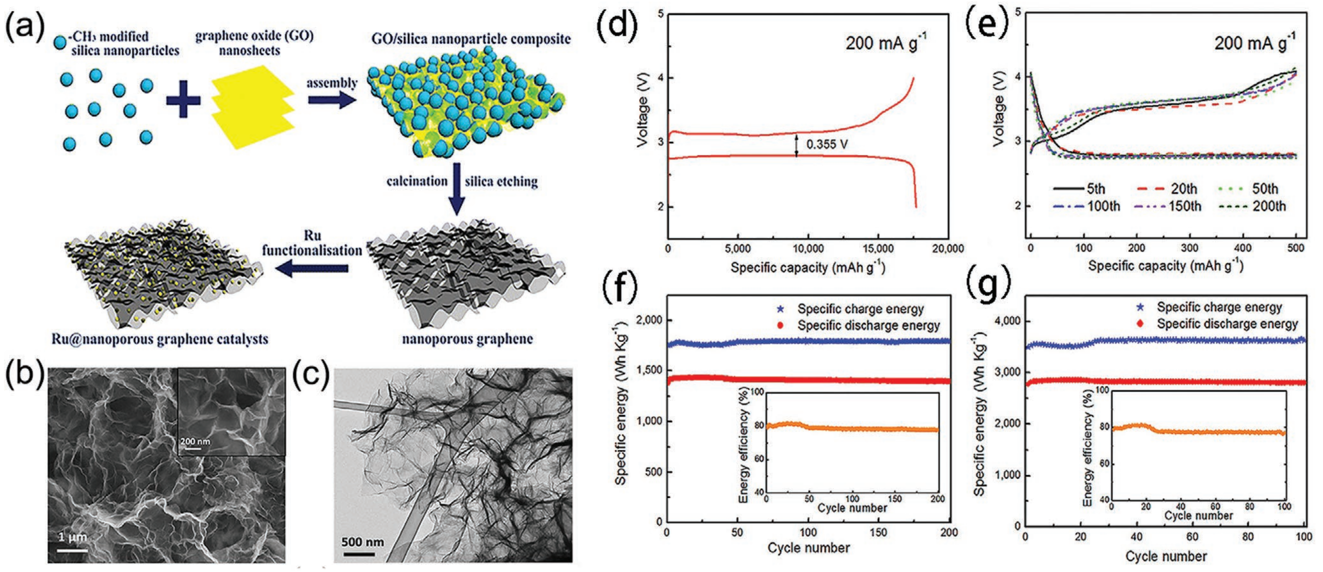

Figure 11. a) Schematic for the synthesis of PG and Ru-functionalized nanoporous graphene structures. b,c) SEM images of PGE-2, and Ru@PGE-2. d) First cycle charge/discharge profiles of LOBs with Ru@PGE-2 as the cathode catalyst at 200 mA g^{-1} in the voltage range 2.0–4.0 V. e) Charge/discharge profiles at different cycles and f) specific energy versus cycle number of a Li–O_2 battery with Ru@PGE-2 catalysts at 200 mA g^{-1} by restricting the capacity to 500 mA h g^{-1} and g) 1000 mA h g^{-1}. a–g) Reproduced with permission.[247] Copyright 2014, American Chemical Society.

well as provided efficient paths for TTF^+ migration and O_2 diffusion within nanopore channels.

5.3. Li-Metal/S Batteries

Sulfur (S) is a promising cathode material for the Li-S battery with high theoretical specific capacity of 1675 mAh g^{-1}, low cost, and environmentally friendly.[250] However, it is still very difficult to develop practical long-life, high-energy-density Li-S batteries due to the low electrical conductivity of S and its solid reduction products (Li_2S and Li_2S_2), dissolution of polysulfides in the electrolyte, the volume expansion of sulfur during discharge, inevitable Li dendrite formation, and the shuttle effect of the polysulfides.[251–254] These main issues in the Li-S batteries lead to low Coulombic efficiency, low active materials utilization, and unstable cycling performance. In this section, we will highlight the vital functions of graphene including PG in Li-S batteries, including cathode, interlayer, separator, and lithium anode.

5.3.1. Cathode

Enormous effort has been dedicated to overcoming the above mentioned issues of Li-S batteries, most of which have been focused on developing novel cathode materials, including i) designing a nanostructured polymer scaffold or conductive carbon to confine the LiPSs,[255] ii) using inorganic yet conductive materials to increase the attachment and surface reduction path,[256,257] and iii) chemical functionalization of the polysulfide complex by adjusting the synergistic effect of the electrolyte solvents.[258,259] Among various carbon-based Li-S battery cathode materials, graphene has enormous potential as 2D conductive support because of its high SSA, chemical stability, mechanical strength, flexibility, high surface functionality, and abundant porosity, which are advantageous for high sulfur loading, stabilizing the anchoring of active materials and effectively preventing polysulfide shuttling.[260–262] In particular, GO with various functional groups is able to chemically bond with polysulfides, giving it a strong polysulfide trapping ability. Due to the abundant OCFG (-OH, -COOH, -O-) on the surface of GO, nano-S can grow in situ on the GO surface. Fei et al. reported an oxidation–reduction reaction between GO and H_2S, and produced graphene-S hybrid nanosheets with chemically bonded G/S interfaces rather than weak physical contact (**Figure 12**a).[251] As a result, the dissolution of polysulfides was effectively reduced, and the cycling performance and rate capability of the batteries were substantially improved.

However, as a typical 2D material, graphene itself cannot effectively confine S (and polysulfides) inside the composite due to its intrinsic geometrical characteristics.[263] Therefore, 3D PG material with an interconnected conductive pore network not only further improves the ion diffusion and electron conduction, and inhibits the volume change of the nano-sulfur electrode during cycling, but also plays an important role in confining the sulfur and polysulfides. For instance, Cao et al. demonstrated a Li-S cathode by the in situ growth of nano-S on GO sheets using the redox reaction between sodium thiosulfate and hydrochloric acid. Because of their large SSA and functional groups, GO sheets not only provide sufficient nucleation sites for sulfur growth, but also significantly anchor sulfur particles and limit their further growth (Figure 12b).[252] The rGO-S hybrid films can serve as the cathodes of flexible Li-S batteries in different shapes, due to their excellent mechanical and electrochemical properties. Based on the high electrical

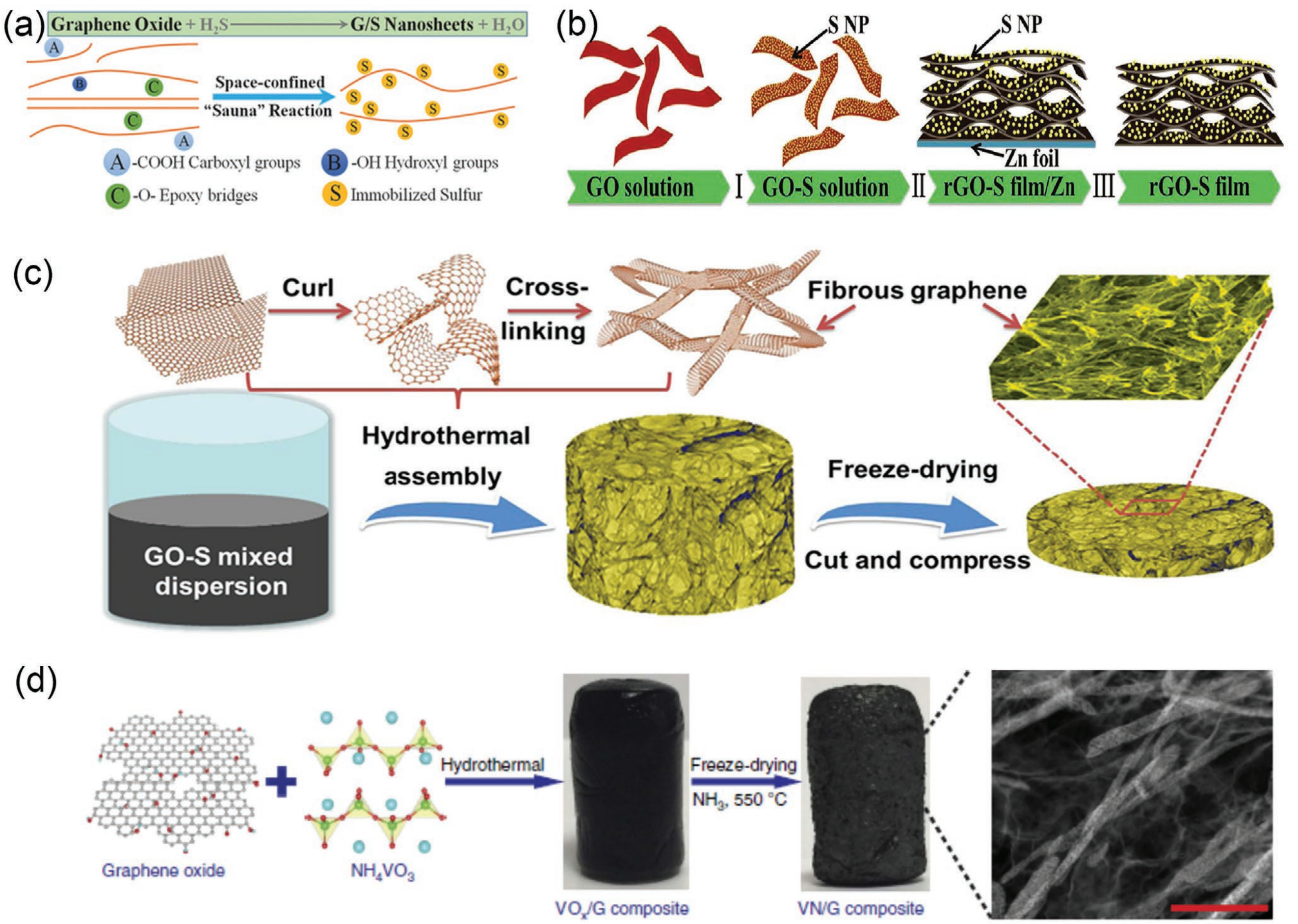

Figure 12. a) Schematic of the space-confined synthesis of G–S hybrid nanosheets in a "sauna" reaction system and the interfacial bonding in it. Reproduced with permission.[251] Copyright 2015, WILEY-VCH. b) Schematic of the fabrication of freestanding rGO–S composite films by depositing S nanoparticles on the surface of GO sheets, self-assembly of the sheets with S nanoparticles on the surface of a Zn foil, and peeling the rGO–S film from the Zn foil. Reproduced with permission.[252] Copyright 2016, WILEY-VCH. c) Illustration of the formation process of the G–S hybrid and fabrication of its self-supporting electrode. Reproduced with permission.[253] Copyright 2013, American Chemical Society. d) Schematic of the fabrication of a VN/G composite and the cell assembly. Reproduced with permission.[254] Copyright 2017, Nature Publishing Group.

conductivity of graphene, Cheng Zhou et al.[253] reported the fabrication of a self-supporting fibrous graphene-sulfur (G-S) hybrid without binder, a metal current collector, and conductive additive, by hydrothermal reduction of GO nanosheet and its assembly with sulfur nanocrystals (Figure 12c).

Moreover, an alternative strategy for improving the performance of Li-S batteries is to composite graphene (or GO) with polar metallic compounds or to dope graphene with heteroatoms.[264–267] For instance, Wang et al.[267] demonstrated the use of amino-functionalized rGO with a strong covalent stabilization of S and its discharge products, which enabled excellent high-rate and stable capacity retention of 80% after 350 cycles with high capacities. Sun et al.[254] developed a conductive porous vanadium nitride (VN) nanoribbon/graphene composite as the cathode of a Li-S battery (Figure 12d). Because of the strong anchoring of the polysulfides and the fast polysulfide conversion and high conductivity of VN, the composite cathode had a faster redox reaction kinetics and lower polarization than a pure rGO cathode. Taking advantage of the excellent conductivity, 3D network and structural support of the PG, Hu et al. constructed Li-S batteries with a high sulfur loading (14.36 mg cm^{-2}) on a graphene aerogel that delivered an impressive capacity of 1000 mAh g^{-1}.[268]

Although recent years have witnessed an increasing interest in the development of graphene-based high-energy Li-S batteries, both the fundamental electrochemistry of Li-S batteries and the interaction of lithium polysulfide species with PG needs to be further understood by the combination of experimental approaches, advanced characterizations, and theoretical calculations. Taking into consideration of keeping pace with the recent fast progress on the S cathode side, more efforts are also needed on the Li anode side in order to accomplish the full potential of Li-S batteries.

5.3.2. Interlayer and Separator

According to the battery operation mechanism, the shuttling of LiPSs not only decreases the cycle life of Li-S batteries, but also limits high energy density. Although a large number of previous studies have had huge success in overcoming the issue of shuttle effect, the dissolution of LiPSs seems inevitable in ether-based liquid electrolytes. Construction of functional separators and interlayers in Li-S batteries is regarded as an alternative route to inhibit the shuttle effect except for modifying the electrode materials and electrolytes.[260,269,270] In order to decrease the negative effect on rate performance caused by inducing the functional groups on the cathode side of the separators,[271] or using a solid electrolyte membrane to inhibit the permeation of LiPSs completely,[272] a Janus separator with graphene framework (CGF)/polypropylene (PP) membrane to improve the utilization of the sulfur cathode was fabricated.[269] As shown in **Figure 13**a, with a CGF layer, the LiPSs were reduced and deposited on the conductive scaffold. The unique structure efficiently inhibited the formation of the insulating film, allowing for the further penetration of LiPSs into the cathode. The interplane pores of the CGFs can be clearly seen in Figure 13b, and they facilitate the transport of lithium ions and prevent the shuttling of the LiPSs. In addition, the CGF separator attached to the PP tightly has a much lighter yellow surface than the PP film (Figure 13c), which captured sulfur compounds and accommodate them without obstructing the ion channels. Taking the advantages of the high SSA, mesopores, large pore volume, and the extraordinary electrical conductivity, CGF layers play a positive role in boosting Li-S batteries with a long life. What is more, by incorporating other polar compounds that strongly interact with polysulfides, the electrochemical performance of Li-S batteries was significantly improved (Figure 13 d–j). For example, Ni et al.[273] reported the use of a highly lithium-ion conductive lithium fluoride/GO (LiF/GO) interlayer to mechanically prevent lithium dendrite formation and mitigate polysulfide shuttling, and obtained remarkable cycling stability with a 0.043% capacity decay per cycle during 400 cycles. Yuan et al.[274] proposed a triple-phase interface in the electrolyte/$CoSe_2$/graphene to provide strong chemisorption and highly-stable Li-S batteries. This is because the interface efficiently increased the kinetic behavior of the soluble lithium polysulfides and regulated the uniform nucleation and controllable growth of solid Li_2S precipitates at large current densities.

5.3.3. Lithium Anode

Li metal, with a high specific capacity of 3860 mAh g^{-1} and a very negative potential of −3.04 V (versus standard hydrogen

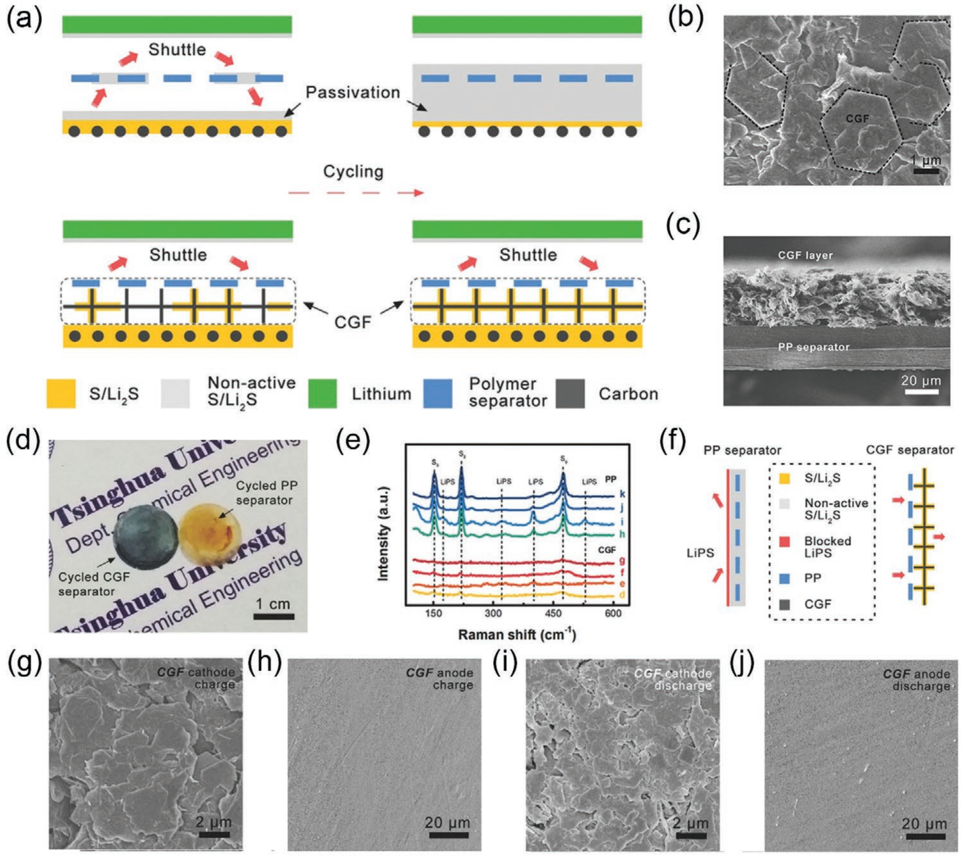

Figure 13. a) Schematic of a routine PP separator and a Janus separator with a CGF layer. b,c) SEM images of b) the CGF separator and c) cross-section of CGF separator. d) Optical image of the cycled PP separator and CGF separator. e) Raman spectra of the cycled PP separator and the CGF separator. f) Schematic of the cycled PP separator where a dense, nonactive film has formed and a CGF separator with unblocked ion channels. g–j) SEM images of the cycled CGF separator showing the g) cathode and h) anode sides in the charged state and i) cathode and j) anode sides in the discharged state. a–j) Reproduced with permission.[269] Copyright 2016, WILEY-VCH.

electrode), is the highest specific energy solid anode material. As the anode of lithium batteries, it will become an important choice for next-generation high-energy lithium batteries.[279–282] However, in the use of Li metal anodes, lithium dendrites formed by the uneven deposition of Li metal are almost inevitable.[283–286] Lithium dendrites can get easily detached from the electrodes and cannot be used for charge and discharge reactions, and become what is called dead lithium, resulting in a fast decrease in battery capacity. If the lithium dendrite grows larger, it will pierce the membrane and cause a short circuit in the battery, and even serious safety problems such as burning or even explosion. The formation of lithium dendrites will also lead to an accelerated reaction with the electrolyte, which would not only corrode the Li metal anode, but also consume the electrolyte, causing the battery to dry up and reduce cycle life.

The study of graphene in Li metal anode has demonstrated its great potential for applications in high-energy-density and stable Li-S, Li-air, and Li-graphene batteries.[287–290] Using the high SSA of a 3D PG nanostructure skeleton as a Li metal anode carrier, the resulting graphene-Li anode significantly reduces the actual current density of the electrode surface during charging and discharging, thereby greatly reducing the deposition rate of lithium and achieving uniform deposition of metallic lithium which avoids dendrite formation. For instance, Zhang et al.[275] proposed an unstacked graphene framework with deposited Li metal to obtain a Li metal anode with high efficiency and stability (**Figure** 14a). Unstacked graphene was a 3D hexagonal "drum" that exhibited large pore volume (1.65 $cm^3\ g^{-1}$), SSA (1666 $m^2\ g^{-1}$), and excellent electrical conductivity (435 S cm^{-1}). The morphology of graphene-based anode

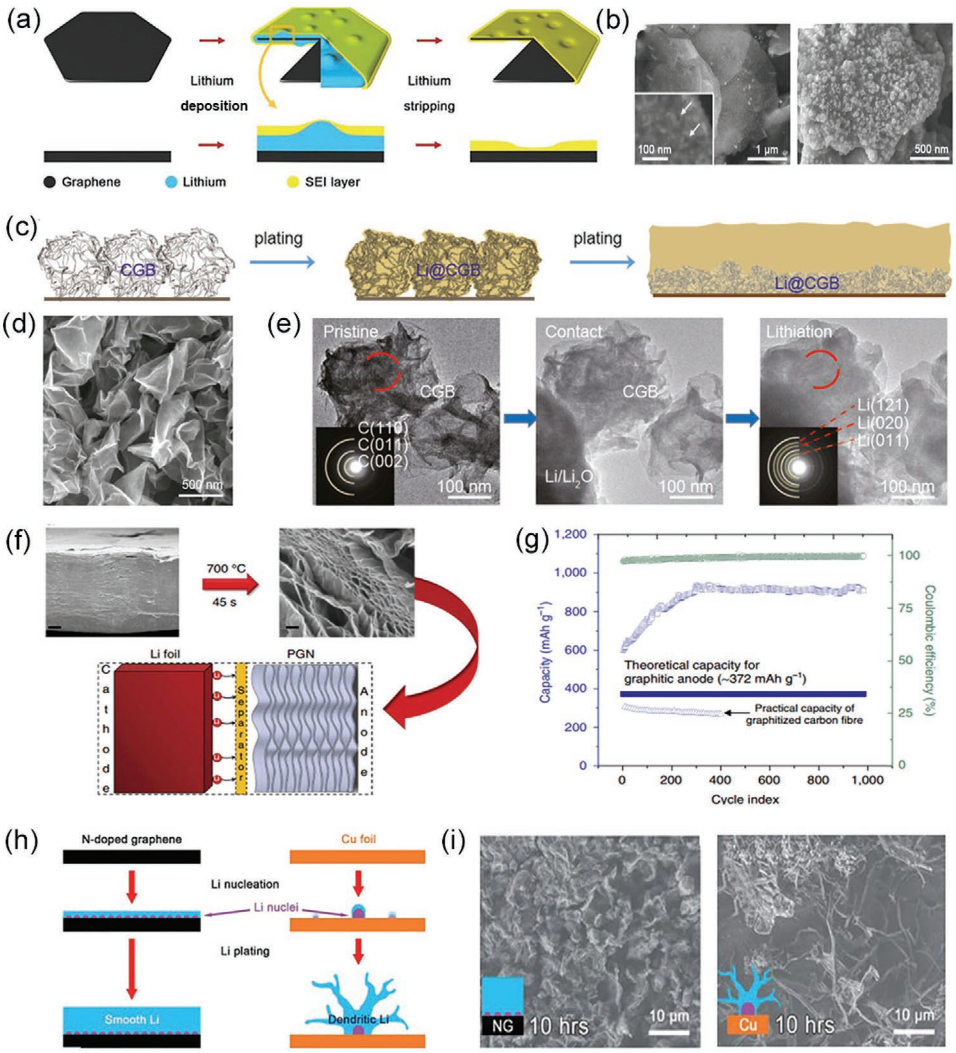

Figure 14. a) Schematic of Li deposition/stripping process on a graphene flake. b) SEM images of a graphene-based anode after Li deposition (left), and after Li stripping (right). a,b) Reproduced with permission.[275] Copyright 2016, WILEY-VCH. c) Schematic of Li plating on a CGB without dendrite growth. d) SEM image of a CGB. e) TEM images taken during the lithiation process in a CGB. c–e) Reproduced with permission.[276] Copyright 2017, Elsevier. f) Reduction of GO paper by thermal shock to produce a freestanding PGN. g) Capacity and Coulombic efficiency of the PGN anode. f,g) Reproduced with permission.[277] Copyright 2014, Nature Publishing Group. h) Schematic of Li nucleation and plating on a N-doped graphene electrode and a Cu foil electrode. i) Morphology of a NG electrode and a Cu foil electrode with the plated Li of 0.50 mAh cm^{-2}. h,i) Reproduced with permission.[278] Copyright 2017, WILEY-VCH.

showed a unique deposition/stripping morphology (Figure 14b). The large SSA provided an ultralow local surface current density, demonstrating the feasibility of regulating the Li deposition morphology. Lin et al.[291] prepared a layered Li-rGO hybrid electrode by injecting molten Li into a rGO film. It contained 7 wt% of rGO with nanoscale gaps that efficiently accommodated the metallic lithium, and had a uniform periodic stack of nanoscale layered Li and rGO. Importantly, the layered rGO provided a stable scaffold for Li stripping/plating that significantly reduced volumetric changes during cycling. The layered Li-rGO surface remained dendrite free after ten cycles, and the uniform deposition was sustained even at 3 mA cm^{-2} whereas a pure Li foil exhibited dendritic Li deposition. The outstanding lithiophilicity of rGO ensured uniform Li implantation and deposition during synthesis and subsequent cycles. The top rGO layer provided a mechanically and electrochemically stable artificial interface that efficiently stabilized the newly formed solid electrolyte interphase (SEI). Consequently, the Li-rGO film achieved highly improved electrochemical performance.

Using a specially designed PG structure, the stability of the graphene-based lithium metal anode can also be improved to some extent. Liu et al. used crumpled graphene balls (CGBs) to achieve high Coulombic efficiency and plating/stripping capacity (Figure 14c).[276] Crumpled spheroidal graphene particles did not aggregate, so that a tightly packed continuous solid was easily formed to an affective scaffold for the Li (Figure 14d). It had a uniform thickness and pore size distribution and was lithiophilic to allow rapid lithium ion diffusion. In situ TEM showed that Li ions were injected into the crumpled graphene spheres when Li/Li$_2$O was in contact with the CGBs and produced a voltage bias. Li was also deposited around the particles, but no dendritic Li growth was observed (Figure 14e). A 40 µm CGB electrode can plate and strip Li up to 12 mAh cm^{-2}, without dendrite growth. As another example, Mukherjee et al. designed a PG network (PGN) that used defects to induce metal lithium plating inside it (Figure 14f).[277] The network acted as a cage to hold the lithium metal, which sufficiently prevented lithium dendritic growth and promoted extended cycling performance of the electrode (Figure 14g).

The stability of lithium metal anodes has also been improved by methods such as doping or compounding the graphene. This can inhibit the formation and growth of lithium dendrites and reduce the volume change during cycling. Zhang et al.[278] and Li et al.[292] demonstrated that nitrogen-doped graphene could efficiently stabilize lithium metal anodes. In addition, 3D porous structures, e.g., a 3D GF, can act as a lithium reservoir and current density reducer, and when N-doped, uniform lithiophilic sites are produced (Figure 14h,i).[278] Typically, Li et al. developed a 3D fluorine-doped graphene shuttle-implanted porous carbon network to control the nucleation and growth of lithium deposits.[293] Graphene shuttle injection promotes a uniform distribution of current density and the homogenous nucleation of Li, and the F-doping ensures a uniform lithium ion distribution by the formation of a LiF-enriched SEI film. Wang et al. proposed a new sulfur-doped graphene matrix design to guide the nucleation and growth of lithium metal. Based on theoretical simulations, it was found that a S atom uniformly increases the adsorption capacity of the surrounding area.[294] This characteristic of homogenous Li adsorption indicates that a large surrounding area can be used as a nucleation region, resulting in dendrite-free lithium deposition by introducing a small number of S atoms.

High-surface-area graphene can act as a Li metal anode support, which significantly reduces the current density of the electrode surface, reduces the deposition rate of lithium, and achieves a uniform deposition of metallic lithium to avoid dendrite formation. The chemical functionality of PG with different structures, doping, and composite modification can also improve the uniform deposition of lithium, and further improve the cycling stability of graphene-Li metal anodes for high-energy-density lithium batteries.

5.4. Non-Lithium Metal Batteries

Because of their limited lithium resources, the use of a flammable electrolyte, and unsatisfactory safety, the large-scale application of LIBs might be limited in the future. To address this issue, the alternative graphene-based non-lithium batteries, such as K-ion, Na-ion, Al-ion, Mg-ion, and Zn-ion batteries have been extensively investigated as next-generation electrochemical energy storage devices.[295–299] In general, the mechanisms of non-lithium ion storage in graphene layers involves the insertion/extraction and adsorption/desorption processes.

5.4.1. Monovalent Metal Ion Batteries

Sodium (Na) is another typical monovalent metal, which shares the chemical properties of lithium in many aspects. Because of their abundance and low cost, sodium-ion batteries (NIBs) are attracting considerable interest as a promising alternative to LIBs for large-scale applications.[300,301] Among the reported electrode materials of SIBs, high-conducting PGMs have been extensively explored as key components in both the cathode and anode to boost Na ion diffusion and intercalation. For instance, Rui et al. reported a 3D meso- and macroporous $Na_3V_2(PO_4)_3$ (NVP)-based composite cathode with continuous Na ion/electron paths for ultrafast charge and discharge (**Figure 15**a).[26] A porous 3D framework with interconnect macropores and single-crystal NVP nanoparticles can be discerned. The small nanograins greatly shorten the distances of Na$^+$ diffusion, and macro/mesoporous network enables rapid ion transport and accommodates strain during repeated Na$^+$ extraction/insertion to maintain structural integrity, delivering outstanding cycling stability (64% capacity retention after 10 000 cycles at 100 C) and high rate capability with 86 mA h g^{-1} at 100 C. Owing to high theoretical capacity (2596 mA h g^{-1}) and commercial availability, red phosphorus (P) is considered as a potential anode material for SIBs. For example, Gao et al. designed a novel 3D integrated carbon@red phosphorus/graphene aerogel (C@P/GA) composite (Figure 15b).[298] In the interconnected 3D pore structure, the graphene and thin carbon layer can significantly minimize the P particle size to prevent the phosphorus volume change, and improve the conductivity by maintaining tight contact between phosphorus and the conducting matrix, and shorten the ion diffusion path in the porous framework, which are favorable for accelerating electron transfer and ion diffusion

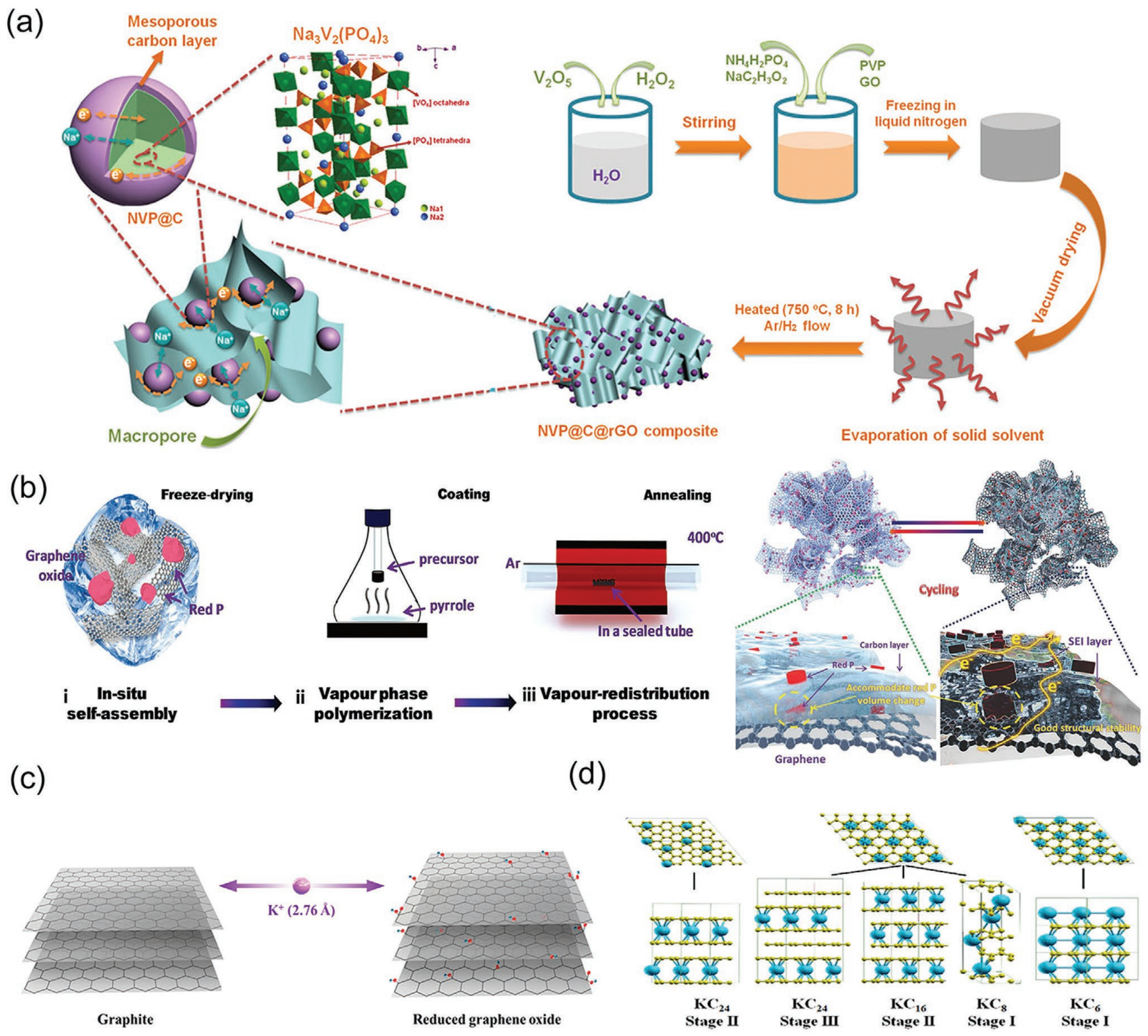

Figure 15. a) Schematic of a 3D meso- and macroporous NVP@C@rGO cathode with paths for both electron and sodium ion transport. Reproduced with permission.[26] Copyright 2015, WILEY-VCH. b) Schematic of the synthesis of a C@P/GA composite and C@P/GA electrode in the SIB system. Reproduced with permission.[298] Copyright 2016, WILEY-VCH. c) Schematic of electrochemical intercalation of K ions into graphite and rGO and d) the different stages of K-intercalated graphite, K shown in blue and C in yellow. c,d) Reproduced with permission.[299] Copyright 2015, American Chemical Society.

during cycling. Cui's group[302] showed that a hybrid material synthesized with few-layer phosphorene sandwiched between graphene layers delivered a specific capacity of 2440 mAh g^{-1} at 0.05 A g^{-1} (based on the mass of phosphorene) and 83% capacity retention after 100 cycles. The graphene layers act as a mechanically stable backbone and electrical conductors, and provide a suitable buffer space for the phosphorene layers for stable cycling operation.

Potassium ion batteries (KIBs) also exhibit great promise due to their low cost, high natural abundance, and lower redox potential (–2.92 V vs standard hydrogen electrode) of the element.[299,303] Luo et al. reported K insertion and extraction in to/from graphitic materials such as graphite and rGO, which occurred in three stages: $C \rightarrow KC_{24}$ (Stage III)$\rightarrow KC_{16}$ (Stage II) $\rightarrow KC_8$ (Stage I).[299] It was disclosed that graphite delivered high capacity of 207 mAh g^{-1}, while a rGO film had a higher reversible capacity of 222 mAh g^{-1} after K^+ insertion (Figure 15c,d). Later, Share et al. demonstrated that the nitrogen doping increased the potassium capacity from 278 mAh g^{-1} (stage I KC_8) in graphite to 350 mAh g^{-1} for few-layer graphene.[303] Meanwhile, the nitrogen doping greatly increased the rate performance, e.g., ≈200 mAh g^{-1} for doped graphene in comparison with ≈30 mAh g^{-1} for undoped graphene at 100 mA g^{-1}. Furthermore, the dual-doping of graphene by phosphorus and oxygen, synthesized by thermal annealing of triphenylphosphine and GO precursors, showed high capacity of 474 mAh g^{-1} at 50 mA g^{-1}, and ultralong cyclability for 600 cycles at 2000 mA g^{-1} with a capacity of 160 mAh g^{-1}.[304]

5.4.2. Multivalent Metal Ion Batteries

Magnesium ion batteries (MIBs) are considered as a typical two-electron redox reaction energy storage system, and are of particular importance in specific applications because of no dendrites formation on magnesium metal. Defective 2D carbon-based structures with 25% divacancy defects are broadly used as anode materials for MIBs, achieving a capacity as high as 1042 mAh g^{-1}.[305] It is predicted that, from density functional theory (DFT) of the adsorption of divalent Mg ions on DG allotropes and graphene, high-concentration vacancies and topological defects significantly increases Mg storage capacity. Different from the previously discussed batteries, the function of graphene in zinc ion batteries are mostly as a supporting material. In this case, metal oxides can be anchored on graphene framework without the aggregation of metal ion nanoparticles. Furthermore, electron transfer is significantly improved by the interconnected graphene sheets, and the abundant pores facilitate good contact between electrode and electrolyte and shorten the ion diffusion paths, while the large spaces in the 3D PG framework provide an effective buffer to prevent volumetric expansion.[296,306–308] In particular, rGO was used to improve the electrical conductivity and cyclability of zinc ion batteries, delivering a high capacity of 423.8 mAh g^{-1} at 100 mA g^{-1} with long-term cyclability.[307]

Rechargeable aluminum ion batteries (AIBs), with the advantageous features of low cost, a three-electron redox reaction, and nonflammability, could satisfy the stringent requirements of electronics and grid energy storage.[309–319] A graphene cathode composed of high-quality graphene nanosheets, with high SSA, nanoporous structure, and large interlayer spacing provides sufficient adsorption sites and enough space for the rapid diffusion and (de)intercalation of $AlCl_4^-$.[314]

As a typical example, Gao's group designed a graphene film cathode that provided a continuous electron conductor, ion-conducting channels, and active material (**Figure 16**a).[315] It was consisted of highly oriented high-quality graphene and gave a high capacity of 120 mAh g^{-1} at ultrahigh current density of 400 A g^{-1} with an extraordinary capacity retention of 91.7% after 250 000 cycles. The GF-HC worked over a wide temperature range between –40 and 120 °C and displayed excellent flexibility, withstanding 1000 folding procedures. The excellent electrochemical performance of this GF-HC cathode was attributed to the defect-free graphene, which offered high conductivity and improved the intercalation of $AlCl_4^-$ into the graphene layers (Figure 16b). In addition, the porous nature of the GF-HC cathode also facilitated the diffusion of $AlCl_4^-$ ions. Dai's group reported a monolithic 3D graphitic foam (3DGF) containing aligned few-layer graphene with a low density of defects or oxygen groups for high-performance AIBs.[316] As shown in Figure 16c, pyrolytic graphite was first charged in the electrolyte at a constant voltage, and heated to provide thermal expansion to accommodate the $AlCl_4^-$ intercalant. The material obtained after the first expansion was used as the cathode for the hydrogen evolution reaction (HER) to create significant void space inside the expanded PG, resulting in a highly porous structure with a dramatic overall expansion of 600 times the original thickness (Figure 16d). The use of this porous and aligned graphitic structure as cathode of an AIB gave a discharge capacity of 60 mAh g^{-1} at a current density of 12 000 mA g^{-1} and could be stably cycled over 4000 cycles. Moreover, the porous graphitic foam provided high rate performance by shortening the diffusion length of $AlCl_4^-$ in the *c* direction. As demonstrated by Zhang et al., the size of the graphitic material in the *ab* plane and in the *c*-direction played an important role in the anion intercalation chemistry.[317] The kinetics and charge transfer of anion intercalation was improved by sharply decreasing the length of the *c*-direction while increasing the size of the planar dimension (*ab* plane) which was attributed to the flexibility of the graphitic material. Very recently, Huang et al. reported the construction of nanoporous densely stacked graphene films derived from 3D graphene aerogels (3D GAs), prepared by the self-propagating combustion reduction of GO aerogels in seconds, which were used as a high-capacity, ultrafast, and binder-free cathode for AIBs (Figure 16e).[318] The obtained films showed high SSA, an expanded interlayer spacing, nanoporous structure, and excellent flexibility, delivering a high capacity of 245 mAh g^{-1} at 1 A g^{-1}, exceptional cycling stability, superior rate capability, and stable operation over a wide temperature range. Importantly, these AIBs showed both surface adsorption charge storage and ion intercalation mechanisms, because the high SSA provided efficient adsorption sites for $AlCl_4^-$, and the large interlayer spacing obtained by the thermal reduction favored ion intercalation. A new electrode material was produced using CVD and Ar^+-plasma etching to form GNRs with a large number of nanovoids in the graphene structure and thus offered a highly porous 3D graphene (GNHPG) foam with large SSA, high flexibility, excellent mechanical strength, and excellent conductivity (Figure 16f).[319] As expected, GNHPG-based AIBs exhibited high capacity of 123 mAh g^{-1} at 5 A g^{-1} with high Coulombic efficiency of about 98%, long cycle life (without capacity decay after more than 10 000 cycles), and impressive performance at high (40, 60, and 80 °C) and low temperature (0 °C) (Figure 16g). Such preliminary investigations on graphene-based cathodes for AIBs indicate the future challenges for the precise preparation of high-quality and defect-free graphene with a porous structure, opening up great opportunities for immediate practical implementation.

5.5. Electrocatalysis

The need for sustainable energy and environmental problems are two major challenges of today's world.[320–322] Electrochemistry is at the heart of many energy technologies, as well as methods of pollutants treatment.[323] Electrochemistry uses the energy in the cleanest possible form to collect or inject electrons through electrodes.[324] Especially, graphene and its derivatives have brought a new perspective to electrochemical systems.[325] In this section, we will demonstrate the role of dopants on graphene electrochemistry and then focus on DG in electrochemical catalysis, clarifying the structure–performance

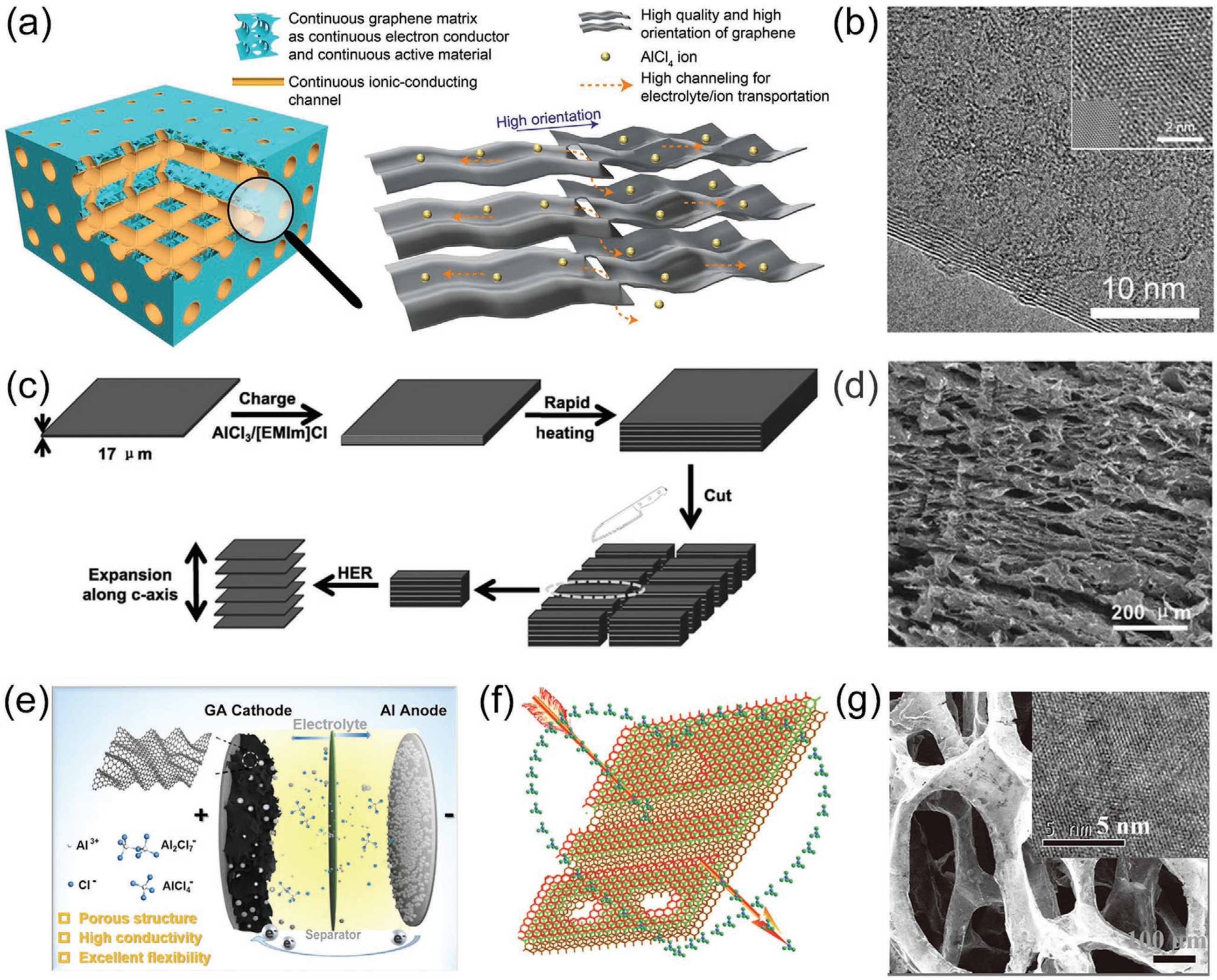

Figure 16. a) Illustration of a triple continuous material and trihigh design for a desired graphene cathode. b) HRTEM image of a trihigh tricontinuous (3H3C) graphene film (GF-HC) with eight neighboring few-layer graphene sheets. Inset: HRTEM image of a GF-HC. a,b) Reproduced with permission.[315] Copyright 2017, American Association for the Advancement of Science. c) Scheme of the preparation of a 3D graphite foam (3DGF) by thermal expansion and electrochemical hydrogen evolution. d) SEM image of 3DGF. c,d) Reproduced with permission.[316] Copyright 2017, WILEY-VCH. e) Battery assembly of a GA film. Reproduced with permission.[318] Copyright 2019, Elsevier. f) Schematic of GNRs on the surface of highly porous 3D graphene. g) SEM image showing GNR formation on the highly porous 3D GF. Inset: HRTEM image of GNRs on highly porous 3D graphene. f,g) Reproduced with permission.[319] Copyright 2017, WILEY-VCH.

relationship. Finally, we describe in details the combined effect of graphene and single atoms on catalytic performance and outline future challenges for graphene-based systems for electrocatalysis.

5.5.1. Doped PG

Substitutional elements related to the type of dopant have large effect on the electronic properties of doped graphene-based materials. Owing to the excellent electronegativity, N atoms are able to induce charge polarization on the surrounding carbon atoms and produce positively charged carbon centers.[326] The resulting high spin density and hybridization freedom of carbon atoms are helpful to improve the critical step for ORR activity via adsorption of oxygen molecules on the materials as a result of the charge transfer.[324] It is found that the electrocatalytic activity of N-doped graphene is dependent on the presence of quaternary-N and pyridinic-N moieties. In addition, pyridinic-N improves the onset potential for ORR, while the quaternary-N determines the limiting current density.[327,328]

Except for N-doped graphene, doping graphenes with sulfur,[329] phosphorus,[330] fluorine,[331] etc., have also been used to produce versatile electrocatalysts with excellent catalytic activity and long-term stability. However, the presence of a dopant in graphene materials is often not of itself sufficient to produce a material that will compete with the performance of the state-of-the-art electrocatalysts in certain applications. In other words, co-doped graphenes with various foreign elements have been explored to further promote the

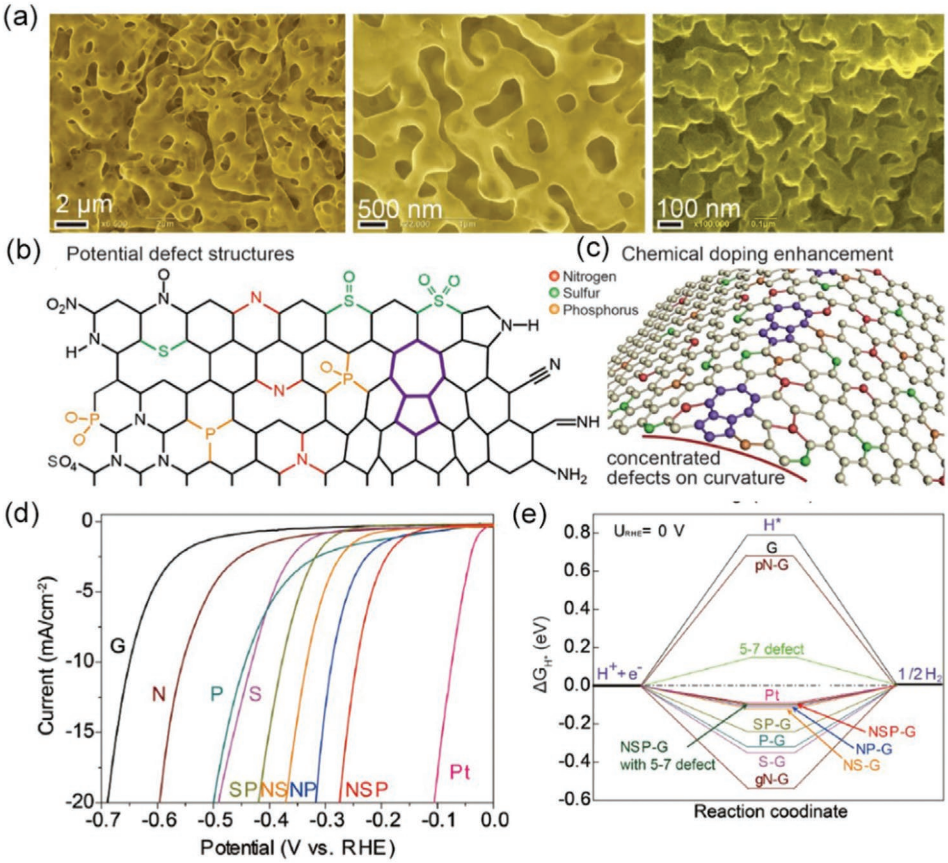

Figure 17. a) SEM images of chemically doped nanoporous (np)-graphene with different pore sizes. b) Possible defect structures of nitrogen–sulfur–phosphorus (NSP)-doped np-graphene. c) Highly curved graphene increases the amount of chemical doping. d) *CV* curves of samples with different chemical dopants. e) DFT calculations of the Gibbs free energy profiles for chemically doped highly curved graphene with topological defects. a–e) Reproduced with permission.[329] Copyright 2016, WILEY-VCH.

catalytic activity of graphene materials for electrocatalysts. For example, systematic investigation by Ito et al. was done about the interaction between surface defects and chemical dopants in curved nanoporous graphene and subsequent synthesis of N, S, and P co-doped 3D np-graphene with a high dopant content (**Figure 17**).[329] The obtained material with large concentration of topological defects can accommodate more dopants as donors or acceptors. In addition, their interaction with the defects can effectively adjust the local electronic structures and lead to a H* adsorption Gibbs free energy comparable to Pt catalysts. Such combined effects increase the number of highly active sites and thus produce superb catalytic performance of the material for highly efficient electrochemical hydrogen production.

5.5.2. Defective PG

From the above discussion, it is obvious that the nitrogen effectively alters the electronic and crystal structure of graphene,[332,333] and changes its chemical stability, surface polarity, electrical conductivity, and electron-donor properties to improve its ORR performance.[334] However, many issues regarding N-doping are the subject of ongoing debate.[335] For example, the relationship between the nitrogen concentration and the ORR performance of N-doped graphene is usually linear.[320,336] The nature of heteroatom doping to improve the ORR activity of carbon materials is most likely to activate the adjacent carbon atoms to make them active for ORR,[337] which means that the real ORR active sites may be the carbon atoms themselves. Although a large number of investigations have been devoted to establishing a catalysis mechanism for ORR based on the defect structures of graphene, direct observation of the proposed defects is still very difficult. This is because most of the prepared defective carbon atoms are present in 3D porous structures and their complexity makes them unsuitable for TEM characterization. In order to obtain direct evidence of the formation of the proposed defects, Yao and co-workers later selected single-layer graphene as a model material for fabricating DG. As illustrated in **Figure 18**a, a simple nitrogen doping and removal approach was used to prepare the DG.[332] It can be seen from the corresponding XPS spectra (Figure 18b) that, compared to the introduction of nitrogen into pristine graphene, few nitrogen atoms are detected after removal of the doped nitrogen in graphene. As expected, various defects can be clearly observed from the DG with the assistance of aberration-corrected HRTEM (Figure 18c). For example, the aforementioned edge pentagons and the G5-8-5 defect. In addition, other types of defects, such as the 7-5,

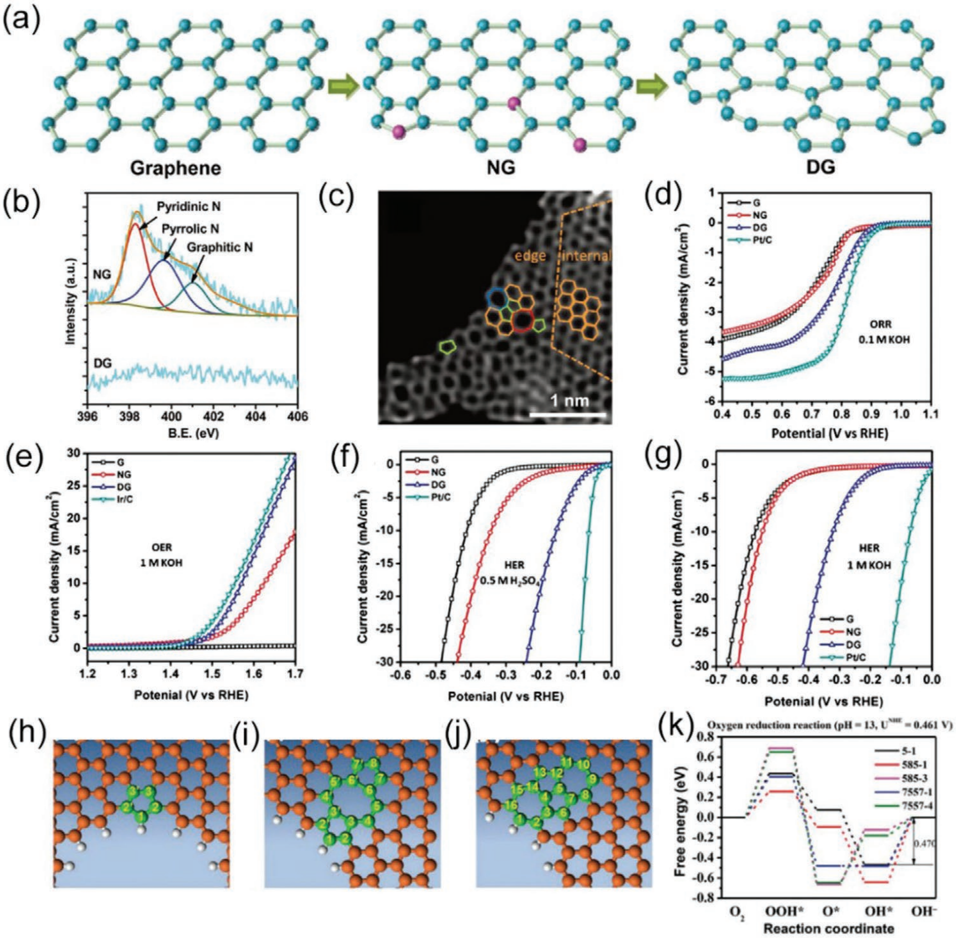

Figure 18. a) A diagram showing the synthesis of DG. b) N 1s XPS spectra of NG and DG. c) High-angle annular dark-field (HAADF) image of DG. Hexagons, pentagons, heptagons, and octagons are labeled in orange, green, blue, and red, respectively. d) ORR performance evaluation of samples prepared under an oxygen-saturated 0.1 M KOH solution. e) OER activity of the prepared samples tested in 1 M KOH. f,g) HER performance of the prepared sample tested in 0.5 M H_2SO_4 and 1 M KOH. h) Edge pentagon. i) 5-8-5 defect. j) 7-55-7 defect. k) Calculated energy profiles for the ORR path on DG in an alkaline solution. a–k) Reproduced with permission.[332] Copyright 2016, WILEY-VCH.

5-8-5 and 5-7-7-5 defects are also found. The direct observation of these effective defects in DG is a solid evidence to support the proposed defect driven catalysis mechanism. It is suggested that the removal of nitrogen is more effective in producing defects in carbon materials than the introduction of heteroatoms. From the electrochemical results in Figure 18d–g, it can be seen that DG not only has a greatly increased ORR activity, but also is an ideal catalyst for the OER and HER. These results prove the versatility of the defect-driven catalysis mechanism for electrocatalysis. The corresponding DFT calculations show that the most active configuration is the edge 5-1 defect for the ORR in alkaline electrolytes (Figure 18h–k) which is consistent with previous modeling and experimental results.[338,339] Therefore, a feasible method for designing efficient ORR catalysts is by creating unique defects for practical fuel cell applications.

Although DG has excellent electrocatalytic performance, the identification of the active sites of this metal-free catalyst is still a controversial issue due to the difficulty in controlling the defect types and their homogeneity in the material. For this purpose, Jia et al. designed a study of the active-site evaluation for a highly oriented pyrolytic graphite (HOPG) catalyst with specific carbon pentagon defects (D-HOPG).[340] The D-HOPG was synthesized by a well-controlled patterning method. Pristine HOPG with a perfect graphitic carbon structure was annealed at 700 °C in an ammonia flow, which allowed only armchair specific nitrogen dopants (Pr-N) to form at the edges of the N-HOPG. Because of the disruption of the hexagonal structure of the carbon matrix caused by nitrogen elimination, the dangling bonds of the nearby carbon atoms were reunited to generate nonhexagonal carbon lattice structures (carbon defects). As expected, the corresponding linear scan voltammogram curves showed efficient ORR activity for D-HOPG with an onset potential of 0.81 V versus reversible hydrogen electrode (RHE) at 0.05 mA cm^{-2} in a 0.1 M H_2SO_4 aqueous solution. In comparison, the onset potentials of Ar-HOPG and N-HOPG were 0.73 and 0.76 V versus RHE, respectively, both inferior to that of D-HOPG.

5.5.3. Single-Atom Catalysts on PG

Except as a catalyst, graphene has recently been of particular interest as a host in electrocatalysis because of its attractive features, including large SSA,[341] high electronic conductivity, chemical stability,[336] and abundant defect sites for attaching to metal atoms.[329] Metal-based single-atom catalysts (SACS) have been attracting extensive attention due to their many advantages of maximum atom efficiency, low metal utilization, controllable reaction selectivity, and superb specific activity.[342] In addition, the tunable electronic structures of the SACS because the different metal and nonmetal coordination possibilities at the atomic level make them appropriate for a wide range of applications.[343] With respect to the design and synthesis of SACS, continuous efforts have focused on graphene-supported SACS because of the strong interactions between the SACS and various types of defect sites at the atomic scale.[344,345]

Currently, a well-defined SAC-graphene would allow an in-depth understanding of the catalytic reaction paths and the rational design of a targeted catalyst with tailored activity. However, it is still quite challenging to prepare such catalysts with exclusive metal-defect coordination structures on graphene at the atomic scale. To solve this, Fei et al. reported a general hydrothermal-annealing method for synthesizing a series of monodispersed atomic transition metals (M = Fe, Co, Ni) trapped on a N-doped graphene with a definitive M-N_4-C_4 moiety.[346] This allows a study of the correlation between the unambiguous structures of the active sites and the specific electrochemical reactions.

The catalytic activity of SACS can be tuned with replacing the bond sites of graphene. For instance, 3D nanoporous graphene with single-atom Ni atom can be used as a catalyst for the HER in acidic solutions (**Figure 19**a,b).[347] In comparison of conventional Ni-based catalysts and graphene, this material exhibited superior HER catalysis with a low overpotential of ≈50 mV and a Tafel slope of 45 mV dec^{-1} in 0.5 м H_2SO_4 solution (Figure 19c). Theoretical investigations further demonstrated that the excellent catalytic performance of this catalyst is attributed to sp-d orbital charge transfer between the surrounding carbon atoms and Ni dopants (Figure 19d).

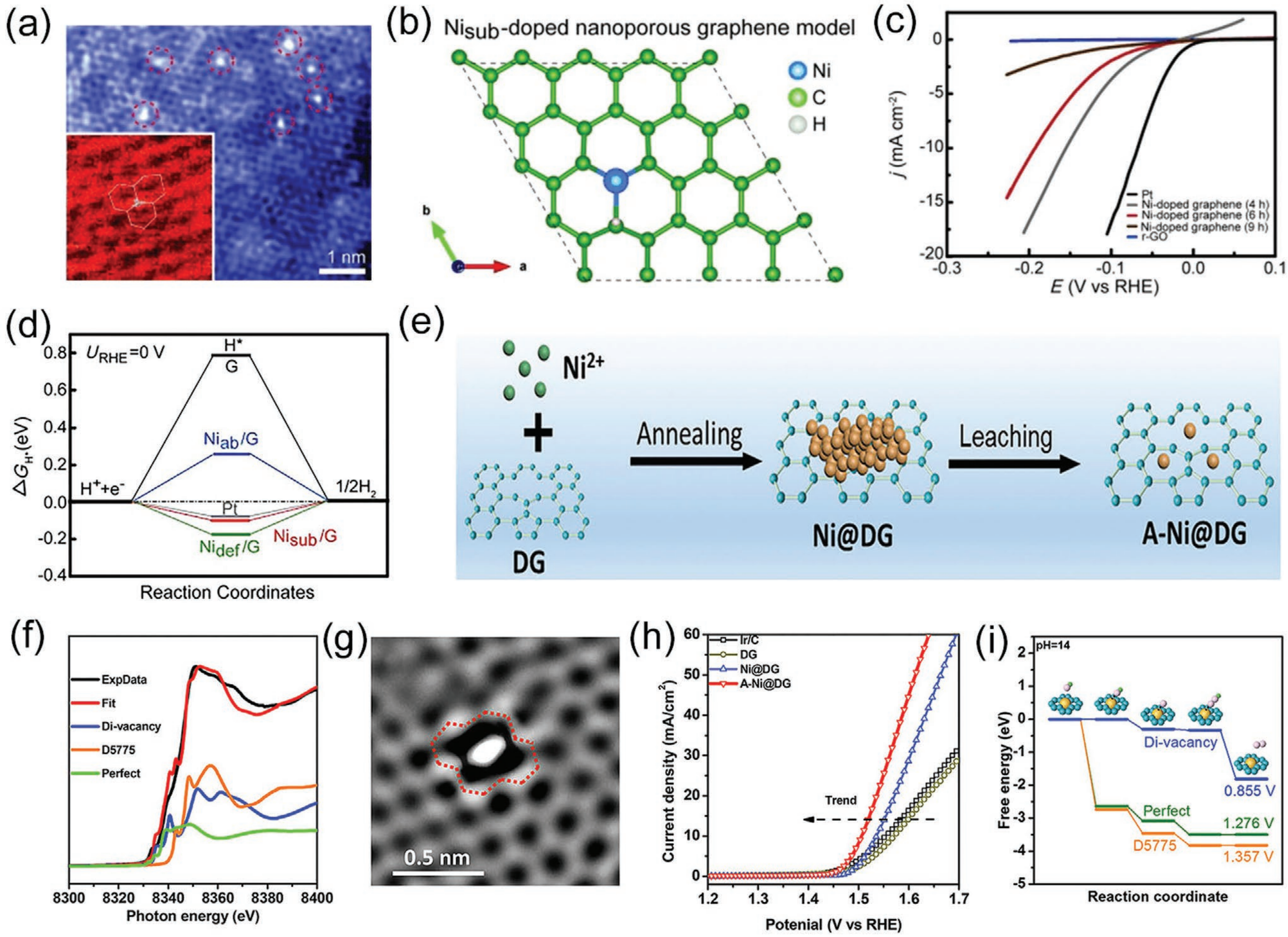

Figure 19. a) HAADF-STEM (scanning transmission electron microscope) image of Ni-doped graphene. Inset: Enlarged HAADF-STEM image. b) Hydrogen adsorption sites and configuration of the Ni_{sub}/G model with $\Delta G_{H^*} = -0.10$ eV. c) Polarization curves of Ni-doped graphene samples with different Ni dissolution periods. d) Calculated Gibbs free-energy diagram of the HER at equilibrium potential for Pt catalyst and Ni-doped graphene samples. a–d) Reproduced with permission.[347] Copyright 2015, WILEY-VCH. e) Schematic of the fabrication of A-Ni@DG. f) LCF analysis of XANES theoretical modeling. g) HAADF-STEM image of the atomic resolution of the di-vacancy for A-Ni@DG. h) OER polarization curves of DG, Ni@DG, A-Ni@DG, and Ir/C measured in a 1 м KOH electrolyte. i) Energy profiles of the three configurations for OER. e–i) Reproduced with permission.[348] Copyright 2018, Elsevier.

Zhang et al. explored the electrocatalytic behavior of catalysts with defects in graphene coordinated with atomic Ni species (Figure 19e).[348] It was demonstrated that coordination structures of atomic Ni trapped in graphene defects exist in the as-prepared atomically dispersed Ni catalyst on the DG (A-Ni@D) catalyst (Figure 19f,g). The A-Ni@DG catalyst has an efficient activity for the OER with superb water-splitting performance, e.g., an overpotential of 270 mV for the OER at a current density of 10 mA cm^{-2}. This performance is superior to the benchmark IrO_2 catalysts (Figure 19h). Furthermore, the DFT calculations reveal that the electronic structures of the atomic Ni can be well tuned by bonding to diverse types of graphene defects. The A-Ni@di-vacancy represents optimal binding energies for *O and *OOH intermediates, thus being beneficial for the OER (Figure 19i).

5.6. Molecule Separation

5.6.1. Gas Adsorption and Separation

As we know, the electron density of graphene aromatic rings is substantial and strong enough to obstruct atoms and molecules trying to pass through the rings. As a result, the perfect graphene sheet is, in principle, impermeable to atoms as small as helium.[349,350] To overcome this issue, it is necessary to design well-defined in-plane pore on monolayer graphene, 2D laminar, or 3D PG membranes to achieve gas permeability.[36] For example, Bunch et al. reported a highly efficient one-atom-thick PG membrane that had two N-functionalization features with hydrogen passivation and all-H passivation, demonstrating the possibility of using PG for gas separation.[349] Molecular building blocks have also been used to assemble porous 2D sheets.[29] Further improvements in these techniques would be helpful in creating ordered subnanometer-size pores in graphene sheets that could be used as 2D molecular-sieve membranes for gas separation. For instance, Celebi et al. reported highly efficient mass transfer double-layer graphene film with narrowly distributed diameters pores (between < 10 nm and 1 µm) (**Figure 20**).[90] Owing to their atomic thicknesses, these PG membranes show outstanding permeance of gases, liquids, and water vapor far in excess of those shown by finite-thickness membranes, highlighting their ultimate permeation.[351]

5.6.2. Water Desalination

Desalination is one of the most appropriate approaches for supplying fresh water in the context of a rapidly growing global water shortage.[352] Owing to their well-defined channels nanoporous materials with fast convective water flow, are of great significance for desalination because they can separate molecules of different sizes. The necessary conditions of an efficient separation membrane are shown as follows. First, it must be as thin as possible to maximize the permeance, and be strong enough to withstand the applied pressure. Second, the separation membrane should have a narrow pore size distribution for excellent selectivity.[13,88,353] However, current PMs have a wide range of pore sizes, poor temperature stability, weak chemical stability, and low mechanical strength are easy-fouled. It is therefore of vital importance to produce novel PMs to satisfy the requirements of targeted applications. For example, Cohen-Tanugi and Grossman reported that graphene with subnanometer pores has better water permeability than existing polymeric reverse osmosis membranes.[354] From the theoretical simulated point, depending critically on the pore size effect and chemical functional groups, the single-layer graphene can effectively separate salt from water. Because of the hydrophilic character of the edges of the graphene pores, hydroxyl groups can roughly double the water flux. As a result, the water permeability of this material is several orders of magnitude higher than conventional reverse osmosis membranes, demonstrative of great potential of nanoporous graphene in water purification.

Surwade et al. reported a single-layer graphene membrane with nanometer-size pores created by oxygen plasma etching, which further validated the effectiveness of the graphene-based desalination of water.[88] These membranes showed both exceptionally rapid water transport properties and a high salt rejection, due to their excellent mechanical properties, single-atom thickness, flexibility, and chemical stability. Volume production of these membranes for use in industrial and commercial processes remains a great challenge. First, maintaining the mechanical stability of the membranes when faced with the high shear rates that are typical in water purification devices is an intractable issue, which requires large area, continuous graphene sheets that can be readily sealed into a membrane module. Supporting such large sheets and scalably creating nanopores in them is a big challenge. Furthermore, the problems of membrane fouling and concentration polarization are always present. Despite the many challenges facing such membranes, current research has shown a proof of concept of the potential and effectiveness of nanoporous graphene for desalination applications.

5.6.3. Bioseparation

Bioseparation of protein structure sequencing, DNA, or RNA at the single-molecule level are another indispensable applications of PGMs.[355–358] Nanopore device with the combination of graphene and Al_2O_3 dielectric layers in stacked membrane structures was unique for its potential to meet the requirements, in which a voltage was used to drive DNA molecules through a nanopore in a thin membrane between two electrolytes. By monitoring the nucleobase-dependent ionic current through the pore when a single DNA chain passed through the nanopore, the sequencing was achieved (**Figure 21**).[355–357] Thus, the membrane used for this purpose should have high robustness and durability, and be as thin as possible to provide high resolution.

6. Conclusions and Future Prospects

We have reviewed the chemistry, different structures, and functionalities (OCFGs, defects, and edge) of graphene and GO,

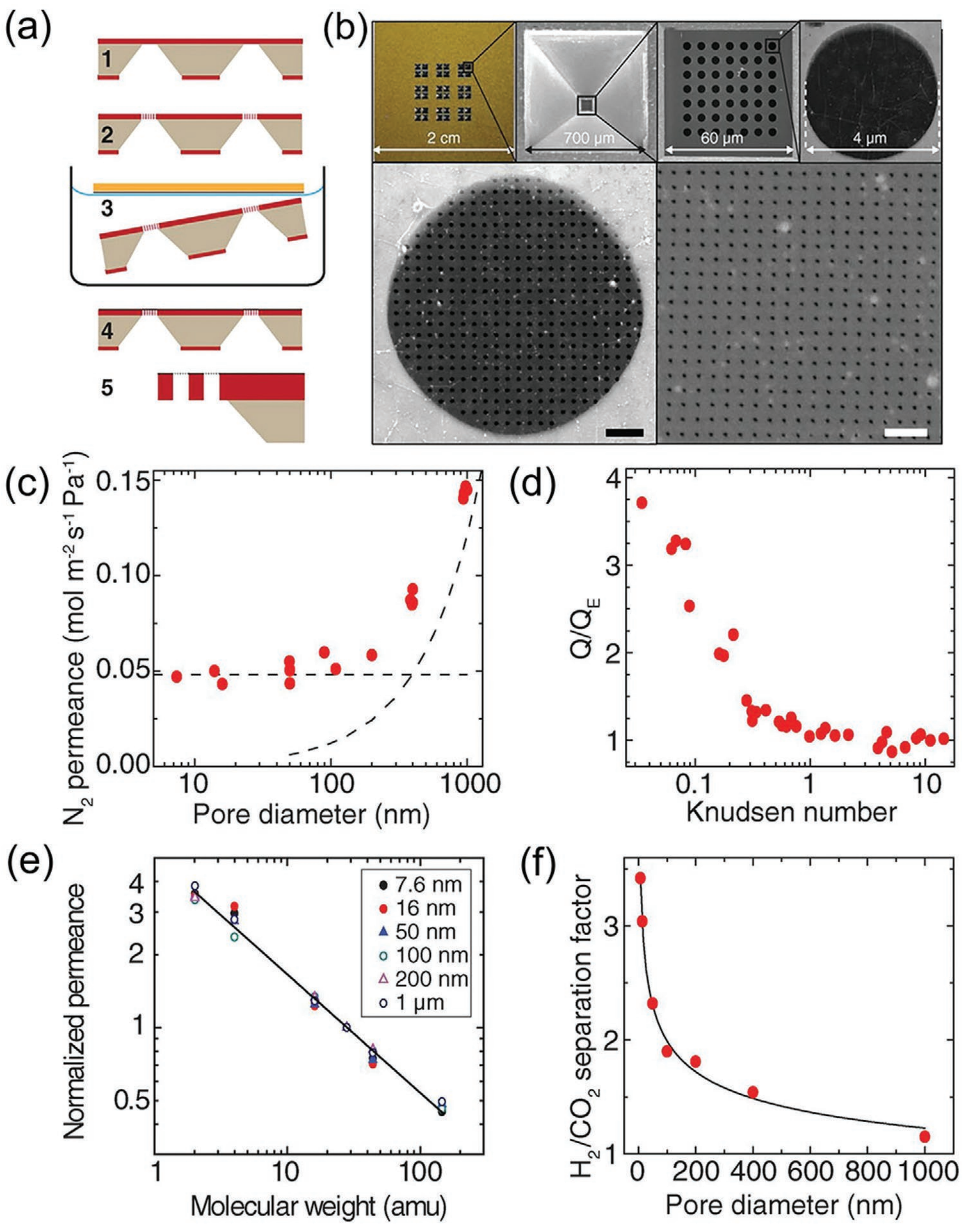

Figure 20. a) Schematic of the PG fabrication process. b) Photograph and SEM (bottom) of the structure of a whole membrane. c) N_2 permeance per pore through different-diameter apertures. d) Permeance normalized with the free-molecular-flow prediction versus Knudsen number. e) Gas permselectivity normalized by N_2 permeance for graphene membranes with different pore diameters. f) H_2/CO_2 gas separation factors versus pore diameter. a–f) Reproduced with permission.[90] Copyright 2014, the American Association for the Advancement of Science.

and systemically summarized the generation and tuning of the physical and chemical properties of pores of different sizes from monolayer PG with in-plane pores, 2D laminar porous films to 3D interconnected porous frameworks. We then generalized the state-of-the-art advances of PGMs in supercapacitors (EDLCs, pseudocapacitors), batteries (LIBs, Li-S, LOBs, and Na/K/Mg/Al ion batteries), electrocatalysts (HER, OER, and ORR), and molecule separation (water desalination and gas separation). The structure–performance relationships between the pore structure of the graphene and its specific applications have been discussed in details. Such PGMs can efficiently combine the advantages of both PMs and graphene for specific applications. Despite the significant advances in the chemistry of PG related to its preparation methods and applications, several key challenges remain unsolved.

I) Bio-inspired synthesis strategies

The development of low-cost efficient methods for the large-scale production of PGMs with controlled structures (e.g., pore size, wall thickness) and large SSA is challenging. The soft and hard template methods are most commonly used for the creation of 2D in-plane PG and the self-assembly of 3D PGMs. However, the high cost and shortage of templates as well as the energy consuming process for template removal always inhibit their applications. One possible method may be learnt from nature which has mastered the construction of nanostructures with well-defined micro/macroscopic effects and purposes. Biological minerals often have porous micro-/nanoscale structures that involve interfacial interactions between inorganic and organic components, and these could provide a good reference. Bioinspired strategies including bio-templating and other construction methods are considered as efficient and promising approaches for large-scale production of PGMs with special morphologies.

II) Design of HPG

The design and controlled fabrication of PG assemblies (e.g., fiber, film, and 3D graphene) are the important topics for preventing the restacking and aggregation of 2D graphene sheets. So far, many studies have been focused on the construction of graphene-based mesoporous nanosheets and the efficient assembly of 3D graphene frameworks. However, the preparation of graphene materials with 2D ordered pores and 3D periodic pores is still a challenging issue. Furthermore, the combination of different pore sizes (i.e., micropores, mesopores, and macropores) is vital for the development of PG-based materials in order to take advantage of the combined effects of different pore sizes, in particular, in applications of EDLCs and the cathodes of Li-S and Li-air batteries.

III) Expanding the category of PG composites

The chemistry of covalent and noncovalent functionalization can also help to expand the variety of graphene composites for different applications. Among the functionalization species, the polymers mainly play an important role in the noncovalent modification of graphene, improving its hydrophilicity and biocompatibility. Another approach of noncovalent functionalization of PG is the creation of PG with graphene analogs hybrids. For instance, the modification of graphene with OH-functionalized MWCNTs results in a highly conductive and hydrophilic hybrid.[359] Designing hybrid PGMs could exhibit higher efficiency and stability of electrochemical performance than pristine TMO nanoparticles or conductive polymers since graphene can greatly improve electron transfer and ion diffusion.

IV) Development of in situ characterization techniques

To fully understand the influence of chemically functionalized graphene on properties, the techniques of both qualitative

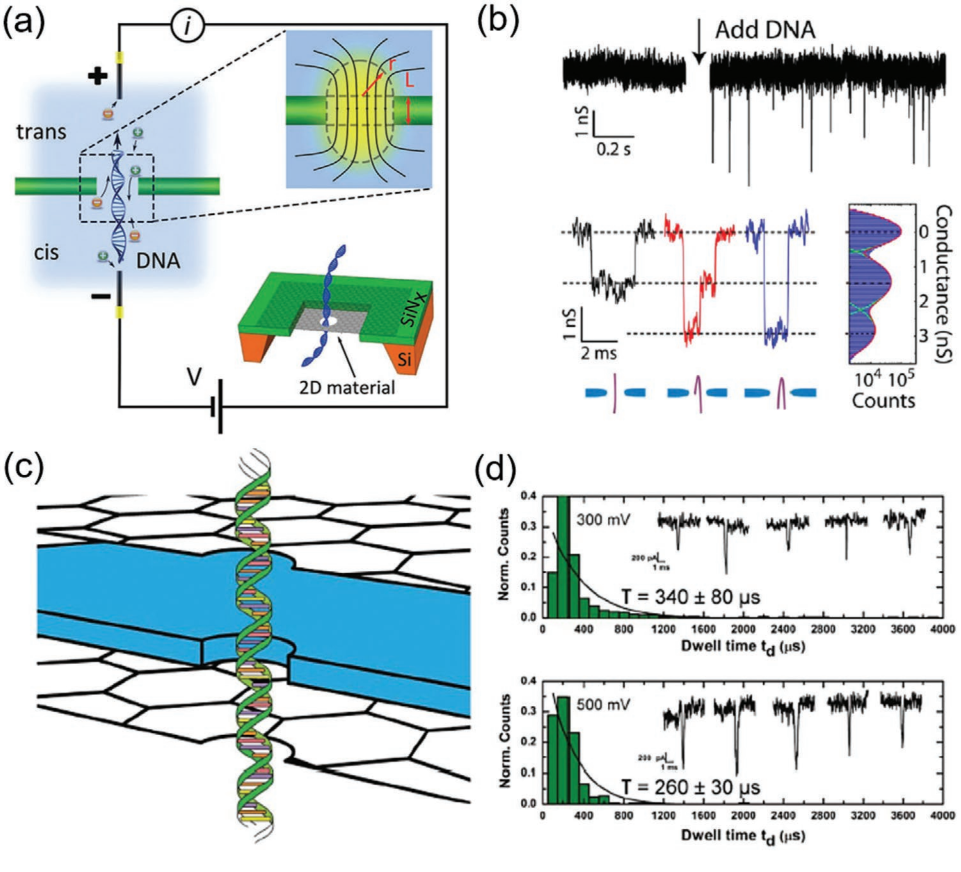

Figure 21. a) Schematic of a typical graphene nanopore device, in which an electrostatic field, applied between two Ag/AgCl electrodes immersed in the cis and trans reservoirs, electrophoretically drives the ions and DNA molecules through the graphene nanopore. The bottom inset illustrates the architecture of a 2D nanopore. Reproduced with permission.[355] Copyright 2011, Nature Publishing Group. b) Measured current in a graphene nanopore system in the absence and presence of dsDNA in the buffer solution. Reproduced with permission.[356] Copyright 2011, American Chemical Society. c) Schematic of graphene-dielectric-graphene membrane used in studying translocation of 850 bp dsDNA. A 6 nm pore is used. d) Translocation histograms for dsDNA translocations at transmembrane voltages of 300 and 500 mV, respectively. c,d) Reproduced with permission.[357] Copyright 2015, WILEY VCH.

characterization and quantitative determination will become more and more important for the direct observations of the structure (doped species, defects) of graphene and PG in order to clarify their differences. However, common characterization techniques cannot fully reveal the structural changes and surface chemistry of PG. Therefore, advanced in situ characterization such as SEM, HRTEM, XPS, atomic force microscopy, STM, and X-ray absorption near edge structure (XANES) need to be used to monitor the real-time reaction dynamics, thermodynamics, structure, and surface chemical environment changes of graphene and PG in specific applications. Some special characterization techniques, e.g., electron cryomicroscopy, and frozen electron microscopy, could be used to precisely observe the reaction process at different temperatures.

V) Pre-lithiation to improve the first Coulombic efficiency

The low initial Coulombic efficiency (or high initial irreversible capacity) caused by the formation of the SEI on high SSA PG-based electrode materials is an unsolved problem for high-energy-density metal ion batteries. To overcome this, one promising strategy is the combination of nanostructural design and prelithiation of electrode materials (i.e., Si, Ge, and S) by regulating the interface chemistry of graphene and GO with strong coupling effects. The construction of pre-lithiated PG-based electrode materials can significantly increase ion transport and prevent volume changes, thus reducing the initial irreversible capacity and improving the initial Coulombic efficiency and cycling stability.

VI) Balancing gravimetric and volumetric energy density

The high volumetric energy density and power density are two important requirements for compact energy storage. Balancing the porosity and mass density of the materials, and optimizing the thickness of the electrodes require the design and precise preparation of PG-based materials, which may have potential uses in compact, flexible energy storage devices. In addition, the freestanding electrodes without binders and additives can avoid sloughing off from current collectors and side reactions with electrolytes, when increasing the mass loading.

VII) Balancing electrical conductivity and electrocatalytic active sites

Chemically derived defects are unavoidable in graphene materials. Therefore, more investigation of their effects on electronic properties of graphene, along with their elimination to improve the functionalities of graphene, needs to be deeply investigated. Such studies might shed new light on the interaction of defects in graphene and the relative design of PGMs with new functionalities. For electrocatalysis, the concentration of heteroatom dopants or defects in graphene must be as low as 1% level to maintain the conductivity.[360] In fact, heteroatom-doped or DG behaves similarly to an insulator and has a charge carrier mobility that is three orders of magnitude smaller than graphene when the concentration of dopants or defects is higher than 5%.[361] Therefore, increasing the concentration of dopants or defects in graphene as catalytic sites while maintaining the superior conductivity of graphene is a big challenge for electrocatalysis. In addition, the introduction of defects with the same single type is still difficult. Thus, creating effective doping or defect production in graphene is worthy of in-depth investigation. This might provide a feasible approach to prepare low cost but highly active metal-free electrocatalysts. Besides, the challenging issue is to reveal the reaction mechanisms of graphene-based electrocatalysts. At present, theoretical simulations are normally used to assist the understanding of the electrochemical reaction paths. However, in situ investigation of the reaction intermediate products is still very difficult. This is because the reaction processes involve three phases (solid–liquid–gas) and are extremely complex. It is therefore crucial to conduct a well-designed experiment to directly probe the reaction intermediates. The experimental results combined with theoretical calculations could be helpful to gain a comprehensive and thorough understanding of the reaction mechanisms involved. After fully understanding these issues, the rational design and controllable fabrication of active electrocatalysts should become feasible for various catalytic reactions and systems. It seems that the use of only one single approach is not enough to solve all the existing issues involving the use of PG in different applications. Multi-strategy approaches with specific aims might bring them to the reality.

All in all, owing to their exceptional chemistry and unique porous structure, PG-based materials are attracting great attention in the fields of such as energy storage and conversion. It is expected that a full understanding of the potential of PGMs has not yet been realized, and further intense collaboration between chemists, physicists, and material scientists should considerably advance these promising materials.

Acknowledgements

This work was financially supported by the National Key R&D Program of China (Grant 2016YFA0200200), National Natural Science Foundation of China (Grants 51872283, 21805273), Natural Science Foundation of Liaoning Province (Grant 20180510038), LiaoNing Revitalization Talents Program (Grant XLYC1807153), DICP (DICP ZZBS201708, DICP ZZBS201802), DNL Cooperation Fund, CAS (DNL180310, DNL180308, DNL201912, and DNL201915), DICP&QIBEBT (Grant DICP&QIBEBT UN201702), and China Postdoctoral Science Foundation (Grants 2018M631831, 2018M633497). P.D. is grateful for the award of a CAS-TWAS President's Fellowship (Fellowship No. 2017CTF018).

Conflict of Interest

The authors declare no conflict of interest.

Keywords

applications, chemistry, graphene, graphene oxide, porous materials

Received: October 31, 2019
Revised: January 18, 2020

---

[1] M. H. Sun, S. Z. Huang, L. H. Chen, Y. Li, X. Y. Yang, Z. Y. Yuan, B. L. Su, *Chem. Soc. Rev.* **2016**, *45*, 3479.
[2] B. Fang, J. H. Kim, M. S. Kim, J. S. Yu, *Acc. Chem. Res.* **2013**, *46*, 1397.

[3] M. E. Davis, *Nature* **2002**, *417*, 813.
[4] K. M. Thomas, *Catal. Today* **2007**, *120*, 389.
[5] A. Stein, Z. Wang, M. A. Fierke, *Adv. Mater.* **2009**, *21*, 265.
[6] J. Lee, J. Kim, T. Hyeon, *Adv. Mater.* **2006**, *18*, 2073.
[7] M. J. Allen, V. C. Tung, R. B. Kaner, *Chem. Rev.* **2010**, *110*, 132.
[8] Y. Zhu, S. Murali, W. Cai, X. Li, J. W. Suk, J. R. Potts, R. S. Ruoff, *Adv. Mater.* **2010**, *22*, 3906.
[9] Y. Dong, Z. S. Wu, W. Ren, H. M. Cheng, X. Bao, *Sci. Bull.* **2017**, *62*, 724.
[10] Y. Xu, G. Shi, X. Duan, *Acc. Chem. Res.* **2015**, *48*, 1666.
[11] S. Wu, R. Ge, M. Lu, R. Xu, Z. Zhang, *Nano Energy* **2015**, *15*, 379.
[12] X. Fan, G. Zhang, F. Zhang, *Chem. Soc. Rev.* **2015**, *44*, 3023.
[13] H. Huang, Y. Ying, X. Peng, *J. Mater. Chem. A* **2014**, *2*, 13772.
[14] X. Sun, Z. Liu, K. Welsher, J. T. Robinson, A. Goodwin, S. Zaric, H. Dai, *Nano Res.* **2008**, *1*, 203.
[15] V. Georgakilas, J. N. Tiwari, K. C. Kemp, J. A. Perman, A. B. Bourlinos, K. S. Kim, R. Zboril, *Chem. Rev.* **2016**, *116*, 5464.
[16] X. Huang, K. Qian, J. Yang, J. Zhang, L. Li, C. Yu, D. Zhao, *Adv. Mater.* **2012**, *24*, 4419.
[17] X. Cao, Z. Yin, H. Zhang, *Energy Environ. Sci.* **2014**, *7*, 1850.
[18] B. G. Choi, M. Yang, W. H. Hong, J. W. Choi, Y. S. Huh, *ACS Nano* **2012**, *6*, 4020.
[19] X. Cao, Y. Shi, W. Shi, G. Lu, X. Huang, Q. Yan, Q. Zhang, H. Zhang, *Small* **2011**, *7*, 3163.
[20] J. Huang, J. Wang, C. Wang, H. Zhang, C. Lu, J. Wang, *Chem. Mater.* **2015**, *27*, 2107.
[21] Y. He, W. Chen, X. Li, Z. Zhang, J. Fu, C. Zhao, E. Xie, *ACS Nano* **2013**, *7*, 174.
[22] J. S. Lee, S. I. Kim, J. C. Yoon, J. H. Jang, *ACS Nano* **2013**, *7*, 6047.
[23] C. Tang, B. Q. Li, Q. Zhang, L. Zhu, H. F. Wang, J. L. Shi, F. Wei, *Adv. Funct. Mater.* **2016**, *26*, 577.
[24] J. Xiao, D. Mei, X. Li, W. Xu, D. Wang, G. L. Graff, W. D. Bennett, Z. Nie, L. V. Saraf, I. A. Aksay, J. Liu, J. G. Zhang, *Nano Lett.* **2011**, *11*, 5071.
[25] M. F. El Kady, Y. Shao, R. B. Kaner, *Nat. Rev. Mater.* **2016**, *1*, 16033.
[26] X. Rui, W. Sun, C. Wu, Y. Yu, Q. Yan, *Adv. Mater.* **2015**, *27*, 6670.
[27] C. Zhang, N. Mahmood, H. Yin, F. Liu, Y. Hou, *Adv. Mater.* **2013**, *25*, 4932.
[28] X. Chen, X. Hai, J. Wang, *Anal. Chim. Acta* **2016**, *922*, 1.
[29] D. E. Jiang, V. R. Cooper, S. Dai, *Nano Lett.* **2009**, *9*, 4019.
[30] H. Du, J. Li, J. Zhang, G. Su, X. Li, Y. Zhao, *J. Phys. Chem. C* **2011**, *115*, 23261.
[31] C. K. Chua, M. Pumera, *Chem. Soc. Rev.* **2014**, *43*, 291.
[32] L. Yan, Y. B. Zheng, F. Zhao, S. Li, X. Gao, B. Xu, P. S. Weiss, Y. Zhao, *Chem. Soc. Rev.* **2012**, *41*, 97.
[33] D. A. C. Brownson, D. K. Kampouris, C. E. Banks, *Chem. Soc. Rev.* **2012**, *41*, 6944.
[34] G. Bottari, M. Á. Herranz, L. Wibmer, M. Volland, L. Rodríguez Pérez, D. M. Guldi, A. Hirsch, N. Martín, F. D'Souza, T. Torres, *Chem. Soc. Rev.* **2017**, *46*, 4464.
[35] V. Chabot, D. Higgins, A. Yu, X. Xiao, Z. Chen, J. Zhang, *Energy Environ. Sci.* **2014**, *7*, 1564.
[36] T. Yang, H. Lin, X. Zheng, K. P. Loh, B. Jia, *J. Mater. Chem. A* **2017**, *5*, 16537.
[37] S. Eigler, A. Hirsch, *Angew. Chem. Int. Ed.* **2014**, *53*, 7720.
[38] A. Ambrosi, C. K. Chua, A. Bonanni, M. Pumera, *Chem. Rev.* **2014**, *114*, 7150.
[39] F. Perreault, A. Fonseca de Faria, M. Elimelech, *Chem. Soc. Rev.* **2015**, *44*, 5861.
[40] C. Chung, Y. K. Kim, D. Shin, S. R. Ryoo, B. H. Hong, D. H. Min, *Acc. Chem. Res.* **2013**, *46*, 2211.
[41] X. Li, L. Zhi, *Chem. Soc. Rev.* **2018**, *47*, 3189.
[42] K. S. Novoselov, A. K. Geim, S. V. Morozov, D. Jiang, Y. Zhang, S. V. Dubonos, I. V. Grigorieva, A. A. Firsov, *Science* **2004**, *306*, 666.
[43] Y. Xu, G. Shi, *J. Mater. Chem.* **2011**, *21*, 3311.
[44] D. Wu, F. Zhang, H. Liang, X. Feng, *Chem. Soc. Rev.* **2012**, *41*, 6160.
[45] K. S. Novoselov, V. I. Fal'ko, L. Colombo, P. R. Gellert, M. G. Schwab, K. Kim, *Nature* **2012**, *490*, 192.
[46] A. K. Geim, K. S. Novoselov, *Nat. Mater.* **2007**, *6*, 183.
[47] D. R. Dreyer, S. Park, C. W. Bielawski, R. S. Ruoff, *Chem. Soc. Rev.* **2010**, *39*, 228.
[48] C. Gómez Navarro, J. C. Meyer, R. S. Sundaram, A. Chuvilin, S. Kurasch, M. Burghard, K. Kern, U. Kaiser, *Nano Lett.* **2010**, *10*, 1144.
[49] X. Zheng, B. Jia, X. Chen, M. Gu, *Adv. Mater.* **2014**, *26*, 2699.
[50] K. P. Loh, Q. Bao, G. Eda, M. Chhowalla, *Nat. Chem.* **2010**, *2*, 1015.
[51] D. A. Dikin, S. Stankovich, E. J. Zimney, R. D. Piner, G. H. Dommett, G. Evmenenko, S. T. Nguyen, R. S. Ruoff, *Nature* **2007**, *448*, 457.
[52] Z. An, O. C. Compton, K. W. Putz, L. C. Brinson, S. T. Nguyen, *Adv. Mater.* **2011**, *23*, 3842.
[53] J. C. Meyer, C. Kisielowski, R. Erni, M. D. Rossell, M. F. Crommie, A. Zettl, *Nano Lett.* **2008**, *8*, 3582.
[54] M. H. Gass, U. Bangert, A. L. Bleloch, P. Wang, R. R. Nair, A. K. Geim, *Nat. Nanotechnol.* **2008**, *3*, 676.
[55] Z. Liang, Z. Xu, T. Yan, F. Ding, *Nanoscale* **2014**, *6*, 2082.
[56] K. Kim, H. B. R. Lee, R. W. Johnson, J. T. Tanskanen, N. Liu, M. G. Kim, C. Pang, C. Ahn, S. F. Bent, Z. Bao, *Nat. Commun.* **2014**, *5*, 4781.
[57] Ç. Ö. Girit, J. C. Meyer, R. Erni, M. D. Rossell, C. Kisielowski, L. Yang, C. H. Park, M. F. Crommie, M. L. Cohen, S. G. Louie, A. Zettl, *Science* **2009**, *323*, 1705.
[58] Y. Ogawa, K. Komatsu, K. Kawahara, M. Tsuji, K. Tsukagoshi, H. Ago, *Nanoscale* **2014**, *6*, 7288.
[59] G. M. Rutter, J. N. Crain, N. P. Guisinger, T. Li, P. N. First, J. A. Stroscio, *Science* **2007**, *317*, 219.
[60] S. Wang, L. Talirz, C. A. Pignedoli, X. Feng, K. Müllen, R. Fasel, P. Ruffieux, *Nat. Commun.* **2016**, *7*, 11507.
[61] M. Terrones, *ACS Nano* **2010**, *4*, 1775.
[62] X. Jia, M. Hofmann, V. Meunier, B. G. Sumpter, J. Campos Delgado, J. M. Romo Herrera, H. Son, Y. P. Hsieh, A. Reina, J. Kong, M. Terrones, M. S. Dresselhaus, *Science* **2009**, *323*, 1701.
[63] L. Dössel, L. Gherghel, X. Feng, K. Müllen, *Angew. Chem. Int. Ed.* **2011**, *50*, 2540.
[64] X. Jia, J. Campos Delgado, M. Terrones, V. Meunier, M. S. Dresselhaus, *Nanoscale* **2011**, *3*, 86.
[65] J. Campos Delgado, J. M. Romo Herrera, X. Jia, D. A. Cullen, H. Muramatsu, Y. A. Kim, T. Hayashi, Z. Ren, D. J. Smith, Y. Okuno, T. Ohba, H. Kanoh, K. Kaneko, M. Endo, H. Terrones, M. S. Dresselhaus, M. Terrones, *Nano Lett.* **2008**, *8*, 2773.
[66] Z. Chen, Y. M. Lin, M. J. Rooks, P. Avouris, *Phys. E* **2007**, *40*, 228.
[67] M. Y. Han, B. Özyilmaz, Y. Zhang, P. Kim, *Phys. Rev. Lett.* **2007**, *98*, 206805.
[68] X. Li, X. Wang, L. Zhang, S. Lee, H. Dai, *Science* **2008**, *319*, 1229.
[69] J. Bai, X. Duan, Y. Huang, *Nano Lett.* **2009**, *9*, 2083.
[70] A. Sinitskii, J. M. Tour, *Appl. Phys. Lett.* **2012**, *100*, 103106.
[71] N. Mohanty, D. Moore, Z. Xu, T. Sreeprasad, A. Nagaraja, A. A. Rodriguez, V. Berry, *Nat. Commun.* **2012**, *3*, 844.
[72] L. Ci, Z. Xu, L. Wang, W. Gao, F. Ding, K. F. Kelly, B. I. Yakobson, P. M. Ajayan, *Nano Res.* **2008**, *1*, 116.
[73] L. C. Campos, V. R. Manfrinato, J. D. Sanchez Yamagishi, J. Kong, P. Jarillo Herrero, *Nano Lett.* **2009**, *9*, 2600.
[74] D. V. Kosynkin, A. L. Higginbotham, A. Sinitskii, J. R. Lomeda, A. Dimiev, B. K. Price, J. M. Tour, *Nature* **2009**, *458*, 872.
[75] L. Jiao, L. Zhang, X. Wang, G. Diankov, H. Dai, *Nature* **2009**, *458*, 877.
[76] A. G. Cano Marquez, F. J. Rodriguez Macias, J. Campos Delgado, C. G. Espinosa González, F. Tristán López, D. Ramírez González,

D. A. Cullen, D. J. Smith, M. Terrones, Y. I. Vega Cantú, *Nano Lett.* **2009**, *9*, 1527.
[77] H. Murayama, T. Maeda, *Nature* **1990**, *345*, 791.
[78] P. Mahanandia, K. K. Nanda, V. Prasad, S. V. Subramanyam, *Mater. Res. Bull.* **2008**, *43*, 3252.
[79] L. Jiao, X. Wang, G. Diankov, H. Wang, H. Dai, *Nat. Nanotechnol.* **2010**, *5*, 321.
[80] A. L. Higginbotham, D. V. Kosynkin, A. Sinitskii, Z. Sun, J. M. Tour, *ACS Nano* **2010**, *4*, 2059.
[81] J. C. Meyer, A. K. Geim, M. I. Katsnelson, K. S. Novoselov, T. J. Booth, S. Roth, *Nature* **2007**, *446*, 60.
[82] K. S. Novoselov, D. Jiang, F. Schedin, T. Booth, V. Khotkevich, S. Morozov, A. K. Geim, *Proc. Natl. Acad. Sci. U. S. A.* **2005**, *102*, 10451.
[83] M. Bieri, M. Treier, J. Cai, K. Ait Mansour, P. Ruffieux, O. Groning, P. Groning, M. Kastler, R. Rieger, X. Feng, K. Mullen, R. Fasel, *Chem. Commun.* **2009**, 6919.
[84] L. Jiang, Z. Fan, *Nanoscale* **2014**, *6*, 1922.
[85] Y. Fang, Y. Lv, R. Che, H. Wu, X. Zhang, D. Gu, G. Zheng, D. Zhao, *J. Am. Chem. Soc.* **2013**, *135*, 1524.
[86] M. D. Fischbein, M. Drndić, *Appl. Phys. Lett.* **2008**, *93*, 113107.
[87] H. W. Yoon, Y. H. Cho, H. B. Park, *Philos. Trans. R. Soc., A* **2016**, *374*, 20150024.
[88] S. P. Surwade, S. N. Smirnov, I. V. Vlassiouk, R. R. Unocic, G. M. Veith, S. Dai, S. M. Mahurin, *Nat.Nanotechnol.* **2015**, *10*, 459.
[89] S. P. Koenig, L. Wang, J. Pellegrino, J. S. Bunch, *Nat. Nanotechnol.* **2012**, *7*, 728.
[90] K. Celebi, J. Buchheim, R. M. Wyss, A. Droudian, P. Gasser, I. Shorubalko, J. I. Kye, C. Lee, H. G. Park, *Science* **2014**, *344*, 289.
[91] Y. Song, J. Yang, K. Wang, S. Haller, Y. Wang, C. Wang, Y. Xia, *Carbon* **2016**, *96*, 955.
[92] S. Han, D. Wu, S. Li, F. Zhang, X. Feng, *Adv. Mater.* **2014**, *26*, 849.
[93] X. Yu, H. Cheng, M. Zhang, Y. Zhao, L. Qu, G. Shi, *Nat. Rev. Mater.* **2017**, *2*, 17046.
[94] J. Bai, X. Zhong, S. Jiang, Y. Huang, X. Duan, *Nat. Nanotechnol.* **2010**, *5*, 190.
[95] Y. Xu, Z. Lin, X. Zhong, X. Huang, N. O. Weiss, Y. Huang, X. Duan, *Nat. Commun.* **2014**, *5*, 4554.
[96] D. Fox, A. O'Neill, D. Zhou, M. Boese, J. N. Coleman, H. Z. Zhang, *Appl. Phys. Lett.* **2011**, *98*, 243117.
[97] O. Akhavan, *ACS Nano* **2010**, *4*, 4174.
[98] X. Zhao, C. M. Hayner, M. C. Kung, H. H. Kung, *ACS Nano* **2011**, *5*, 8739.
[99] Y. Zhu, S. Murali, M. D. Stoller, K. J. Ganesh, W. Cai, P. J. Ferreira, A. Pirkle, R. M. Wallace, K. A. Cychosz, M. Thommes, D. Su, E. A. Stach, R. S. Ruoff, *Science* **2011**, *332*, 1537.
[100] Z. Fan, Q. Zhao, T. Li, J. Yan, Y. Ren, J. Feng, T. Wei, *Carbon* **2012**, *50*, 1699.
[101] L. L. Zhang, X. Zhao, M. D. Stoller, Y. Zhu, H. Ji, S. Murali, Y. Wu, S. Perales, B. Clevenger, R. S. Ruoff, *Nano Lett.* **2012**, *12*, 1806.
[102] K. Chen, S. Song, F. Liu, D. Xue, *Chem. Soc. Rev.* **2015**, *44*, 6230.
[103] D. Zhou, Y. Cui, P. W. Xiao, M. Y. Jiang, B. H. Han, *Nat. Commun.* **2014**, *5*, 4716.
[104] V. Cecen, R. Thomann, R. Mülhaupt, C. Friedrich, *Polymer* **2017**, *132*, 294.
[105] W. Hooch Antink, Y. Choi, K. d. Seong, J. M. Kim, Y. Piao, *Adv. Mater. Interfaces* **2018**, *5*, 1701212.
[106] W. M. Wu, C. S. Zhang, S. B. Yang, *New Carbon Mater.* **2017**, *32*, 1.
[107] S. B. Yang, X. L. Feng, L. Wang, K. Tang, J. Maier, K. Müllen, *Angew. Chem. Int. Ed.* **2010**, *49*, 4795.
[108] H. S. Kim, Y. H. Kim, K. C. Roh, K. B. Kim, *Nano Res.* **2016**, *9*, 2696.
[109] X. Zhuang, F. Zhang, D. Wu, X. Feng, *Adv. Mater.* **2014**, *26*, 3081.
[110] Y. Wang, K. Wang, J. Zhao, X. Liu, J. Bu, X. Yan, R. Huang, *J. Am. Chem. Soc.* **2013**, *135*, 4799.
[111] S. Yang, W. Yue, J. Zhu, Y. Ren, X. Yang, *Adv. Funct. Mater.* **2013**, *23*, 3570.
[112] R. Liu, L. Wan, S. Liu, L. Pan, D. Wu, D. Zhao, *Adv. Funct. Mater.* **2015**, *25*, 526.
[113] Z. Tong, S. Liu, Y. Zhou, J. Zhao, Y. Wu, Y. Wang, Y. Li, *Energy Storage Mater.* **2018**, *13*, 223.
[114] S. Liu, P. Gordiichuk, Z. S. Wu, Z. Liu, W. Wei, M. Wagner, N. Mohamed Noriega, D. Wu, Y. Mai, A. Herrmann, K. Müllen, X. Feng, *Nat. Commun.* **2015**, *6*, 8817.
[115] Z. Liu, S. Liu, R. Dong, S. Yang, H. Lu, A. Narita, X. Feng, K. Müllen, *Small* **2017**, *13*, 1603388.
[116] W. Wei, H. Liang, K. Parvez, X. Zhuang, X. Feng, K. Müllen, *Angew. Chem. Int. Ed.* **2014**, *53*, 1570.
[117] Z. S. Wu, S. Yang, Y. Sun, K. Parvez, X. Feng, K. Müllen, *J. Am. Chem. Soc.* **2012**, *134*, 9082.
[118] K. Chen, L. Chen, Y. Chen, H. Bai, L. Li, *J. Mater. Chem.* **2012**, *22*, 20968.
[119] Z. Chen, W. Ren, L. Gao, B. Liu, S. Pei, H. M. Cheng, *Nat. Mater.* **2011**, *10*, 424.
[120] M. F. El Kady, V. Strong, S. Dubin, R. B. Kaner, *Science* **2012**, *335*, 1326.
[121] Y. Xu, X. Huang, Z. Lin, X. Zhong, Y. Huang, X. Duan, *Nano Res.* **2013**, *6*, 65.
[122] Q. Wu, Y. Sun, H. Bai, G. Shi, *Phys. Chem. Chem. Phys.* **2011**, *13*, 11193.
[123] Y. Wang, Y. Wu, Y. Huang, F. Zhang, X. Yang, Y. Ma, Y. Chen, *J. Phys. Chem. C* **2011**, *115*, 23192.
[124] M. Q. Zhao, X. F. Liu, Q. Zhang, G. L. Tian, J. Q. Huang, W. Zhu, F. Wei, *ACS Nano* **2012**, *6*, 10759.
[125] J. Liu, Z. Wang, Y. Zhao, H. Cheng, C. Hu, L. Jiang, L. Qu, *Nanoscale* **2012**, *4*, 7563.
[126] Y. Zhao, F. Zhao, X. Wang, C. Xu, Z. Zhang, G. Shi, L. Qu, *Angew. Chem. Int. Ed.* **2014**, *53*, 13934.
[127] Y. Zhao, C. Hu, Y. Hu, H. Cheng, G. Shi, L. Qu, *Angew. Chem. Int. Ed.* **2012**, *51*, 11371.
[128] P. Chen, J. J. Yang, S. S. Li, Z. Wang, T. Y. Xiao, Y. H. Qian, S. H. Yu, *Nano Energy* **2013**, *2*, 249.
[129] Y. Gong, S. Yang, Z. Liu, L. Ma, R. Vajtai, P. M. Ajayan, *Adv. Mater.* **2013**, *25*, 3979.
[130] Z. Zhang, F. Xiao, Y. Guo, S. Wang, Y. Liu, *ACS Appl. Mater. Interfaces* **2013**, *5*, 2227.
[131] Z. Tang, S. Shen, J. Zhuang, X. Wang, *Angew. Chem. Int. Ed.* **2010**, *49*, 4603.
[132] C. Hu, Y. Zhao, H. Cheng, Y. Hu, G. Shi, L. Dai, L. Qu, *Chem. Commun.* **2012**, *48*, 11865.
[133] C. Hu, H. Cheng, Y. Zhao, Y. Hu, Y. Liu, L. Dai, L. Qu, *Adv. Mater.* **2012**, *24*, 5493.
[134] Q. Zhou, J. Gao, C. Li, J. Chen, G. Shi, *J. Mater. Chem. A* **2013**, *1*, 9196.
[135] W. Chen, L. Yan, *Nanoscale* **2011**, *3*, 3132.
[136] L. Qiu, J. Z. Liu, S. L. Y. Chang, Y. Wu, D. Li, *Nat. Commun.* **2012**, *3*, 1241.
[137] L. Zhang, G. Chen, M. N. Hedhili, H. Zhang, P. Wang, *Nanoscale* **2012**, *4*, 7038.
[138] X. Zhang, Z. Sui, B. Xu, S. Yue, Y. Luo, W. Zhan, B. Liu, *J. Mater. Chem.* **2011**, *21*, 6494.
[139] K. X. Sheng, Y. X. Xu, C. Li, G. Q. Shi, *New Carbon Mater.* **2011**, *26*, 9.
[140] W. Chen, S. Li, C. Chen, L. Yan, *Adv. Mater.* **2011**, *23*, 5679.
[141] K. Sheng, Y. Sun, C. Li, W. Yuan, G. Shi, *Sci. Rep.* **2012**, *2*, 247.
[142] B. G. Choi, S. J. Chang, Y. B. Lee, J. S. Bae, H. J. Kim, Y. S. Huh, *Nanoscale* **2012**, *4*, 5924.
[143] D. Du, X. Liu, G. Korn, J. Squier, G. Mourou, *Appl. Phys. Lett.* **1994**, *64*, 3071.
[144] Y. Zhang, L. Guo, S. Wei, Y. He, H. Xia, Q. Chen, H. B. Sun, F. S. Xiao, *Nano Today* **2010**, *5*, 15.

[145] J. Lin, Z. Peng, Y. Liu, F. Ruiz Zepeda, R. Ye, E. L. G. Samuel, M. J. Yacaman, B. I. Yakobson, J. M. Tour, *Nat. Commun.* **2014**, *5*, 5714.
[146] X. Shi, F. Zhou, J. Peng, R. A. Wu, Z. S. Wu, X. Bao, *Adv. Funct. Mater.* **2019**, *29*, 1902860.
[147] Z. Xiong, C. Liao, W. Han, X. Wang, *Adv. Mater.* **2015**, *27*, 4469.
[148] X. Yu, Y. Kang, H. S. Park, *Carbon* **2016**, *101*, 49.
[149] Y. Zhou, C. H. Yen, S. Fu, G. Yang, C. Zhu, D. Du, P. C. Wo, X. Cheng, J. Yang, C. M. Wai, Y. Lin, *Green Chem.* **2015**, *17*, 3552.
[150] Y. Zhao, C. Hu, L. Song, L. Wang, G. Shi, L. Dai, L. Qu, *Energy Environ. Sci.* **2014**, *7*, 1913.
[151] S. H. Lee, H. W. Kim, J. O. Hwang, W. J. Lee, J. Kwon, C. W. Bielawski, R. S. Ruoff, S. O. Kim, *Angew. Chem. Int. Ed.* **2010**, *49*, 10084.
[152] S. Chen, S. Z. Qiao, *ACS Nano* **2013**, *7*, 10190.
[153] J. E. Johns, M. C. Hersam, *Acc. Chem. Res.* **2013**, *46*, 77.
[154] Z. Wang, C. Xu, L. Chen, J. Si, W. Li, S. Huang, Y. Jiang, Z. Chen, B. Zhao, *Electrochim. Acta* **2019**, *312*, 282.
[155] V. Georgakilas, M. Otyepka, A. B. Bourlinos, V. Chandra, N. Kim, K. C. Kemp, P. Hobza, R. Zboril, K. S. Kim, *Chem. Rev.* **2012**, *112*, 6156.
[156] C. A. Hunter, J. K. M. Sanders, *J. Am. Chem. Soc.* **1990**, *112*, 5525.
[157] S. E. Wheeler, *Acc. Chem. Res.* **2013**, *46*, 1029.
[158] S. Grimme, *Angew. Chem. Int. Ed.* **2008**, *47*, 3430.
[159] F. X. Xiao, J. Miao, B. Liu, *J. Am. Chem. Soc.* **2014**, *136*, 1559.
[160] A. Das, S. Pisana, B. Chakraborty, S. Piscanec, S. K. Saha, U. V. Waghmare, K. S. Novoselov, H. R. Krishnamurthy, A. K. Geim, A. C. Ferrari, A. K. Sood, *Nat. Nanotechnol.* **2008**, *3*, 210.
[161] C. Berger, Z. Song, X. Li, X. Wu, N. Brown, C. Naud, D. Mayou, T. Li, J. Hass, A. N. Marchenkov, E. H. Conrad, P. N. First, W. A. de Heer, *Science* **2006**, *312*, 1191.
[162] H. Liu, Y. Liu, D. Zhu, *J. Mater. Chem.* **2011**, *21*, 3335.
[163] E. Hwang, S. Adam, S. D. Sarma, *Phys. Rev. B* **2007**, *76*, 195421.
[164] T. Wehling, K. Novoselov, S. Morozov, E. Vdovin, M. Katsnelson, A. Geim, A. Lichtenstein, *Nano Lett.* **2008**, *8*, 173.
[165] B. Das, R. Voggu, C. S. Rout, C. N. R. Rao, *Chem. Commun.* **2008**, *41*, 5155.
[166] A. Lherbier, X. Blase, Y. M. Niquet, F. Triozon, S. Roche, *Phys. Rev. Lett.* **2008**, *101*, 036808.
[167] H. Wang, T. Maiyalagan, X. Wang, *ACS Catal.* **2012**, *2*, 781.
[168] D. Wei, Y. Liu, Y. Wang, H. Zhang, L. Huang, G. Yu, *Nano Lett.* **2009**, *9*, 1752.
[169] Z. Luo, S. Lim, Z. Tian, J. Shang, L. Lai, B. MacDonald, C. Fu, Z. Shen, T. Yu, J. Lin, *J. Mater. Chem.* **2011**, *21*, 8038.
[170] L. Qu, Y. Liu, J. B. Baek, L. Dai, *ACS Nano* **2010**, *4*, 1321.
[171] A. L. M. Reddy, A. Srivastava, S. R. Gowda, H. Gullapalli, M. Dubey, P. M. Ajayan, *ACS Nano* **2010**, *4*, 6337.
[172] Z. Jin, J. Yao, C. Kittrell, J. M. Tour, *ACS Nano* **2011**, *5*, 4112.
[173] N. Li, Z. Wang, K. Zhao, Z. Shi, Z. Gu, S. Xu, *Carbon* **2010**, *48*, 255.
[174] Y. Qin, J. Yuan, J. Li, D. Chen, Y. Kong, F. Chu, Y. Tao, M. Liu, *Adv. Mater.* **2015**, *27*, 5171.
[175] X. Li, H. Wang, J. T. Robinson, H. Sanchez, G. Diankov, H. Dai, *J. Am. Chem. Soc.* **2009**, *131*, 15939.
[176] J. Liang, X. Du, C. Gibson, X. W. Du, S. Z. Qiao, *Adv. Mater.* **2013**, *25*, 6226.
[177] H. M. Jeong, J. W. Lee, W. H. Shin, Y. J. Choi, H. J. Shin, J. K. Kang, J. W. Choi, *Nano Lett.* **2011**, *11*, 2472.
[178] R. Imran Jafri, N. Rajalakshmi, S. Ramaprabhu, *J. Mater. Chem.* **2010**, *20*, 7114.
[179] Y. Shao, S. Zhang, M. H. Engelhard, G. Li, G. Shao, Y. Wang, J. Liu, I. A. Aksay, Y. Lin, *J. Mater. Chem.* **2010**, *20*, 7491.
[180] Y. Wang, Y. Shao, D. W. Matson, J. Li, Y. Lin, *ACS Nano* **2010**, *4*, 1790.
[181] D. Long, W. Li, L. Ling, J. Miyawaki, I. Mochida, S. H. Yoon, *Langmuir* **2010**, *26*, 16096.
[182] D. W. Wang, I. R. Gentle, G. Q. Lu, *Electrochem. Commun.* **2010**, *12*, 1423.
[183] Z. H. Sheng, H. L. Gao, W. J. Bao, F. B. Wang, X. H. Xia, *J. Mater. Chem.* **2012**, *22*, 390.
[184] T. Lin, F. Huang, J. Liang, Y. Wang, *Energy Environ. Sci.* **2011**, *4*, 862.
[185] Z. Peng, R. Ye, J. A. Mann, D. Zakhidov, Y. Li, P. R. Smalley, J. Lin, J. M. Tour, *ACS Nano* **2015**, *9*, 5868.
[186] H. Wang, Y. Zhou, D. Wu, L. Liao, S. Zhao, H. Peng, Z. Liu, *Small* **2013**, *9*, 1316.
[187] Z. S. Wu, W. Ren, L. Xu, F. Li, H. M. Cheng, *ACS Nano* **2011**, *5*, 5463.
[188] Z. S. Wu, A. Winter, L. Chen, Y. Sun, A. Turchanin, X. Feng, K. Müllen, *Adv. Mater.* **2012**, *24*, 5130.
[189] L. S. Panchakarla, K. S. Subrahmanyam, S. K. Saha, A. Govindaraj, H. R. Krishnamurthy, U. V. Waghmare, C. N. R. Rao, *Adv. Mater.* **2009**, *21*, 4726.
[190] Y. Jin, Y. Meng, W. Fan, H. Lu, T. Liu, S. Wu, *Electrochim. Acta* **2019**, *318*, 865.
[191] P. Chen, Y. Fu, Z. Wu, J. Xia, Y. Zhou, J. Xu, J. Zhu, X. Wang, *J. Power Sources* **2019**, *434*, 226728.
[192] A. Wu, G. Wei, F. Yang, G. Xia, X. Yan, S. Shen, F. Zhu, C. Ke, J. Zhang, *Electrochim. Acta* **2019**, *318*, 354.
[193] T. Schlegel, S. Schuster, *Science* **2008**, *319*, 104.
[194] G. P. Wang, L. Zhang, J. J. Zhang, *Chem. Soc. Rev.* **2012**, *41*, 797.
[195] Y. G. Wang, Y. F. Song, Y. Xia, *Chem. Soc. Rev.* **2016**, *45*, 5925.
[196] X. Yang, C. Cheng, Y. Wang, L. Qiu, D. Li, *Science* **2013**, *341*, 534.
[197] J. Yan, Z. J. Fan, W. Sun, G. Q. Ning, T. Wei, Q. Zhang, R. F. Zhang, L. J. Zhi, F. Wei, *Adv. Funct. Mater.* **2012**, *22*, 2632.
[198] M. F. El Kady, R. B. Kaner, *Nat. Commun.* **2013**, *4*, 1475.
[199] F. Liu, Z. Wang, H. Zhang, L. Jin, X. Chu, B. Gu, H. Huang, W. Yang, *Carbon* **2019**, *149*, 105.
[200] G. Zhao, C. Chen, D. Yu, L. Sun, C. Yang, H. Zhang, Y. Sun, F. Besenbacher, M. Yu, *Nano Energy* **2018**, *47*, 547.
[201] T. Kim, G. Jung, S. Yoo, K. S. Suh, R. S. Ruoff, *ACS Nano* **2013**, *7*, 6899.
[202] R. Raccichini, A. Varzi, S. Passerini, B. Scrosati, *Nat. Mater.* **2015**, *14*, 271.
[203] B. Xu, S. Yue, Z. Sui, X. Zhang, S. Hou, G. Cao, Y. Yang, *Energy Environ. Sci.* **2011**, *4*, 2826.
[204] Y. Yoon, K. Lee, S. Kwon, S. Seo, H. Yoo, S. Kim, Y. Shin, Y. Park, D. Kim, J. Y. Choi, H. Lee, *ACS Nano* **2014**, *8*, 4580.
[205] S. Zheng, Z. Li, Z. S. Wu, Y. Dong, F. Zhou, S. Wang, Q. Fu, C. Sun, L. Guo, X. Bao, *ACS Nano* **2017**, *11*, 4009.
[206] K. H. Lee, Y. W. Lee, S. W. Lee, J. S. Ha, S. S. Lee, J. G. Son, *Sci. Rep.* **2015**, *5*, 13696.
[207] J. Azadmanjiri, V. K. Srivastava, P. Kumar, J. Wang, A. Yu, *J. Mater. Chem. A* **2018**, *6*, 13509.
[208] J. Azadmanjiri, V. K. Srivastava, P. Kumar, M. Nikzad, J. Wang, A. Yu, *J. Mater. Chem. A* **2018**, *6*, 702.
[209] X. C. Dong, H. Xu, X. W. Wang, Y. X. Huang, M. B. Chan Park, H. Zhang, L. H. Wang, W. Huang, P. Chen, *ACS Nano* **2012**, *6*, 3206.
[210] J. Wen, X. Wang, S. Mao, Z. Bo, H. Kim, S. Cui, G. Lu, X. Feng, J. Chen, *Adv. Mater.* **2012**, *24*, 5610.
[211] C. N. R. Rao, K. Gopalakrishnan, A. Govindaraj, *Nano Today* **2014**, *9*, 324.
[212] J. Han, L. L. Zhang, S. Lee, J. Oh, K. S. Lee, J. R. Potts, J. Ji, X. Zhao, R. S. Ruoff, S. Park, *ACS Nano* **2013**, *7*, 19.
[213] L. Sun, L. Wang, C. Tian, T. Tan, Y. Xie, K. Shi, M. Li, H. Fu, *RSC Adv.* **2012**, *2*, 4498.
[214] Z. Zuo, Z. Jiang, A. Manthiram, *J. Mater. Chem. A* **2013**, *1*, 13476.
[215] Z. S. Wu, Y. Z. Tan, S. Zheng, S. Wang, K. Parvez, J. Qin, X. Shi, C. Sun, X. Bao, X. Feng, K. Mullen, *J. Am. Chem. Soc.* **2017**, *139*, 4506.

[216] F. Zhou, H. Huang, C. Xiao, S. Zheng, X. Shi, J. Qin, Q. Fu, X. Bao, X. Feng, K. Mullen, Z. S. Wu, *J. Am. Chem. Soc.* **2018**, *140*, 8198.
[217] I. Y. Jeon, Y. R. Shin, G. J. Sohn, H. J. Choi, S. Y. Bae, J. Mahmood, S. M. Jung, J. M. Seo, M. J. Kim, D. Wook Chang, L. Dai, J. B. Baek, *Proc. Natl. Acad. Sci. U. S. A.* **2012**, *109*, 5588.
[218] N. A. Kumar, H. Nolan, N. McEvoy, E. Rezvani, R. L. Doyle, M. E. G. Lyons, G. S. Duesberg, *J. Mater. Chem. A* **2013**, *1*, 4431.
[219] C. Z. Yuan, L. Yang, L. R. Hou, L. F. Shen, X. G. Zhang, X. W. Lou, *Energy Environ. Sci.* **2012**, *5*, 7883.
[220] H. L. Guo, P. Su, X. Kang, S. K. Ning, *J. Mater. Chem. A* **2013**, *1*, 2248.
[221] F. M. Hassan, V. Chabot, J. Li, B. K. Kim, L. Ricardez Sandoval, A. Yu, *J. Mater. Chem. A* **2013**, *1*, 2904.
[222] M. Beidaghi, Y. Gogotsi, *Energy Environ. Sci.* **2014**, *7*, 867.
[223] N. A. Kyeremateng, T. Brousse, D. Pech, *Nat. Nanotechnol.* **2017**, *12*, 7.
[224] J. J. Yoo, K. Balakrishnan, J. Huang, V. Meunier, B. G. Sumpter, A. Srivastava, M. Conway, A. L. Mohana Reddy, J. Yu, R. Vajtai, *Nano Lett.* **2011**, *11*, 1423.
[225] Z. S. Wu, X. Feng, H. M. Cheng, *Natl. Sci. Rev.* **2014**, *1*, 277.
[226] H. Xiao, Z. S. Wu, L. Chen, F. Zhou, S. Zheng, W. Ren, H. M. Cheng, X. Bao, *ACS Nano* **2017**, *11*, 7284.
[227] W. Gao, N. Singh, L. Song, Z. Liu, A. L. M. Reddy, L. Ci, R. Vajtai, Q. Zhang, B. Wei, P. M. Ajayan, *Nat. Nanotechnol.* **2011**, *6*, 496.
[228] L. Peng, X. Peng, B. Liu, C. Wu, Y. Xie, G. Yu, *Nano Lett.* **2013**, *13*, 2151.
[229] Z. S. Wu, K. Parvez, S. Li, S. Yang, Z. Liu, S. Liu, X. Feng, K. Müllen, *Adv. Mater.* **2015**, *27*, 4054.
[230] Z. Liu, Z. S. Wu, S. Yang, R. Dong, X. Feng, K. Müllen, *Adv. Mater.* **2016**, *28*, 2217.
[231] Z. S. Wu, Y. Zheng, S. Zheng, S. Wang, C. Sun, K. Parvez, T. Ikeda, X. Bao, K. Müllen, X. Feng, *Adv. Mater.* **2017**, *29*, 1602960.
[232] Y. Qiu, X. Zhang, S. Yang, *Phys. Chem. Chem. Phys.* **2011**, *13*, 12554.
[233] L. Hou, C. Yuan, L. Yang, L. Shen, F. Zhang, X. Zhang, *CrystEngComm* **2011**, *13*, 6130.
[234] S. Dai, Z. Liu, B. Zhao, J. Zeng, H. Hu, Q. Zhang, D. Chen, C. Qu, D. Dang, M. Liu, *J. Power Sources* **2018**, *387*, 43.
[235] L. Niu, Z. Li, W. Hong, J. Sun, Z. Wang, L. Ma, J. Wang, S. Yang, *Electrochim. Acta* **2013**, *108*, 666.
[236] S. J. Deng, N. Chen, D. Y. Deng, Y. X. Li, X. X. Xing, Y. D. Wang, *Ceram. Int.* **2015**, *41*, 11004.
[237] J. Huo, P. Zheng, X. Wang, S. Guo, *Appl. Surf. Sci.* **2018**, *442*, 575.
[238] Z. S. Wu, A. Winter, L. Chen, Y. Sun, A. Turchanin, X. Feng, K. Mullen, *Adv. Mater.* **2012**, *24*, 5130.
[239] W. Zhang, Z. Chen, X. Guo, K. Jin, Y. Wang, L. Li, Y. Zhang, Z. Wang, L. Sun, T. Zhang, *Electrochim. Acta* **2018**, *278*, 51.
[240] Y. Chen, Z. Liu, L. Sun, Z. Lu, K. Zhuo, *J. Power Sources* **2018**, *390*, 215.
[241] K. Xia, Z. Huang, L. Zheng, B. Han, Q. Gao, C. Zhou, H. Wang, J. Wu, *J. Power Sources* **2017**, *365*, 380.
[242] H. Sun, L. Mei, J. Liang, Z. Zhao, C. Lee, H. Fei, M. Ding, J. Lau, M. Li, C. Wang, X. Xu, G. Hao, B. Papandrea, I. Shakir, B. Dunn, Y. Huang, X. Duan, *Science* **2017**, *356*, 599.
[243] J. Qin, C. He, N. Zhao, Z. Wang, C. Shi, E. Z. Liu, J. Li, *ACS Nano* **2014**, *8*, 1728.
[244] D. Lin, Z. Lu, P. C. Hsu, H. R. Lee, N. Liu, J. Zhao, H. Wang, C. Liu, Y. Cui, *Energy Environ. Sci.* **2015**, *8*, 2371.
[245] X. Wang, L. Lv, Z. Cheng, J. Gao, L. Dong, C. Hu, L. Qu, *Adv. Energy Mater.* **2016**, *6*, 1502100.
[246] B. Wang, W. Al Abdulla, D. Wang, X. S. Zhao, *Energy Environ. Sci.* **2015**, *8*, 869.
[247] B. Sun, X. Huang, S. Chen, P. Munroe, G. Wang, *Nano Lett.* **2014**, *14*, 3145.
[248] J. Han, G. Huang, Y. Ito, X. Guo, T. Fujita, P. Liu, A. Hirata, M. Chen, *Adv. Energy Mater.* **2017**, *7*, 1601933.
[249] W. Zhang, J. Zhu, H. Ang, Y. Zeng, N. Xiao, Y. Gao, W. Liu, H. H. Hng, Q. Yan, *Nanoscale* **2013**, *5*, 9651.
[250] H. Wang, Y. Yang, Y. Liang, J. T. Robinson, Y. Li, A. Jackson, Y. Cui, H. Dai, *Nano Lett.* **2011**, *11*, 2644.
[251] L. Fei, X. Li, W. Bi, Z. Zhuo, W. Wei, L. Sun, W. Lu, X. Wu, K. Xie, C. Wu, H. L. W. Chan, Y. Wang, *Adv. Mater.* **2015**, *27*, 5936.
[252] J. Cao, C. Chen, Q. Zhao, N. Zhang, Q. Lu, X. Wang, Z. Niu, J. Chen, *Adv. Mater.* **2016**, *28*, 9629.
[253] G. Zhou, L. C. Yin, D. W. Wang, L. Li, S. Pei, I. R. Gentle, F. Li, H. M. Cheng, *ACS Nano* **2013**, *7*, 5367.
[254] Z. Sun, J. Zhang, L. Yin, G. Hu, R. Fang, H.-M. Cheng, F. Li, *Nat. Commun.* **2017**, *8*, 14627.
[255] J. Wang, Y. S. He, J. Yang, *Adv. Mater.* **2015**, *27*, 569.
[256] X. Liang, A. Garsuch, L. F. Nazar, *Angew. Chem. Int. Ed.* **2015**, *54*, 3907.
[257] Z. W. Seh, J. H. Yu, W. Li, P. C. Hsu, H. Wang, Y. Sun, H. Yao, Q. Zhang, Y. Cui, *Nat. Commun.* **2014**, *5*, 5017.
[258] F. Pei, L. Lin, D. Ou, Z. Zheng, S. Mo, X. Fang, N. Zheng, *Nat. Commun.* **2017**, *8*, 482.
[259] H. Pan, X. Wei, W. A. Henderson, Y. Shao, J. Chen, P. Bhattacharya, J. Xiao, J. Liu, *Adv. Energy Mater.* **2015**, *5*, 1500113.
[260] A. Manthiram, S. H. Chung, C. Zu, *Adv. Mater.* **2015**, *27*, 1980.
[261] J. Q. Huang, X. F. Liu, Q. Zhang, C. M. Chen, M. Q. Zhao, S. M. Zhang, W. Zhu, W. Z. Qian, F. Wei, *Nano Energy* **2013**, *2*, 314.
[262] H. Bai, C. Li, G. Shi, *Adv. Mater.* **2011**, *23*, 1089.
[263] X. Yang, L. Zhang, F. Zhang, Y. Huang, Y. Chen, *ACS Nano* **2014**, *8*, 5208.
[264] X. Tao, J. Wang, C. Liu, H. Wang, H. Yao, G. Zheng, Z. W. Seh, Q. Cai, W. Li, G. Zhou, *Nat. Commun.* **2016**, *7*, 11203.
[265] W. Ren, W. Ma, S. Zhang, B. Tang, *Energy Storage Mater.* **2019**, *23*, 707.
[266] J. P. Paraknowitsch, A. Thomas, *Energy Environ. Sci.* **2013**, *6*, 2839.
[267] Z. Wang, Y. Dong, H. Li, Z. Zhao, H. B. Wu, C. Hao, S. Liu, J. Qiu, X. W. Lou, *Nat. Commun.* **2014**, *5*, 5002.
[268] G. Hu, C. Xu, Z. Sun, S. Wang, H. M. Cheng, F. Li, W. Ren, *Adv. Mater.* **2016**, *28*, 1603.
[269] H. J. Peng, D. W. Wang, J. Q. Huang, X. B. Cheng, Z. Yuan, F. Wei, Q. Zhang, *Adv. Sci.* **2016**, *3*, 1500268.
[270] S. K. Lee, S. M. Oh, E. Park, B. Scrosati, J. Hassoun, M. S. Park, Y. J. Kim, H. Kim, I. Belharouak, Y. K. Sun, *Nano Lett.* **2015**, *15*, 2863.
[271] J. Q. Huang, Q. Zhang, H. J. Peng, X. Y. Liu, W. Z. Qian, F. Wei, *Energy Environ. Sci.* **2014**, *7*, 347.
[272] L. Wang, Y. Wang, Y. Xia, *Energy Environ. Sci.* **2015**, *8*, 1551.
[273] X. Ni, T. Qian, X. Liu, N. Xu, J. Liu, C. Yan, *Adv. Funct. Mater.* **2018**, *28*, 1706513.
[274] H. Yuan, H. Peng, B. Li, J. Xie, L. Kong, M. Zhao, X. Chen, J. Huang, Q. Zhang, *Adv. Energy Mater.* **2019**, *9*, 1802768.
[275] R. Zhang, X. B. Cheng, C. Z. Zhao, H. J. Peng, J. L. Shi, J. Q. Huang, J. Wang, F. Wei, Q. Zhang, *Adv. Mater.* **2016**, *28*, 2155.
[276] S. Liu, A. Wang, Q. Li, J. Wu, K. Chiou, J. Huang, J. Luo, *Joule* **2018**, *2*, 184.
[277] R. Mukherjee, A. V. Thomas, D. Datta, E. Singh, J. Li, O. Eksik, V. B. Shenoy, N. Koratkar, *Nat. Commun.* **2014**, *5*, 3710.
[278] R. Zhang, X. R. Chen, X. Chen, X. B. Cheng, X. Q. Zhang, C. Yan, Q. Zhang, *Angew. Chem. Int. Ed.* **2017**, *129*, 7872.
[279] X. B. Cheng, R. Zhang, C. Z. Zhao, Q. Zhang, *Chem. Rev.* **2017**, *117*, 10403.
[280] D. Lin, Y. Liu, Y. Cui, *Nat. Nanotechnol.* **2017**, *12*, 194.
[281] J. Qian, W. A. Henderson, W. Xu, P. Bhattacharya, M. Engelhard, O. Borodin, J. G. Zhang, *Nat. Commun.* **2015**, *6*, 6362.
[282] W. Xu, J. Wang, F. Ding, X. Chen, E. Nasybulin, Y. Zhang, J. G. Zhang, *Energy Environ. Sci.* **2014**, *7*, 513.
[283] S. Bai, Y. Sun, J. Yi, Y. He, Y. Qiao, H. Zhou, *Joule* **2018**, *2*, 2117.
[284] Q. Li, H. Pan, W. Li, Y. Wang, J. Wang, J. Zheng, X. Yu, H. Li, L. Chen, *ACS Energy Lett.* **2018**, *3*, 2259.

[285] C. Yan, X. B. Cheng, Y. X. Yao, X. Shen, B. Q. Li, W. J. Li, R. Zhang, J. Q. Huang, H. Li, Q. Zhang, *Adv. Mater.* **2018**, *30*, 1804461.
[286] Y. Zhao, L. V. Goncharova, Q. Zhang, P. Kaghazchi, Q. Sun, A. Lushington, B. Wang, R. Li, X. Sun, *Nano Lett.* **2017**, *17*, 5653.
[287] X. B. Cheng, H. J. Peng, J. Q. Huang, R. Zhang, C. Z. Zhao, Q. Zhang, *ACS Nano* **2015**, *9*, 6373.
[288] S. S. Chi, Y. Liu, W. L. Song, L. Z. Fan, Q. Zhang, *Adv. Funct. Mater.* **2017**, *27*, 1700348.
[289] J. Zhao, G. Zhou, K. Yan, J. Xie, Y. Li, L. Liao, Y. Jin, K. Liu, P. C. Hsu, J. Wang, *Nat. Nanotechnol.* **2017**, *12*, 993.
[290] A. A. Assegie, C. C. Chung, M. C. Tsai, W. N. Su, C. W. Chen, B. J. Hwang, *Nanoscale* **2019**, *11*, 2710.
[291] D. Lin, Y. Liu, Z. Liang, H. W. Lee, J. Sun, H. Wang, K. Yan, J. Xie, Y. Cui, *Nat. Nanotechnol.* **2016**, *11*, 626.
[292] Z. Li, X. Li, L. Zhou, Z. Xiao, S. Zhou, L. Li, L. Zhi, *Nanoscale* **2018**, *10*, 4675.
[293] Z. Li, X. Li, L. Zhou, Z. Xiao, S. Zhou, X. Zhang, L. Li, L. Zhi, *Nano Energy* **2018**, *49*, 179.
[294] T. Wang, P. Zhai, D. Legut, L. Wang, X. Liu, B. Li, C. Dong, Y. Fan, Y. Gong, Q. Zhang, *Adv. Energy Mater.* **2019**, *9*, 1804000.
[295] C. Zhu, P. Kopold, P. A. van Aken, J. Maier, Y. Yu, *Adv. Mater.* **2016**, *28*, 2409.
[296] G. Li, B. Huang, Z. Pan, X. Su, Z. Shao, L. An, *Energy Environ. Sci.* **2019**, *12*, 2030.
[297] X. Cheng, D. Li, Y. Wu, R. Xu, Y. Yu, *J. Mater. Chem. A* **2019**, *7*, 4913.
[298] H. Gao, T. Zhou, Y. Zheng, Y. Liu, J. Chen, H. Liu, Z. Guo, *Adv. Energy Mater.* **2016**, *6*, 1601037.
[299] W. Luo, J. Wan, B. Ozdemir, W. Bao, Y. Chen, J. Dai, H. Lin, Y. Xu, F. Gu, V. Barone, L. Hu, *Nano Lett.* **2015**, *15*, 7671.
[300] S. W. Kim, D. H. Seo, X. Ma, G. Ceder, K. Kang, *Adv. Energy Mater.* **2012**, *2*, 710.
[301] H. Pan, Y. S. Hu, L. Chen, *Energy Environ. Sci.* **2013**, *6*, 2338.
[302] J. Sun, H. W. Lee, M. Pasta, H. Yuan, G. Zheng, Y. Sun, Y. Li, Y. Cui, *Nat. Nanotechnol.* **2015**, *10*, 980.
[303] K. Share, A. P. Cohn, R. Carter, B. Rogers, C. L. Pint, *ACS Nano* **2016**, *10*, 9738.
[304] G. Ma, K. Huang, J. S. Ma, Z. Ju, Z. Xing, Q. C. Zhuang, *J. Mater. Chem. A* **2017**, *5*, 7854.
[305] D. Er, E. Detsi, H. Kumar, V. B. Shenoy, *ACS Energy Lett.* **2016**, *1*, 638.
[306] X. Dai, F. Wan, L. Zhang, H. Cao, Z. Niu, *Energy Storage Mater.* **2019**, *17*, 143.
[307] Y. Cai, F. Liu, Z. Luo, G. Fang, J. Zhou, A. Pan, S. Liang, *Energy Storage Mater.* **2018**, *13*, 168.
[308] B. Wu, G. Zhang, M. Yan, T. Xiong, P. He, L. He, X. Xu, L. Mai, *Small* **2018**, *14*, 1703850.
[309] F. Ambroz, T. J. Macdonald, T. Nann, *Adv. Energy Mater.* **2017**, *7*, 1602093.
[310] S. K. Das, S. Mahapatra, H. Lahan, *J. Mater. Chem. A* **2017**, *5*, 6347.
[311] P. F. Smith, K. J. Takeuchi, A. C. Marschilok, E. S. Takeuchi, *Acc. Chem. Res.* **2017**, *50*, 544.
[312] H. Yang, H. Li, J. Li, Z. Sun, K. He, H. M. Cheng, F. Li, *Angew. Chem. Int. Ed.* **2019**, *58*, 11978.
[313] G. A. Elia, K. Marquardt, K. Hoeppner, S. Fantini, R. Lin, E. Knipping, W. Peters, J. F. Drillet, S. Passerini, R. Hahn, *Adv. Mater.* **2016**, *28*, 7564.
[314] S. K. Das, *Angew. Chem. Int. Ed.* **2018**, *57*, 16606.
[315] H. Chen, H. Xu, S. Wang, T. Huang, J. Xi, S. Cai, F. Guo, Z. Xu, W. Gao, C. Gao, *Sci. Adv.* **2017**, *3*, eaao7233.
[316] Y. Wu, M. Gong, M. C. Lin, C. Yuan, M. Angell, L. Huang, D. Y. Wang, X. Zhang, J. Yang, B. J. Hwang, H. Dai, *Adv. Mater.* **2016**, *28*, 9218.
[317] L. Zhang, L. Chen, H. Luo, X. Zhou, Z. Liu, *Adv. Energy Mater.* **2017**, *7*, 1700034.
[318] H. Huang, F. Zhou, X. Shi, J. Qin, Z. Zhang, X. Bao, Z. S. Wu, *Energy Storage Mater.* **2019**, *23*, 664.
[319] X. Yu, B. Wang, D. Gong, Z. Xu, B. Lu, *Adv. Mater.* **2017**, *29*, 1604118.
[320] P. Chen, T. Y. Xiao, Y. H. Qian, S. S. Li, S. H. Yu, *Adv. Mater.* **2013**, *25*, 3192.
[321] H. B. Yang, S. F. Hung, S. Liu, K. Yuan, S. Miao, L. Zhang, X. Huang, H. Y. Wang, W. Cai, R. Chen, J. Gao, X. Yang, W. Chen, Y. Huang, H. M. Chen, C. M. Li, T. Zhang, B. Liu, *Nat. Energy* **2018**, *3*, 140.
[322] S. Chu, A. Majumdar, *Nature* **2012**, *488*, 294.
[323] H. Fei, J. Dong, M. J. Arellano Jiménez, G. Ye, N. Dong Kim, E. L. G. Samuel, Z. Peng, Z. Zhu, F. Qin, J. Bao, M. J. Yacaman, P. M. Ajayan, D. Chen, J. M. Tour, *Nat. Commun.* **2015**, *6*, 8668.
[324] S. Chen, J. Duan, J. Ran, M. Jaroniec, S. Z. Qiao, *Energy Environ. Sci.* **2013**, *6*, 3693.
[325] Z. Cai, B. Liu, X. Zou, H. M. Cheng, *Chem. Rev.* **2018**, *118*, 6091.
[326] H. B. Yang, J. Miao, S. F. Hung, J. Chen, H. B. Tao, X. Wang, L. Zhang, R. Chen, J. Gao, H. M. Chen, L. Dai, B. Liu, *Sci. Adv.* **2016**, *2*, e1501122.
[327] D. Deng, X. Pan, L. Yu, Y. Cui, Y. Jiang, J. Qi, W.-X. Li, Q. Fu, X. Ma, Q. Xue, *Chem. Mater.* **2011**, *23*, 1188.
[328] L. Lai, J. R. Potts, D. Zhan, L. Wang, C. K. Poh, C. Tang, H. Gong, Z. Shen, J. Lin, R. S. Ruoff, *Energy Environ. Sci.* **2012**, *5*, 7936.
[329] Y. Ito, Y. Shen, D. Hojo, Y. Itagaki, T. Fujita, L. Chen, T. Aida, Z. Tang, T. Adschiri, M. Chen, *Adv. Mater.* **2016**, *28*, 10644.
[330] Z. W. Liu, F. Peng, H. J. Wang, H. Yu, W. X. Zheng, J. Yang, *Angew. Chem. Int. Ed.* **2011**, *50*, 3257.
[331] J. J. Duan, S. Chen, M. Jaroniec, S. Z. Qiao, *ACS Catal.* **2015**, *5*, 5207.
[332] Y. Jia, L. Zhang, A. Du, G. Gao, J. Chen, X. Yan, C. L. Brown, X. Yao, *Adv. Mater.* **2016**, *28*, 9532.
[333] X. R. Wang, J. Y. Liu, Z. W. Liu, W. C. Wang, J. Luo, X. P. Han, X. W. Du, S. Z. Qiao, J. Yang, *Adv. Mater.* **2018**, *30*, 1800005.
[334] T. Feng, X. R. Zhao, C. K. Dong, H. Liu, X. W. Du, J. Yang, *Nanoscale* **2018**, *10*, 22140.
[335] S. Chen, J. Duan, M. Jaroniec, S. Z. Qiao, *Angew. Chem. Int. Ed.* **2013**, *52*, 13567.
[336] D. Geng, Y. Chen, Y. Chen, Y. Li, R. Li, X. Sun, S. Ye, S. Knights, *Energy Environ. Sci.* **2011**, *4*, 760.
[337] G. Giovannetti, P. A. Khomyakov, G. Brocks, V. M. Karpan, J. van den Brink, P. J. Kelly, *Phys. Rev. Lett.* **2008**, *101*, 026803.
[338] H. Zhao, C. Sun, Z. Jin, D. W. Wang, X. Yan, Z. Chen, G. Zhu, X. Yao, *J. Mater. Chem. A* **2015**, *3*, 11736.
[339] Y. Jiang, L. Yang, T. Sun, J. Zhao, Z. Lyu, O. Zhuo, X. Wang, Q. Wu, J. Ma, Z. Hu, *ACS Catal.* **2015**, *5*, 6707.
[340] Y. Jia, L. Zhang, L. Zhuang, H. Liu, X. Yan, X. Wang, J. Liu, J. Wang, Y. Zheng, Z. Xiao, E. Taran, J. Chen, D. Yang, Z. Zhu, S. Wang, L. Dai, X. Yao, *Nat. Catal.* **2019**, *2*, 688.
[341] L. Dai, Y. Xue, L. Qu, H. J. Choi, J. B. Baek, *Chem. Rev.* **2015**, *115*, 4823.
[342] P. Song, M. Luo, X. Liu, W. Xing, W. Xu, Z. Jiang, L. Gu, *Adv. Funct. Mater.* **2017**, *27*, 1700802.
[343] W. Li, Y. Yanhui, W. Chunfei, G. Hongchen, T. Xin, *Angew. Chem., Int. Ed.* **2017**, *129*, 13867.
[344] W. Chen, J. Pei, C. T. He, J. Wan, H. Ren, Y. Zhu, Y. Wang, J. Dong, S. Tian, W. C. Cheong, S. Lu, L. Zheng, X. Zheng, W. Yan, Z. Zhuang, C. Chen, Q. Peng, D. Wang, Y. Li, *Angew. Chem. Int. Ed.* **2017**, *129*, 16302.
[345] N. Cheng, S. Stambula, D. Wang, M. N. Banis, J. Liu, A. Riese, B. Xiao, R. Li, T. K. Sham, L. M. Liu, G. A. Botton, X. Sun, *Nat. Commun.* **2016**, *7*, 13638.
[346] H. Fei, J. Dong, Y. Feng, C. S. Allen, C. Wan, B. Volosskiy, M. Li, Z. Zhao, Y. Wang, H. Sun, P. An, W. Chen, Z. Guo, C. Lee, D. Chen,

I. Shakir, M. Liu, T. Hu, Y. Li, A. I. Kirkland, X. Duan, Y. Huang, *Nat. Catal.* **2018**, *1*, 63.
[347] H. J. Qiu, Y. Ito, W. Cong, Y. Tan, P. Liu, A. Hirata, T. Fujita, Z. Tang, M. Chen, *Angew. Chem. Int. Ed.* **2015**, *54*, 14031.
[348] L. Zhang, Y. Jia, G. Gao, X. Yan, N. Chen, J. Chen, M. T. Soo, B. Wood, D. Yang, A. Du, X. Yao, *Chem* **2018**, *4*, 285.
[349] J. S. Bunch, S. S. Verbridge, J. S. Alden, A. M. van der Zande, J. M. Parpia, H. G. Craighead, P. L. McEuen, *Nano Lett.* **2008**, *8*, 2458.
[350] O. Leenaerts, B. Partoens, F. M. Peeters, *Appl. Phys. Lett.* **2008**, *93*, 193107.
[351] R. K. Joshi, P. Carbone, F. C. Wang, V. G. Kravets, Y. Su, I. V. Grigorieva, H. A. Wu, A. K. Geim, R. R. Nair, *Science* **2014**, *343*, 752.
[352] T. A. Larsen, S. Hoffmann, C. Lüthi, B. Truffer, M. Maurer, *Science* **2016**, *352*, 928.
[353] E. N. Wang, R. Karnik, *Nat. Nanotechnol.* **2012**, *7*, 552.
[354] D. Cohen Tanugi, J. C. Grossman, *Nano Lett.* **2012**, *12*, 3602.
[355] B. M. Venkatesan, R. Bashir, *Nat. Nanotechnol.* **2011**, *6*, 615.
[356] G. F. Schneider, S. W. Kowalczyk, V. E. Calado, G. Pandraud, H. W. Zandbergen, L. M. K. Vandersypen, C. Dekker, *Nano Lett.* **2010**, *10*, 3163.
[357] S. Banerjee, J. Wilson, J. Shim, M. Shankla, E. A. Corbin, A. Aksimentiev, R. Bashir, *Adv. Funct. Mater.* **2015**, *25*, 936.
[358] T. Nelson, B. Zhang, O. V. Prezhdo, *Nano Lett.* **2010**, *10*, 3237.
[359] M. Y. Yen, M. C. Hsiao, S. H. Liao, P. I. Liu, H. M. Tsai, C. C. M. Ma, N. W. Pu, M. D. Ger, *Carbon* **2011**, *49*, 3597.
[360] K. Chen, H. Li, L. P. Ma, W. Ren, J. Y. Zhou, H. M. Cheng, T. Lai, *J. Appl. Phys.* **2014**, *115*, 203701.
[361] R. Afrin, N. A. Shah, R. Zhang, F. Wei, A. S. Bhatti, *J. Mater. Sci.* **2014**, *49*, 7023.